Lattice Simulations of QCD-like Theories at Finite Baryon Density

Vom Fachbereich Physik
der Technischen Universität Darmstadt

zur Erlangung des Grades
eines Doktors der Naturwissenschaften
(Dr. rer. nat.)

genehmigte Dissertation von
M.Sc. Philipp Friedrich Scior
aus Groß-Umstadt

Darmstadt 2016
D17

Referent: Prof. Dr. Lorenz von Smekal
Korreferent: Prof. Dr. Jochen Wambach

Tag der Einreichung: 14.06.2016
Tag der Prüfung: 13.07.2016

The results of presented in this thesis are solely due to the author. However, parts of the thesis have been done in collaboration with other authors. Results for Polyakov loop distributions and effective potentials in two-color QCD in section 3.1 were obtained in collaboration with David Scheffler, Dominik Smith and Lorenz von Smekal. Parts of the section are published in [1]. Parts of the results in chapter 4 were obtained together with Björn Wellegehausen and Lorenz von Smekal and published in [2, 3]

Zusammenfassung

Die Untersuchung des Phasendiagramms der Quantenchromodynamik (QCD) ist von großer Bedeutung zur Beschreibung der Eigenschaften von Neutronensternen oder Schwerionenkollisionen. Aufgrund des Vorzeichenproblems der Gitter-QCD bei endlichem chemischen Potential benötigen wir effektive Theorien zur Beschreibung der QCD bei endlicher Dichte. Wir verwenden hier dreidimensionale Polyakov-Loop Theorien zur Analyse der Phasendiagramme QCD-artiger Theorien. Insbesondere untersuchen wir den Fall schwerer Quarks, für den wir diese effektiven Theorien durch Entwicklung nach inverser Kopplung und inverser Quarkmasse systematisch herleiten und Ordnung für Ordung verbessert können. Da die von uns untersuchten QCD-artigen Theorien kein Vorzeichenproblem aufweisen, ist es uns möglich, unsere Resultate mit Daten von abinito Gittersimulationen dieser Theorien zu vergleichen, um qualitative und quantitative Aussagen über Anwendbarkeit und Gültigkeitsbereich der effektiven Theorien zu machen.

Wir starten mit der Herleitung der effektiven Theorien bis zur übernächsten Ordnung im sogenannten Hoppingparameter, invers zur Quarkmasse, für Zwei-Farb-QCD und G_2-QCD. Dies sind QCD-artige Theorien mit nur zwei anstelle der üblichen drei Farben bzw. mit Eichgruppe G_2 anstelle der SU(3) der QCD. Wir beginnen die Analyse der Phasendiagramme bei endlicher Temperatur, um die effektive Theorie und ihre numerische Implementierung zu testen. Darüber hinaus können wir Vorhersagen für den Deconfinement-Phasenübergang in G_2 Yang-Mills-Theorie treffen. Schlussendlich wenden wir uns der kalten und dichten Region der Phasendiagramme zu. Hier beobachten wir, dass die Baryonendichte abrupt mit dem chemischen Potential für Quarks an zu wachsen beginnt, sobald diese die halbe Diquarkmasse erreicht hat. Bei verschwindender Temperatur erwartet man, dass dies in einem Quantenphasenübergang mit Bose-Einstein-Kondensation der Diquarks passiert, der im Gegensatz zum Flüssig-Gas-Übergang der QCD kontinuierlich ist. In der Tat finden wir sehr gute Evidenz dafür, dass die effektiven Gittertheorien für schwere Quarks diesen qualitativen Unterschied zwischen Übergängen erster und zweiter Ordnung beschreiben können. Bei noch größerem chemischen Potential finden wir einen Anstieg des Polyakov-Loop und der Teilchenzahldichte der Quarks bis hin zur charakteristischen Sättigung der jeweiligen Theorie auf einem endlichen Gitter.

Abstract

The exploration of the phase diagram of quantum chromodynamics (QCD) is of great importance to describe e.g. the properties of neutron stars or heavy-ion collisions. Due to the sign problem of lattice QCD at finite chemical potential we need effective theories to study QCD at finite density. Here, we will use a three-dimensional Polyakov-loop theory to study the phase diagrams of QCD-like theories. In particular, we investigate the heavy quark limit of the QCD-like theories where the effective theory can be derived from the full theory by a combined strong coupling and hopping expansion. This expansion can be systematically improved order by order. Since there is no sign problem for the QCD-like theories we consider, we can compare our results to data from lattice calculations of the full theories to make qualitative and quantitative statements of the effective theory's validity.

We start by deriving the effective theory up to next-to-next-to leading-oder, in particular for two-color and G_2-QCD where replace the three colors in QCD with only two colors or respectively replace the gauge group SU(3) of QCD with G_2. We will then apply the effective theory at finite temperature mainly to test the theory and the implementation but also to make some predictions for the deconfinement phase transition in G_2 Yang-Mills theory. Finally, we will turn our attention to the cold and dense regime of the phase diagram where we observe a sharp increase of the baryon density with the quark chemical potential μ, when μ reaches half the diquark mass. At vanishing temperature this is expected to happen in a quantum phase transition with Bose-Einstein-condensation of diquarks. In contrast to the liquid-gas transition in QCD, the phase transition to the Bose-Einstein condensate is continuous. We find evidence that the effective theories for heavy quarks are able to describe the qualitative difference between first and second order phase transitions. For even higher μ we find the rise of the Polyakov loop as well as the quark number density up to the characteristic saturation of the respective Theory on a finite lattice.

Contents

1 Introduction

The theoretical framework for the description of particle physics as well as collider and high precision experiments is the Standard Model of particle physics. It combines the description of Quantum Chromodynamics (QCD) and the electroweak theory, contains all known elementary particles and all forces with the exception of gravity. The Standard Model was and still is highly successful in explaining and predicting experimental data for about four decades. Though we know, we have to extend the Standard Model to describe neutrino masses, dark matter, dark energy and to incorporate a quantum theory of gravitation, apart from cosmological observations, there is almost no experimental evidence for how and where the Standard Model could go wrong. Even with possible hints at new physics in the muon's anomalous magnetic moment [4] or an observed excess in the diphoton channel around 750 GeV at the Large Hadron Collider [5] the Standard Model is one of the most successful and extensively verified models in physics.

Yet, our physical understanding of the Standard Model remains incomplete. Especially in the case of QCD there are a lot of open questions, and much theoretical and experimental effort is directed towards answering these questions. The reason for the complexity of QCD is its non-Abelian nature, that comes in the form of asymptotic freedom, which is a blessing and a curse at the same time. Asymptotic freedom was discovered by Wilczek, Politzer and Gross in 1973 [6, 7]. It states that the coupling constant of QCD is – despite its name – not constant but scale-dependent, leading to an asymptotically vanishing coupling strength as energy increases. On one hand asymptotic freedom guarantees the renormalizability of QCD, so that it may be valid to the smallest length/ high energy scales, but on the other hand the physics, guaranteeing weak coupling at high energies, leads to increasing interactions at lower energies until the theory eventually becomes non-perturbative. At some scale the interaction becomes so strong, that quarks and gluons – QCDs elementary fields – become locked into hadrons,

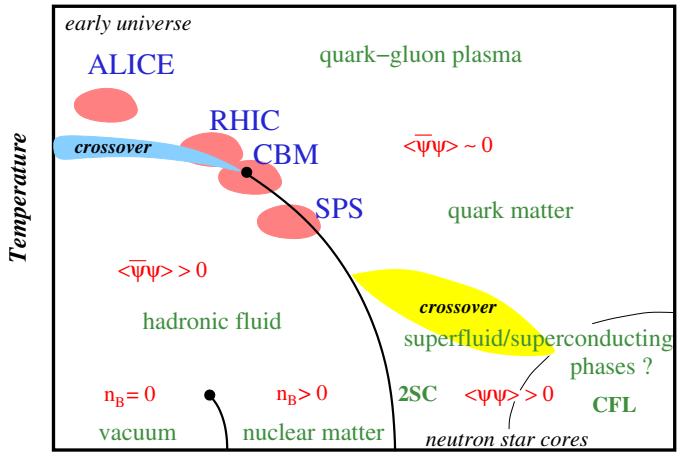

Figure 1.1.: Schematic view of the QCD phase diagram in the $T - \mu$ plane. Taken from [8].

like mesons and baryons. This effect is called Confinement and is the reason why we have never been able to directly observe an isolated quark or a gluon in a detector. Even though quark confinement can be intuitively understood as a concentration of the chromoelectrix flux between two quarks into a flux-tube leading to a linear rising potential between the quarks, its underlying physical mechanism is yet unknown [9]. In general the ultra-violet features of QCD are well understood as perturbation theory is applicable and able to explain experimental data from e.g. deep in-elastic scattering to high accuracy [10]. The infrared physics of QCD with important effects like confinement and dynamical chiral symmetry breaking is much harder to study as we need non-perturbative methods to do so.
The most successful ab-intio method to study the infrared physics of QCD is lattice QCD, where the theory is formulated on a finite Euclidean space-time grid. The discretization turns the path integral in the generating functional into a finite set of integrals, which can be evaluated by using Monte-Carlo methods. Lattice QCD has produced tremendous results. The first of these were the reproduction of hadron masses to high accuracy [11]. In the last years it has become possible to extract hadron form factors for electromagnetic and strong decays [12] or even nucleon scattering phase shifts [13].
Despite all these results, there remain areas where there was little progress over the last years. Maybe the two most pressing, still standing issues are the nature of confinement and the exploration of the QCD phase diagram.

The knowledge about the thermodynamic properties and the phase structure of strongly interacting matter in thermal equilibrium is summarized in the QCD phase diagram. In QCD one is usually interested in the temperature-chemical potential plane of the phase diagram. A conjectured view of the phase diagram is shown in Fig. 1.1. At low tempera-

tures T and small chemical potential μ the quarks and gluons are confined into hadrons. Perturbative QCD calculations and heavy ion collisions show that at high temperatures quarks and gluons are no longer confined into hadrons and form a quark-gluon plasma (QGP) [14]. Parallel to this deconfinement phase transition we expect another phase transition to happen: We know from hadron spectra that chiral symmetry is broken at low temperatures, characterized by a finite chiral condensate $\langle\bar{\psi}\psi\rangle$, while at higher temperatures chiral symmetry is expected to be restored. Even though the phase diagram has been studied experimentally and theoretically for many years, we know only its most basic properties [15]. It is now well established by lattice QCD that the deconfinement and chiral phase transitions at $\mu = 0$ are analytic cross-overs[1] and happen around 155 MeV [16, 17]. Unfortunately, lattice QCD is unable to provide us with results for the bigger part of the phase diagram as it suffers from the so called fermion sign problem: At finite chemical potential $\mu > 0$ the fermion determinant becomes complex and can not be used as a statistical weight in Monte-Carlo simulations [18]. Perturbative QCD is also of limited use for the study of the phase diagram as it is only valid for very high T and μ. There is evidence from model calculations that point to a rich phase structure at finite chemical potential, e.g. in Nambu–Jona-Lasinio (NJL) and (Polyakov-)quark-meson model as well as Dyson-Schwinger calculations the deconfinement and chiral cross-over transitions will eventually become true phase transitions at finite chemical potential, that end in a critical point [15]. Inside the hadronic phase we further find the nuclear first order liquid-gas transition also ending in a critical point. Both existence and location of this phase transition are well established by experiments [19]. Large N_c arguments suggest that at some point the chiral and deconfinement phase transitions will move apart from each other and in between emerges a phase of matter called quarkyonic [20]. NJL model, quark-meson model and other calculations also suggest a region of the phase diagram with inhomogeneous chiral matter characterized by a spatially modulated chiral condensate $\langle\bar{\psi}\psi\rangle$ [21]. Further, NJL and perturbative QCD studies suggest color superconducting phases at high chemical potential [22].
Experimentally, the phase diagram is explored by heavy-ion collision experiments, e.g. ALICE at CERN [23], experiments at RHIC [24] or planned future experiments at FAIR [19]. Heavy-ion experiments where able to confirm the formation of a quark-gluon plasma and also to show that the QGP behaves almost like an ideal fluid. Related experiments, like the beam energy scan at RHIC [24] are trying to locate the critical point by analyzing fluctuations in specific observables.
The properties of the QCD phase diagram at finite μ are not only important for the theoretical description of heavy-ion collisions, but also for astrophysical observations concerning neutron stars. The mass-radius relation and other properties of neutron stars are directly influenced by the QCD equation of state at intermediate to high μ [25].
As we already mentioned, most of our knowledge of the QCD phase diagram comes from functional methods in low energy effective models of QCD, that share the chiral properties with QCD but are much simpler, e.g. studies of the (Polyakov-)quark-meson

[1] Hence, they are not phase transitions in the thermodynamic sense.

model with the functional renormalization group [26]. Even though studies with effective models can be used to gain qualitative insight into parts of the phase diagram [27], they are also not suited to study other parts of the phase diagram or to extract quantitative results. One of the reasons is that it is difficult to include gauge fields and therefore confinement in these models. Confinement is usually effectively introduced by a Polyakov loop potential, generated by a background gauge field. However, this is a purely classical field without quantum fluctuations. By fitting the undetermined constants to experimental or lattice data these models are able to reproduce the correct bulk thermodynamic properties of QCD, but still include processes forbidden by confinement, e.g. the decay of a pion into two free quarks [28, 29]. Further, these models usually include vector mesons also only on the mean field level and struggle to incorporate baryons. Baryonic fluctuations are believed to be important for the fate of the chiral and deconfinement phase transitions at finite μ. Another functional approach to explore the QCD phase diagram are Dyson-Schwinger equations (DSEs). DSEs studies were able to find a the critical point in the phase diagram [30]. DSEs are able to do a better job modeling confinement, by using gluon propagators from the lattice as input, also the first steps to take baryonic fluctuations into account were done [31]. The drawback of DSE framework is, that the DSE for a given n-point function depends also on higher n-point functions. Thus, one needs to truncate the system of coupled equations at some point. Unfortunately, it is quite difficult to check the systematic errors of the used truncations schemes, and to estimate the effects of higher order corrections. A functional method with better control over the truncation errors is the functional renormalization group.
In the recent years, the lattice community has seen much attention being directed to deal with the sign problem. Reweighting techniques and analytic continuation from imaginary to real μ [32] can be used to get results in the vicinity of the $\mu = 0$ axis. Taylor expansion of the grand potential is used to explore the phase diagram at small $\frac{\mu}{T}$ [33, 34]. Monte-Carlo on a Lefshetz thimble has shown to work for complex scalar fields with chemical potential [35], complex Langevin dynamics [36] have been tested successfully at QCD with dynamical quarks on small lattices [37]. Formulation of the theory in dual lattice variables can solve the sign problem for massless fermions with Abelian fields in 1+1 dimensions and other toy models [38]. Similar in spirit, graph representations in terms of hadrons can be used at finite chemical potential in the strong coupling limit [39].
Another way to circumvent the sign problem is the use of effective Polyakov-loop theories on the lattice. Here, the sign problem is weaker than in the full theory and can be solved by e.g. using the complex Langevin algorithm [40]. Effective Polyakov-loop theories can be derived systematically from the full theory in a combined strong coupling and hopping expansion from QCD with heavy quarks, by integrating out spatial links [41]. It has been shown that such theories can reproduce the critical couplings for deconfinement in the pure SU(2) and SU(3) gauge theories, and the critical quark masses, limiting the region of the first-order deconfinement transition in SU(3) with heavy quarks, within less than 10% accuracy [41, 42]. Also, studies of the cold and dense regime of the QCD phase diagram have produced first results on the nuclear liquid-gas transition [40]. Further, there are efforts going on to extract the couplings in the effective theory for arbitrary

lattice coupling and masses via inverse Monte-Carlo or relative weights methods [43, 44]. A totally different way to learn something about genuine features of strongly interacting matter at finite density is to avoid the sign problem altogether, by studying the phase diagram of QCD-like theories, that share crucial features with QCD but do not have a sign problem. This can be achieved by replacing the gauge group of QCD, namely SU(3), with other gauge groups. The most popular and well studies example is two-color QCD with the gauge group SU(2). Two-color QCD shares its principle features with QCD, it is asymptotically free and in the infrared it includes confinement and chiral symmetry breaking. However, there are also important differences: The deconfinement phase transition in the case of pure gauge theory is of 2nd order in contrast to the case of SU(3) [45]. An additional symmetry between quarks and anti-quarks leads to a modification of the chiral symmetry pattern. Further, the baryons of two-color QCD consist of two quarks, and thus are bosons not fermions, and some of those baryons are also pseudo-Goldstone bosons from the breaking of chiral symmetry. Still, there has been and still is much work devoted to the exploration of the phase diagram of two-color QCD [46–49]. Another QCD-like theory without a sign problem is G_2-QCD. Here, the gauge group is G_2, the smallest exceptional Lie group. The deconfinement phase transition of pure G_2 gauge theory is of 1st order, as in SU(3) gauge theory [50]. The spectrum of G_2-QCD contains bosonic baryons made out of two quarks but also, like in QCD, fermionic baryons, consisting of three quarks [51]. G_2-QCD therefore provides a unique opportunity to study a gauge theory with dynamic quarks in the fundamental representation, including fermionic baryons without a sign problem. Of course, one could also study QCD with quarks in the adjoint representation to get a QCD-like theory with fermionic baryons and without a sign problem. However, with adjoint quarks the finite T deconfinement phase transition will not be a cross-over but a true phase transition and the chiral and deconfinement phase transitions do not coincide [52]. One particular advantage of QCD-like theories is that they are an excellent testing ground for effective theories, since it is possible to make qualitative and quantitative comparisons between results from effective theories and from lattice simulations at finite density. This for example has been done in [53, 54], where results from a (Polyakov-)quark-meson model in a functional renormalization group approach were compared to two-color QCD lattice data.

The goal of this thesis is to derive effective Polyakov loop models on the lattice for QCD-like theories with heavy quarks from a combined strong coupling and hopping expansion and get results in the cold and dense regime of the phase diagram that can be compared to lattice calculations of the full theory. The document will be organized as follows: First, we will give an overview over lattice field theory in general and an introduction in the two particular QCD-like theories used in this thesis: two-color QCD and G_2-QCD. Next, we will discuss the systematic derivation of the effective theory. Following the derivation, we will first give results at finite temperature and compare our results to lattice results form the full theories. We will then give results for the cold and dense regime of the phase diagram and also compare some of our results to results from the full theory. An overall summary and outlook will be given at the end.

2
Theoretical Framework

2.1. Lattice Field Theory

Before we start with the main part of this thesis, let us briefly review the basic properties of lattice field theory, as it is our approach to calculate the thermodynamic properties of QCD-like theories. This introduction serves to establish conventions, notations and to give a background for the non-expert reader.

Gauge theories in the continuum

Let us start, by writing down the Lagrangian of a gauge theory similar to QCD[2]

$$\mathcal{L} = -\frac{1}{4}F^a_{\mu\nu}F^{a\,\mu\nu} + \bar{\psi}^a(i\gamma_\mu D^\mu - m)\psi^a \,. \tag{2.1}$$

The form of the Lagrangian[3] is almost fully constrained by locality, Poincaré invariance, local gauge invariance and renormalizability. Fermions are represented as Dirac fields ψ in the fundamental representation of the gauge group. The covariant derivative is defined as $D_\mu = \partial_\mu - giA^a_\mu T^a$, where g is the coupling constant, A^a_μ is the gauge field. The field strength tensor is given by

$$F_{\mu\nu} = -\frac{i}{g}[D_\mu, D_\nu] = F^a_{\mu\nu}T^a = (\partial_\mu A^a_\nu - \partial_\nu A^a_\mu + igf^{abc}A^b_\mu A^c_\nu)T^a \,. \tag{2.2}$$

The T^a are the generators of the gauge group, fulfilling

$$[T^a, T^b] = if^{abc}T^c \,, \quad \operatorname{tr} T^a T^b = \frac{1}{2}\delta^{ab} \,.$$

[2]Here, similar to QCD, is used in the sense that the matter content of the theory are fermions in the fundamental representation of the gauge group.

[3]We work with natural units: $\hbar = c = k_B = 1$.

The f^{abc} are the structure constants of the given gauge group, for Abelian gauge theories all f^{abc} vanish, for non-Abelian theories they are proportional to the self-interactions of the gauge fields. Finally, the covariant derivative is contracted with the anti-commuting Dirac matrices that are defined by

$$\{\gamma_\mu, \gamma_\nu\} = 2g_{\mu\nu} = 2\ \mathrm{diag}(1, -1, -1, -1)\ . \tag{2.3}$$

Quantization

Up to now all fields are classical, to go to a quantum theory of fields we have to quantize accordingly. The standard way in quantum mechanics would be to promote our classical fields to operators and impose (anti-)commutation relations for our fields. However it turns out, that this is a rather painful way to quantize the theory, as it is impossible to quantize the gauge fields in this way without fixing a gauge [55]. So, instead of promoting our classical fields to operators we will take another way of quantization. We use the path integral formulation to formulate a quantized theory, here an observable is given by the expectation value of a given operator

$$\begin{aligned} \langle \mathcal{O} \rangle &= \frac{1}{Z} \int \mathcal{D}A\, \mathcal{D}\psi\, \mathcal{D}\bar{\psi}\, \mathcal{O}\, e^{iS[A,\psi,\bar{\psi}]}\ , \\ Z &= \int \mathcal{D}A\, \mathcal{D}\psi\, \mathcal{D}\bar{\psi}\, e^{iS[A,\psi,\bar{\psi}]}\ , \end{aligned} \tag{2.4}$$

where $S = \int d^4x\, \mathcal{L}$ is the classical action, Z is called the generating functional and we have to integrate over all field configurations, not only the ones minimizing the classical action. Even though we have now quantized our theory, we did not make real progress. It turns out that gauge equivalent field configurations lead to a massive over-counting of the physical degrees of freedom and the infinite dimensional integrals over the fields will diverge. Of course, this is again fixable by choosing a gauge. Yet, gauge fixing for a non-Abelian gauge theory is a non-trivial procedure. In the perturbative regime, this can be achieved by the BRST formalism and the introduction of non-physical auxiliary fields [55]. Unfortunately BRST quantization becomes problematic in the non-perturbative regime, as the Gribov ambiguity becomes important here.
Nevertheless, let us quantize our theory by the path integral formalism. We will see, that because of our chosen regularization, we can just solve the arising integrals by brute force and we do not have to care about the finicky matter of gauge fixing at all.

Lattice discretization

To perform the integrations over the gauge fields in eq. (2.4) we have to regulate our theory properly. We do this by discretizing space-time to a 4 dimensional hypercubic lattice with finite lattice-spacing a.
Before we go into technical details of the discretization, there is one more thing we have to address. The integrand in eq. (2.4) always comes with the phase factor e^{iS}, hence it

is highly oscillating. In case of a free field theory one can show that such an integral is only defined by adding a small imaginary part $i\epsilon$ to the action, performing the integral and taking $\epsilon \to 0$, otherwise the integral does not converge. A convenient way to do this, is by a Wick-rotation of the time direction to imaginary time $t \to it$, this corresponds to changing from Minkowski metric to Euclidean metric and we find

$$Z = \int \mathcal{D}A\, \mathcal{D}\psi\, \mathcal{D}\bar{\psi}\, e^{-S_E[A,\psi,\bar{\psi}]} \,, \tag{2.5}$$

$$S_E = \int d^4x \, \left(\frac{1}{4} F^a_{\mu\nu} F^a_{\mu\nu} + \bar{\psi}^a (i\gamma_\mu D_\mu + m)\psi^a \right) \,. \tag{2.6}$$

S_E is now the Euclidean action and we do not have to distinguish between co- and contra-variant indices. Another interesting feature is that the generating functional (2.5) now has the same form as a statistical partition function with the Boltzmann weight e^{-S_E}. This allows us to assign a temperature to the system as we identify the inverse temperature of the system $\beta = 1/T$ with the extend of the compact temporal direction, when we use appropriate boundary conditions

$$Z = \underset{\text{periodic b.c.}}{\int \mathcal{D}A} \quad \underset{\text{anti-periodic b.c.}}{\int \mathcal{D}\psi\, \mathcal{D}\bar{\psi}} \quad \exp\left(- \int_0^\beta dt \int d^3x\, \mathcal{L}_E \right) \,. \tag{2.7}$$

The Wick rotation is well defined, and using Euclidean quantum field theory is a well established method when using numerical computations and simulations. The only problem arises when one wants to calculate real-time quantities like e.g. spectral functions. In principle we can do all calculations in the Euclidean framework with imaginary time and use analytic continuation to translate our results back to Minkowski space with real time. However as most numerical calculations depend on some discretization in space or momentum space one has only a finite set of data points to construct the analytic continuation back to real time. This gets problematic, when there are numerical errors in those data points, as the analytic continuation of a finite set of noisy data points is an ill-defined problem. Nevertheless, it is still possible to perform the analytic continuation. It was shown in a functional renormalization group approach, that this can be done in a well defined way on the level of the flow equations [56]. Another well established method is the maximum entropy method [57].
Now let us come back to the lattice discretization. We regulate our Euclidean quantum field theory by introducing a finite lattice spacing a. We further work in a finite box with N_t sites in temporal direction, N_s sites in spatial direction and periodic boundary conditions. This way, we introduced an UV cutoff by having a shortest length scale a. The finite extend of the lattice $L = aN_s$ acts as an IR regulator. Finally, because of the finite number of the lattice sites, we only have to perform a finite number of field integrations.

Fermions on the lattice

Let us start our discussion of the discretization of the action with the theory's fermion content. The discretization of the free fermion action is achieved by placing the spinor fields on the discrete lattice sites $\psi(x),\ \bar{\psi}(x),\ x \in \Lambda$, where we take Λ as the finite set of all sites in our 4d lattice. The x are now discrete 4 vectors and, by discretizing the differential symmetrically, the fermion action reads

$$S_f = a^4 \sum_{x\in\Lambda} \bar{\psi}(x) \left(\sum_\mu \gamma_\mu \frac{\psi(x+\hat{\mu}) - \psi(x-\hat{\mu})}{2a} + m\psi(x) \right) . \tag{2.8}$$

The $\hat{\mu}$ denotes a unit vector in the direction μ. We now want to couple the quarks to gluons and therefore have to promote the discretized derivative to a discrete version of a covariant derivative. This is easiest done by demanding gauge invariance of S_f. The discretized fermion fields transform exactly as the continuum fields under gauge transformations:

$$\psi'(x) = \Omega(x)\psi(x) , \quad \bar{\psi}'(x) = \bar{\psi}(x)\Omega^\dagger(x) . \tag{2.9}$$

Is is immediately clear that the mass term is already gauge invariant. However, the derivative terms are not. Consider e.g. the term

$$\bar{\psi}(x)\psi(x+\hat{\mu}) \to \bar{\psi}'(x)\psi'(x+\hat{\mu}) = \bar{\psi}(x)\Omega^\dagger(x)\Omega(x+\hat{\mu})\psi(x+\hat{\mu}) , \tag{2.10}$$

this is not a gauge invariant quantity. It would be gauge invariant, if we inserted some quantity $U(x, x+\hat{\mu})$ in between the fermion fields that transforms like $U(x, x+\hat{\mu}) \to U'(x, x+\hat{\mu}) = \Omega(x)U(x, x+\hat{\mu})\Omega^\dagger(x+\hat{\mu})$. Luckily, we already know a function with the desired transformation properties from the continuum formulation of gauge fields, it is called a parallel transporter

$$U(x,y) = \mathcal{P} \exp\left(i \int_{C(x,y)} A_\mu dx_\mu \right) , \tag{2.11}$$

where $C(x,y)$ is a curve between the points x and y and $\mathcal{P}$ denotes the path ordering of the exponential. As A_μ is a gauge field, living in the algebra of the gauge group, the parallel transporter is an element of the gauge group itself and thus transforms like $\Omega(x)U(x,y)\Omega^\dagger(y)$. We will use the notations

$$U(x, x+\hat{\mu}) = U_\mu(x) = \exp[iaA_\mu(x)] \quad \text{and} \quad U_{-\mu}(x) = U^\dagger(x-\hat{\mu}) \tag{2.12}$$

and call the $U_\mu(x)$ link-variables, as they are directed and can be thought of elements connecting two neighboring sites. There is a one-to-one correspondence between $A_\mu(x)$ and $U_\mu(x)$, hence we will now treat the $U_\mu(x)$'s as our elementary fields. By doing so, our gauge fields are now elements of the gauge group, not the Lie algebra as in the continuum formulation.
The fermion action reads

$$S_f = a^4 \sum_{x\in\Lambda} \bar{\psi}(x) \left(\sum_{\pm\mu} \gamma_\mu \frac{1}{2a} U_\mu(x)\psi(x+\hat{\mu}) + m\psi(x) \right) . \tag{2.13}$$

The above equation is a valid and gauge invariant discretization of the continuum action, however there is a problem. One can easily show that the propagator of free and massless fermions, discretized in that way, has poles not only at the physical $p^2 = 0$, but also in all corners of the first Brillouin zone resulting in 15 additional poles for 4 dimensions [58]. One way to remove these unphysical doublers is by adding a special term to the fermion action that vanishes in the continuum limit but gives the doublers an additional mass $\sim 1/a$, so that the doublers will decouple from the theory as $a \to 0$. This is called the Wilson fermion formalism and the fermion action reads

$$S_f = a^4 \sum_{x,y\in\Lambda} \bar{\psi}(x) D(x,y) \psi(y) \ , \tag{2.14}$$

where the Wilson Dirac operator is defined as

$$D(x,y) = \left(m + \frac{4}{a}\right) \delta_{xy} - \frac{1}{2a} \sum_{\pm\mu} (1 - \gamma_\mu) U_\mu(x) \delta_{y,x+\hat{\mu}} \ . \tag{2.15}$$

The shortcoming of Wilson fermions is that the additional term, giving the extra mass to the unphysical doublers, breaks chiral symmetry explicitly. There are other fermion discretizations that do not break chiral symmetry, e.g. the staggered fermion formulation but they will again contain doublers. In fact, the Nilson-Ninoyima theorem states, there is no local fermion discretization with the right continuum limit that respects chiral symmetry and has no doublers [59].

Yang-Mills action

We already saw that on the lattice the gauge fields are naturally described by parallel transporters $U_\mu(x)$, living on the links of the lattice. We now have to find a combination of Us that is gauge invariant and reduces to the standard Yang-Mills action in the limit $a \to 0$. Let us start by defining gauge invariant quantities consisting only of gauge fields. The gauge fields transform as $U_\mu(x) \to U'_\mu(x) = \Omega(x) U_\mu(x) \Omega^\dagger(x + \hat{\mu})$. Therefore, gauge invariant quantities made of gauge fields will be color traces of closed loops of gauge fields. The smallest possible loop is made out of four gauge fields and is called a plaquette

$$U_{\mu\nu}(x) = U_\mu(x) U_\nu(x + \hat{\mu}) U^\dagger(x + \hat{\nu}) U^\dagger_\nu(x) \ . \tag{2.16}$$

These plaquettes are the building blocks of the most simple gauge action, the Wilson gauge action

$$S_g = -\frac{\beta}{N_c} \sum_{x,\mu<\nu} \mathrm{Re}\,\mathrm{tr}\, U_{\mu\nu}(x) \ , \tag{2.17}$$

with the lattice coupling $\beta = \frac{2N_c}{g^2}$. A straight forward calculation shows that S_g has the right continuum limit

$$\lim_{a\to 0} S_g = \int d^4x \ F^a_{\mu\nu} F^a_{\mu\nu} \ . \tag{2.18}$$

Continuum limit and renormalization

We were able to show that our chosen lattice discretization has the right continuum limit, but we still have to answer how to get to the continuum limit in our numerical calculations. In principle we could just do our calculations with some different values a and extrapolate $a \to 0$. However this is problematic, since the gauge action does not even explicitly depend on a! Furthermore, for the computer a is just a number, so does $a = 0.01$ stand for 0.01 fm or 0.01 ly, and is that already close enough to the continuum limit? So part of the problem is that we simply do not know the scale of the system. From continuum physics we know that to avoid unphysical divergences in loop diagrams we have to renormalize the theory, i.e. the bare parameters of the theory will have a non-trivial dependence on the UV cutoff. This implies that the bare coupling is also a dependent $g(a)$. This turns out to be the solution to our problem: from the property of asymptotic freedom we know that to 1-loop oder we have [60]

$$g^2(a) = \frac{1}{\left(\frac{11}{3}N_c - \frac{2}{3}N_f\right)\log(\frac{\Lambda^2_{\mathrm{QCD}}}{a^2})} \,. \tag{2.19}$$

If we invert this we get $a(g)$ and we find $\lim_{g\to 0} a = 0$. This tells us that we can take the continuum limit of lattice calculations by computing observables at different lattice couplings β and then take the limit $\beta = \frac{2N_c}{g^2} \to \infty$. Of course $a \to 0$ also means that the lattice is shrinking. We therefore have to simultaneously take the thermodynamic limit

$$\beta,\ N_t,\ N_s \to \infty\,, \quad \text{with} \quad T = aN_t,\ L = aN_s \ \text{ finite.} \tag{2.20}$$

To remove finite volume effects one has to repeat this $a \to 0$ extrapolation for various values of L and extrapolate to $L \to \infty$.

2.1.1. Monte-Carlo Integration

We now take a look a how to do the numerical simulations of QCD-like theories on the lattice. Vacuum or thermal expectation values of any observable in the Euclidean lattice framework are given by

$$\langle \mathcal{O} \rangle = \frac{1}{Z} \int [dU]\,[d\psi]\,[d\bar{\psi}]\,\mathcal{O}\; e^{-S[U,\psi,\bar{\psi}]}\,, \tag{2.21}$$

where $[d\psi] = \prod_{x\in\Lambda} d\psi_x$ and $[dU] = \prod_{x\in\Lambda}\prod_{\mu=1}^{\pm 4} dU_\mu(x)$ where $dU_\mu(x)$ is now an invariant measure on the group manifold, called the Haar measure. Solving these integrals numerically is quite challenging, as the integral are of very high dimensions. An efficient way to perform highly dimensional integrals is Monte-Carlo integration. Here, one approximates the integral by summing over field configurations that are already distributed according to the Boltzmann factor e^{-S}

$$\langle \mathcal{O} \rangle \approx \sum_{\text{config.s}\sim e^{-S}} \mathcal{O}(\mathcal{U}, \psi, \bar{\psi})\,. \tag{2.22}$$

Since we sum only over a finite number of configurations this introduces a statistical error, however one can show that the error will reduce with the number of configurations taken into account. The only thing we have to do, is to generate configurations $\{U, \psi, \bar{\psi}\}$ distributed according $\sim e^{-S}$. This can be done by generating a Markov-Chain with e.g. the Metropolis algorithm as update algorithm or more advanced algorithms like heat-bath or hybrid-Monte-Carlo [58].

Fermion determinant and the sign problem

Taking a look at the partition function of a QCD-like theory, we recognize that the integral in the fermion fields is Gaussian. Therefore, the integration can be done analytically

$$\begin{aligned} Z &= \int [dU]\,[d\psi]\,[d\bar{\psi}]\, e^{-(S_g[U]+\bar{\psi}D[U]\psi)}\,, \\ &= \int [dU]\, e^{-S_g[U]} \det[D(U)]\,, \end{aligned} \tag{2.23}$$

where $D(U)$ is the Dirac operator of our chosen discretization and its determinant is called the fermion determinant. Usually, the fermion determinant is treated numerically, like the gauge action, as a weight factor. This is in principle equivalent to using the full action as a Boltzmann weight though it is handled differently by the numerical algorithms, to avoid the Grassmann valued fermion fields on the computer. There is one important constraint on using the fermion determinant (or equivalently the full action) in this way. A well-defined probability weight has to be real and positive! For arbitrary but well defined actions S this is not necessarily the case. However in most cases we are fortunate and the Dirac operator obeys

$$\gamma_5 D \gamma_5 = D^\dagger \quad \Rightarrow \quad \det[D]^* = \det[\gamma_5 D \gamma_5] = \det[D]\,. \tag{2.24}$$

This property is called γ_5-hermicity and we can indeed check that the relation holds for the Dirac operator in (2.15). This ensures that for every complex eigenvalue of D, the complex conjugate eigenvalue is also part of the spectrum and the determinant is real. It is not necessarily positive, however by taking two degenerate quark flavors we get $\det[D]^2 > 0$.
In QCD there is a serious problem when we want to introduce chemical potential for the quarks, to investigate the QCD phase diagram at finite densities. Chemical potential is usually introduced by a modification of the time-like links

$$U_4(x) \to \exp(a\mu) U_4(x) \quad \text{and} \quad U_{-4}(x) \to \exp(-a\mu) U_{-4}(x)\,. \tag{2.25}$$

Some quick lines of algebra show that this modification leads to

$$\gamma_5 D(\mu) \gamma_5 = D(-\mu)^\dagger\,. \tag{2.26}$$

γ_5-hermicity is no longer valid, the fermion determinant is in general complex and we are not able to interpret it as a probability weight at finite μ. Now one could just split

the determinant into absolute value and a complex phase $\det[D] = e^{i\varphi_D}|\det[D]|$ and include the phase into the measured operator. By defining an effective action

$$S_{\text{eff}} = S_g - \log(|\det[D]|) \,, \tag{2.27}$$

we can rewrite (2.21) as

$$\langle \mathcal{O} \rangle = \frac{\langle \mathcal{O} e^{i\varphi_D} \rangle_{S_{\text{eff}}}}{\langle e^{i\varphi_D} \rangle_{S_{\text{eff}}}} \,, \tag{2.28}$$

which is well-defined also at finite chemical potential. The problem is that this does not work numerically. The complex phase $e^{i\varphi_D}$ is rapidly fluctuating in the update process generated by S_{eff} and one needs exponentially many configurations to get reliable expectation values for observables [61]. The obstacle even gets worse when one increases the lattice size. This is called the QCD-sign problem[4] at finite density and so far it has prohibited lattice QCD to fully explore the phase diagram of strongly interacting matter. One should however note that QCD is not unique in having this property, the QCD sign problem is just one particular example of a so called complex action problem and there are many more systems known, where such problems are present.
Recent years have seen much activity in overcoming the sign problem. Taylor expansion of the grand potential in small $\frac{\mu}{T}$, reweighing or canonical approaches [62, 63] have allowed us to get some information of the phase diagram not to far away from $\mu = 0$. New algorithms for circumventing the sign problem, like complex Langevin or simulations on Lefshetz thimbles [35] have been developed. Other approaches include e.g. switching to the polymer representation of the fermion determinant [39] or the density of states method [64]. All of the methods stated above were applied successfully to circumvent sign problems for toy models. The most promising results come from the complex Langevin simulations that were able to get results for QCD at finite chemical potential on small lattices [37]. So far however, all these methods are not quite there yet. In the next sections we will discuss a class of QCD-like theories that share many features with QCD but do not show a sign problem.

2.2. Two-Color QCD

Yang-Mills theory and quantum chromodynamics with only two colors have been and still are the subjects of extensive research. Two-color QCD has the advantage that it is cheaper to simulate than QCD because it has less color degrees of freedom. Yet, two-color QCD shares a lot of qualitative features with QCD: It is strongly coupled, confining in the infrared and asymptotically free at high energies. Two-color QCD exhibits a chiral symmetry breaking pattern very similar to QCD. Moreover, and in contrast to QCD with adjoint matter, the chiral and deconfinement cross-overs at vanishing chemical potential coincide [65, 66]. Still there are also important differences, e.g. the deconfinement transition in the pure gauge theory is a second order phase transition in contrast to the

[4] Though it is actually the strongly fluctuating complex phase of the fermion determinant, that causes the problems.

first order transition in QCD. The biggest difference is the fact that the sign problem, that hinders simulations of QCD at finite baryon density, can be easily solved in two-color QCD. Therefore, two-color QCD is an excellent playground to explore the finite density phase diagram of a QCD-like theory from first principles. In particular, one can study the effects of baryonic degrees of freedom on the phase structure since they are often omitted in effective models and it can be shown in this case that the phase diagram changes drastically if baryonic fluctuations are taken into account, e.g. the chiral phase transition is modified heavily if baryons are taken into account properly [54]. Recent studies with Dyson-Schwinger equations have shown evidence that this might not be the case in QCD [31]. Another significant difference to QCD is the fact that in two-color QCD the baryons, the diquarks, are pseudo Goldstone bosons. One result of this is that at intermediate chemical potential we expect Bose-Einstein condensation of the diquarks [67]. This is the two-color analog to the nuclear liquid-gas transition in QCD.
Two-color QCD is naturally a very rich testing ground for effective theories that might be used to explore the QCD phase diagram, as the effective theories can be compared to first principle lattice calculations in the whole phase diagram.
We will now discuss the symmetries of two-color QCD that lead to the absence of a sign problem.

2.2.1. Anti-Unitary Symmetries and Dyson's Classification

γ_5-hermiticity ensures the reality of the fermion determinant only at vanishing chemical potential. In contrast to QCD with three colors, there is an additional symmetry in two-color QCD that ensures the reality of the fermion determinant for all μ.
If there is an isometry between the generators of a given representation of the gauge group and the complex conjugate representation, like

$$T^{a*} = T^T = -ST^aS^{-1} \,, \tag{2.29}$$

one is able to construct an anti-unitary symmetry A for the Dirac operator in the given representation

$$[A, D] = [SCK, D] = 0 \,, \tag{2.30}$$

where C is the charge conjugation operator and complex conjugation is denoted K. Dyson showed that there are only three scenarios for anti-unitary symmetries of D [68]. If there is no such anti-unitary symmetry, the representation of the group is complex, i.e. the eigenvalues of D are complex, we associate this case with the Dyson index $\beta = 2$. If there is a symmetry with $A^2 = +1$, the complex eigenvalues of D come in complex conjugate pairs and the fermion determinant is always real, but not necessarily positive. We assign this situation with $\beta = 1$. The last case is $\beta = 4$: There is an anti-unitary symmetry and $A^2 = -1$, here D has only real eigenvalues and the eigenvalues are two-fold degenerate, resulting in a positive fermion determinant.
In fundamental two-color QCD we find $S = i\sigma_2$, σ_2 being the second Pauli matrix, to be an isometry between the generators and for Wilson fermions[5] we find $T^2 = 1$. Therefore

[5] Without the additional minus sign from C^2 the anti-unitary symmetries of staggered fermions are opposite to the continuum formulation or Wilson's formulation of lattice fermions.

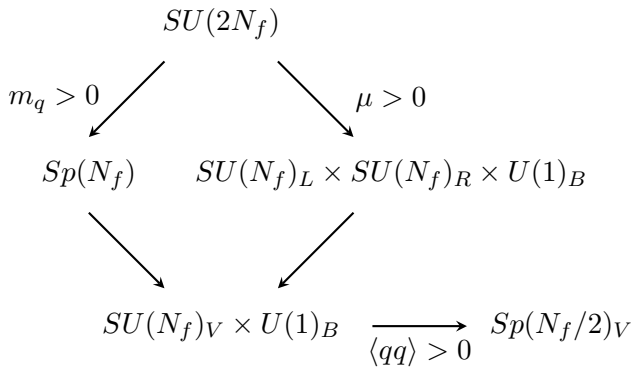

Figure 2.1.: Patterns of chiral symmetry breaking in two-color QCD with fundamental quarks.

we can solve the sign problem by taking two degenerate quark flavors with $\det[D]^2 > 0$.

2.2.2. Extended Flavor Symmetry and Spectrum of Two-Color QCD

Due to the isometry between the fundamental generators, quarks and anti-quarks belong to equivalent representations and we will find an extended flavor symmetry in this case. Let us start with the kinetic part of the Euclidean quark Lagrangian in the chiral basis

$$\mathcal{L} = \bar{\psi} \not{D} \psi = \psi_L^\dagger i \sigma_\mu D_\mu \psi_L - \psi_R^\dagger i \sigma_\mu^\dagger D_\mu \psi_L \ , \tag{2.31}$$

with the transformation

$$\widetilde{\psi}_R = \sigma_2 \tau_2 \psi_R^* \ , \qquad \widetilde{\psi}_R^* = \sigma_2 \tau_2 \psi_R \ , \tag{2.32}$$

where σ_2 and τ_2 are Pauli matrices in spinor and color space, and after some lines of algebra we can rewrite the Lagrangian as

$$\mathcal{L} = \Psi^\dagger i \sigma_\mu D_\mu \Psi \ , \tag{2.33}$$

where we introduced the $4N_cN_f$ dimensional Nambu-Gorkov spinors

$$\Psi = \begin{pmatrix} \psi_L \\ \widetilde{\psi}_R \end{pmatrix} \ . \tag{2.34}$$

Now from eq. (2.33) we can readily see that the Lagrangian is invariant under $U(2N_f)$ chiral symmetry transformations. However just as in the case of QCD the axial $U(1)_A$ is broken by the Adler-Bell-Jackiw anomaly [69, 70] and the symmetry group reduces to $SU(2N_f)$ which contains the usual chiral $SU(N_f)_L \times SU(N_f)_R \times U(1)_B$ as a subgroup. And indeed, if we introduce a chemical potential $\mu > 0$, quarks and anti-quarks do no longer belong to the same representation and the enlarged symmetry group is broken down to the familiar $SU(N_f)_L \times SU(N_f)_R \times U(1)_B$ [46]. For vanishing μ, the

extended $SU(2N_f)$ can be broken down explicitly by a Dirac mass term for the quarks or spontaneously by a dynamical formation of a chiral condensate $\langle q\bar{q}\rangle$. In this case the remaining symmetry is given by the compact symplectic group $Sp(N_f)$[6] [71]. The coset $SU(2N_f)/Sp(N_f)$ has dimension $N_f(2N_f-1)-1$ and we expect as many (pseudo-)Goldstone bosons in the spectrum of the theory. With both, $m_q > 0$ and $\mu > 0$, one is left with the usual isospin-like and baryon number symmetries, $SU(N_f)_V \times U(1)_B$. For two-color QCD with two degenerate quark flavors the enlarged flavor symmetry is $SU(4)$ which is spontaneously (explicitly) broken by a chiral condensate (Dirac mass) to $Sp(2)$ resulting in five (pseudo-)Goldstone bosons: the three pions and a scalar diquark/anti-diquark pair. The chiral symmetry breaking pattern is shown in Fig. 2.1

Diquark condensation

Let us start from the vacuum of two-color QCD with two degenerate quark flavors, where a finite Dirac mass breaks the chiral symmetry explicitly. Still, the quarks and anti-quarks belong to the same representation of the gauge group and all pseudo-Goldstone bosons will have the same mass m_π. By dialing up chemical potential the excitation energy of the diquark will decrease like $\omega_d = m_\pi - 2\mu$, the excitation energy of the anti-diquark will increase, while the pion energy will stay unchanged. At a critical $\mu_c = \frac{m_\pi}{2}$ we can excite diquarks essentially for free and a Bose-Einstein condensate of diquarks will form. There is exactly one way to write down a gauge invariant scalar diquark condensate

$$\langle qq\rangle = \langle q^T C\gamma_5 T_2\tau_2 q\rangle \ . \tag{2.35}$$

The formation of the diquark condensate again restricts the remaining chiral symmetry. In the presence of a $\langle qq\rangle$ condensate the remainder of the chiral symmetry is given by $Sp(N_f/2)_V$.

2.3. G_2-QCD

We will now turn our attention to a QCD-like theory, where we replace the gauge group $SU(3)$ by the group G_2. G_2 is the smallest of the exceptional Lie groups in Weyl's classification of classical Lie groups. One particular definition is that G_2 is the automorphism group of the octonions algebra, or equivalently, the subgroup of $SO(7)$ that obeys

$$\begin{aligned} c_{abc} &= c_{def}U_{da}U_{eb}U_{fc} \ , \\ c_{abc} &= \frac{1}{\sqrt{3}}\psi_{abc} \quad a,b,c \in 1,2,3,4,5,6,7 \ , \end{aligned} \tag{2.36}$$

where ψ_{abc} is the totally antisymmetric octonionic tensor defined by [72]

$$\psi_{123} = \psi_{147} = \psi_{165} = \psi_{246} = \psi_{257} = \psi_{354} = \psi_{367} = 1 \ . \tag{2.37}$$

[6] Since the anti-unitary symmetry is different for staggered quarks, we also find a different chiral symmetry breaking pattern. Here, chiral symmetry gets broken down spontaneously to $O(2N_f)$

This amounts to seven non-trivial constraints, reducing the 21 generators of $SO(7)$ to the 14 generators of G_2. G_2 has rank 2 and includes $SU(3)$ as a subgroup

$$G_2/SU(3) \sim SO(7)/SO(6) \sim S_6 \ . \tag{2.38}$$

G_2 has two fundamental representations a 7-dimensional and a 14-dimensional, they carry the Dynkin labels

$$(7) = [1,0] \ , \quad (14) = [0,1] \ , \tag{2.39}$$

The 14-dimensional fundamental representation is also the adjoint representation which is an unfamiliar feature coming from SU(N) gauge theories. G_2 gauge theory was first investigated by Pepe and Wiese [50] and was introduced to clarify the influence of the group-center on deconfinement. It was shown that G_2 Yang-Mills theory exhibits a first order phase transition even though it has a trivial center.

2.3.1. Symmetries of G_2-QCD

There is another feature of G_2 that makes it very interesting to use as a gauge group of a QCD-like theory. As a subgroup of $SO(7)$, G_2 is real, i.e. all representations of G_2 are real and there is a trivial isometry between the generators of a given representation and its complex conjugate, leading to an anti-unitary symmetry for the Dirac operator $[A, D] = 0$ with $A^2 = -1$. That implies $\beta = 4$ for the Dirac operator and there is no sign problem. The reality of G_2 also has important consequences on the fermion content of the theory. Let us start this discussion with the G_2-QCD action with N_f quark flavors in the continuum

$$S = \int d^4x \left(-\frac{1}{4} F_{\mu\nu} F^{\mu\nu} + \bar{\psi}^i (i\gamma_\mu D^\mu - m)\psi^i \right) \ , \tag{2.40}$$

where summation over the flavor index $i = 1, \ldots, N_f$ is implied and color indices are suppressed. The matter part of the Lagrangian transforms under charge conjugation (up to irrelevant boundary terms) as

$$\begin{aligned} \mathcal{L}^C &= \bar{\psi}^C (i\gamma_\mu(\partial_\mu - gA_\mu) - m)\psi^C \ , \\ &= \bar{\psi}(i\gamma_\mu(\partial_\mu + gA_\mu^T) - m)\psi \ . \end{aligned} \tag{2.41}$$

$$\tag{2.42}$$

That is, if

$$A_\mu^T = -A_\mu = -A_\mu^a T^a \ , \tag{2.43}$$

then the Lagrangian is invariant under charge conjugation. Since every representation of G_2 is real, eq. (2.43) holds and we can replace the N_f Dirac spinors by $2N_f$ Majorana spinors

$$S = \int d^4x \left(-\frac{1}{4} F_{\mu\nu} F^{\mu\nu} + \bar{\lambda}^i (i\gamma_\mu D^\mu - m)\lambda^i \right) \ , \tag{2.44}$$

with $\lambda^C = C\bar{\lambda}^T$. The connection between the Majorana and Dirac spinors is given by $\lambda = (\chi, \eta)$ and $\psi = \chi + i\eta$.

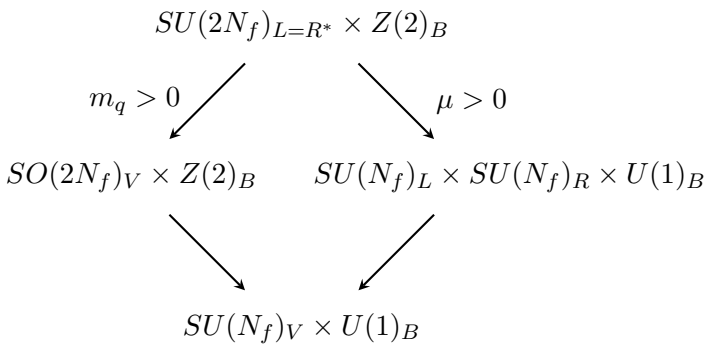

Figure 2.2.: Patterns of chiral symmetry breaking in G_2-QCD.

Now, what is the chiral symmetry and the breaking patterns of G_2-QCD? Eq. (2.44) suggest a $U(2N_f)$ symmetry. This is broken down by the axial anomaly to $SU(2N_f)_{L=R^*} \times Z(2)_B$, which looks unfamiliar because we consider Majorana fermions. Because of the Majorana condition, we are not free to transform the left- and right-handed components independently. In fact, the Majorana condition requires $L = R^*$ [73]. In the same way the $U(1)_B = U(1)_{L=R}$ is reduced to $U(1)_B = U(1)_{L=R=R^*} = Z(2)_B$. As we cannot distinguish between quarks and anti-quarks, the $U(1)_B$ baryon number symmetry is reduced to $Z(2)_B$ that distinguishes between states with even and odd numbers of quarks. As in ordinary QCD, the introduction of a finite Dirac mass or a chiral condensate breaks the axial part of the $SU(2N_f)_{L=R^*} \times Z(2)_B$ and we are left with the vector part of the symmetry $SU(2N_f)_{L=R=R^*} \times Z(2)_B = SO(2N_f)_{L=R} \times Z(2)_B$, leading to $4N_f^2 - 1 - N_f(2N_f - 1) = N_f(2N_f + 1) - 1$ Goldstone bosons. Already for $N_f = 1$ we will find (pseudo-)Goldstone bosons in our spectrum: a scalar and a pseudo-scalar diquark

$$
\begin{aligned}
d(0^+) &= \bar{\chi}\gamma_5\eta = \bar{\psi}^C\gamma_5\psi - \bar{\psi}\gamma_5\psi^C \\
d(0^-) &= \frac{1}{\sqrt{2}}(\bar{\chi}\gamma_5\chi - \bar{\eta}\gamma_5\eta) = \bar{\psi}^C\gamma_5\psi + \bar{\psi}\gamma_5\psi^C \ .
\end{aligned}
$$

The introduction of chemical potential corresponds to an off-diagonal term in the Lagrangian with Majorana fields

$$
\bar{\psi}(i\not{D} - m + i\gamma_0\mu)\psi = \left(\bar{\chi}, \bar{\eta}\right) \begin{pmatrix} i\not{D} - m & i\gamma_0\mu \\ -i\gamma_0\mu & i\not{D} - m \end{pmatrix} \begin{pmatrix} \chi \\ \eta \end{pmatrix} \ , \tag{2.45}
$$

violating the Majorana decomposition and we are left with the usual $SU(N_f)_L \times SU(N_f)_R \times U(1)_B$. The chiral symmetry breaking pattern is summarized in Fig. 2.2.
Now let us analyze the expected colorless spectrum of the theory by decomposing the

tensor products of the fundamental representations

$$\begin{aligned}
(7) \otimes (7) &= (1) \oplus (7) \oplus (14) \oplus (27) \\
(7) \otimes (7) \otimes (7) &= (1) \oplus 4 \cdot (7) \oplus 2 \cdot (14) \oplus 3 \cdot (27) \oplus \dots \, , \\
(14) \otimes (14) &= (1) \oplus (14) \oplus (27) \oplus \dots \, , \\
(14) \otimes (14) \otimes (14) &= (1) \oplus (7) \oplus 5 \cdot (14) \oplus \dots \, , \\
(7) \otimes (14) \otimes (14) \otimes (14) &= (1) \dots \, .
\end{aligned} \tag{2.46}$$

We find a rich spectrum containing glueballs, mesons and baryons. From the first two lines in (2.46) we can conclude that the spectrum of G_2 contains two kinds of baryons: bosonic diquarks as in two-color QCD and fermionic three-quark states as in QCD. We already saw that the scalar diquarks are Goldstone modes of the theory. In contrast to other QCD-like theories with matter in the fundamental representation, we can also find hybrid states that consist of quarks and gluons. The existence of those lead to string breaking already in G_2 Yang-Mills theory.
Since there is no sign problem in G_2-QCD, Lattice Monte-Carlo techniques allows us to explore the phase diagram of a QCD-like theory with fermionic baryons from first principles, i.e. the investigation of a nuclear liquid-gas transition, that is also present in QCD, or the search for a critical point in the phase digram without the need of effective models.

2.4. Effective Polyakov-Loop Theories

In this work we will make extensive use of effective theories for QCD-like theories that use the so called Polyakov loops as degrees of freedom. Let us first discuss the role of the Polyakov loop in the case of pure gauge theory. The Polyakov loop is defined as

$$L(\vec{x}) = \mathrm{tr} \prod_{t=1}^{t=N_t} U_0(\vec{x}, t) \, . \tag{2.47}$$

It thus is the trace of a loop holonomy of gauge links that winds around the lattice in the compact, periodic time direction. Under a global center transformation $U_0(\vec{x}, t_0) \to zU_0(\vec{x}, t_0)$ the Polyakov loop transforms according to

$$L(\vec{x}) \to zL(\vec{x}) \, . \tag{2.48}$$

Therefore, the Polyakov loop acts as an order parameter for the spontaneous breaking of center symmetry. One also finds that the expectation value of the Polyakov loop probes the screening properties of a static color test charge. In particular the difference in the free energy $F_q(T)$ of a gauge theory with and without a single color test charge is

$$e^{-F_q(T)/T} \propto |\langle L \rangle| \, . \tag{2.49}$$

Thus the Polyakov loop also acts as an order parameter for confinement. When the vacuum is center symmetric we have $|\langle L \rangle| = 0$ and the free energy for putting a single

quark into the system is infinite. When center symmetry is spontaneously broken we have $|\langle L \rangle| > 0$ and the free energy of a single quark in the systems becomes finite.
Now we know that the Polyakov loop is an order parameter for the deconfinement phase transition in the pure gauge theory. That alone already justifies a phenomenological model with the Polyakov loop as the degree of freedom in a Ginzburg-Landau theory for the deconfinement phase transition. Note, that this is a phenomenological argument that is only valid on mean-field level. However, the Svetitsky-Yaffe conjecture [74] states that if one integrates out all spatial links in a d+1 dimensional SU(N) gauge theory, one ends up with a d dimensional SU(N) Polyakov-loop theory with only short-range interactions. If the phase transition of the original gauge theory is of 2nd order, the Polyakov-loop theory and the underlying d+1 dimensional gauge theory belong to the same universality class and we can compute the order of the finite temperature confinement-deconfinement phase transition and the critical exponents with the effective Polyakov-loop theory which is easier to handle numerically. Even though the arguments by Svetitsky and Yaffe are only conjectures, there is reasonable evidence for these conjectures to be true. High precision analysis of 3+1 dimensional SU(2) gauge theory shows that it belongs to the 3d Ising universality class [75] according to the Svetitsky-Yaffe conjecture. Also data for SU(2) and SU(3) gauge theory in 2+1 dimensions shows that these gauge theories belong to the same universality classes as the according spin models [76].
Now, strictly speaking the universality arguments of Svetitsky and Yaffe are only valid for theories with a 2nd order phase transition where the correlation length of the system ξ diverges. SU(3) Yang-Mills theory in 3+1 dimensions shows a weak 1st order confinement-deconfinement phase transition. Thus, an effective Polyakov-loop theory can only provide an effective description of the phase transition because the correlation length ξ is finite and the differences in the microscopic physics will show up at some scale. Nevertheless there are many efforts to explore SU(3) gauge theories by the means of effective SU(3) or Z_3 spin models in the literature [77–79].
In the past effective Polyakov loop models were popular to determine properties like e.g. the order of the phase transition of the underlying d+1 dimensional gauge theory via the Svetitsky-Yaffe conjecture. When it became numerically feasible to simulate the full theory people lost interest in effective Polyakov-loop theories. The most important reason for that might be, that QCD in not only pure SU(3) gauge theory but there are also dynamical fermions. These dynamical fermions break center symmetry explicitly. Therefore, in QCD and QCD-like theories with fundamental fermions we do not have a real phase transition but a smooth cross-over between the confined and the deconfined phase. Since there is no real phase transition if we include dynamical fermions, we can no longer rely on universality arguments. And it is quite unclear how to relate the cross-over deconfinement transition in QCD to the one in an effective Polyakov loop model.
In the last decade effective Polyakov-loop theories had quite a resurgence. Maybe the most important reason for that is the sign problem of QCD at finite chemical potential. There has been a lot of effort to solve the sign problem of QCD, see section 2.1.1, however, all those methods so far work only for theories simpler than QCD. Effective Polyakov-loop theories are one class of theories, where the sign problem at finite chemical potential is solvable by e.g. the complex Langevin method. Therefore, they are an

important testing ground for the algorithms. Further, as Polyakov-loop theories are still effective theories for QCD, one can hope that we might be able to extract information about the properties of QCD at finite density.
Now let us take a look at how to actually derive an effective Polyakov-loop theory. In general the effective action for the Polyakov-loop theory is defined by

$$\exp(-S_{\text{eff}}[L]) = \int \mathcal{D}U \delta(L - L[U]) \exp(-S[U]) \; . \tag{2.50}$$

The only task we have to do is to evaluate the integral. However for most theories this is a quite indomitable task. The good thing is, that we know the basic form of the effective action just from symmetry arguments

$$\begin{aligned} S_{\text{eff}} = &\sum_{\vec{x}\vec{y}} L_{\vec{x}} K^{(2)}(\vec{x},\vec{y}) L^{\dagger}_{\vec{y}} + \sum_{\vec{w}\vec{x}\vec{y}\vec{z}} L_{\vec{w}} L_{\vec{x}} K^{(4)}(\vec{w},\vec{x},\vec{y},\vec{z}) L^{\dagger}_{\vec{y}} L^{\dagger}_{\vec{z}} + \dots \\ &+ \sum_{\vec{x}} \left(h^{(1)} L_{\vec{x}} + h^{(1)} L^{\dagger}_{\vec{x}} \right) + \dots \; . \end{aligned} \tag{2.51}$$

The first terms contain only even numbers of Polyakov loops and respect center symmetry. Their origin lies in the Yang-Mills part of the underlying QCD-like theory. The latter terms contain odd numbers of Polyakov loops and break center symmetry explicitly. Those terms originate in the fermonic part of the action[7]. Note that eq. (2.51) contains infinitely many terms. Not only with arbitrary numbers of Polyakov loops in the fundamental representation of the gauge group but also with loops in the adjoint or even higher representations [80][43].
Now we know the general form of the effective action. What we now need to do is to determine the form of the kernels $K^{(2n)}$, they will in general depend on the lattice coupling β, the temperature T and the fermion mass m[8], and the form of the center-breaking couplings $h^{(n)}$, they will also depend on β, T and m. There are several methods how to determine the effective kernels and couplings. One method is to find the effective kernels $K^{(2n)}$ via inverse Monte-Carlo calculations [81] [43]. Here one generates an ensemble of gauge configurations with the underlying gauge theory. One uses these configurations to calculate the expectation values of an appropriate set of operators $\langle X \rangle$. Now one can look at the Dyson-Schwinger equations for the effective theory. They will depend on the kernels $K^{(2n)}$ and some coefficients. It turns out that those coefficients are given by the expectation values of our set of operators $\langle X \rangle$ that we have computed by Monte-Carlo simulations. So now one has a set of equations for the kernels or respectively for the effective couplings of the effective Polyakov-loop theory.
Another way to compute the effective kernels and couplings is the relative weights

[7] The fermionic part will also generate terms that contain even numbers of Polyakov loops. Those terms respect center symmetry. However, all terms that do not respect center symmetry will come from the fermionic part not from the Yang-Mills part of the action

[8] Since the terms containing the kernels $K^{(2n)}$ originate in the Yang-Mills part of the action we would not expect the kernels to depend on the fermion mass. However we will see later, that non-winding fermion loops can be absorbed in the Yang-Mills action and thus lead to mass depended corrections of the lattice coupling β

method [44, 82, 83]. Here one uses a slight modification of a standard Monte-Carlo algorithm for the full gauge theory. The algorithm is chosen such that the configurations of the untraced Polykov loop is fixed. This is done for some set of different Polyakov loop configurations. This way, one can calculate derivatives of the effective Polyakov loop action in the configuration space of our effective theory. When one uses an ansatz for the spatial distribution of the values of the Polyakov loop one can use the derivatives of the effective action to construct the effective kernels and couplings of the effective theory.
The methods described above have been applied very successfully, e.g. Polyakov loop correlators computed by an effective theory via the relative weights method match the correlators from the full gauge theory perfectly well over a large range of values for β even in the deconfined phase [44]. However, all methods described above need somewhat heuristic truncations and ansatzes for the effective action. Further, so far none of those methods were able to include dynamical fermions in the effective theory. Thus we will take a different approach to derive our effective action from the full QCD-like theory. The method we will use relies on a combined strong coupling and hopping expansion and was developed by Langelage, Philipsen et al.[40–42, 84]. In this way we are able to derive the effective action for the Polyakov-loop theory from the underlying gauge theory in a systematic way and we are in principle able to improve the effective action order by order. In the following sections we will see how to derive the effective action from the full QCD-like theory. We will start with Yang-Mills theory and later we will see how to add dynamical fermions to the theory.

2.4.1. Yang-Mills Theory

Consider the partition function of the non-Abelian gauge field action

$$Z = \int [dU_0][dU_i] \exp\left[\frac{\beta}{2N_c}\sum_p (\operatorname{tr} U_p + \operatorname{tr} U_p^\dagger)\right] , \quad \beta = \frac{2N}{g^2} . \tag{2.52}$$

In order to arrive at an effective Polyakov-loop theory we integrate out the spatial degrees of freedom of the gauge fields.

$$\begin{aligned} Z &= \int [dU_0] \exp[-S_{eff}] , \\ -S_{eff} &= \ln \int [dU_i] \exp\left[\frac{\beta}{2N_c}\sum_p (\operatorname{tr} U_p + \operatorname{tr} U_p^\dagger)\right] , \\ &\equiv + \lambda_1 S_1 + \lambda_2 S_2 + \dots . \end{aligned} \tag{2.53}$$

The effective couplings $\lambda_n = \lambda_n(\beta, N_t)$ are arranged in increasing order in β, thus the λ_n get neglectable the higher n is. Using the character expansion of the gauge group (details of group representations and character analysis may be found in appendix A),

we can write the effective action in (2.53) as

$$-S_{eff} = \ln \int [dU_i] \prod_p \left[1 + \sum_{j \neq 0} d_j a_j(\beta) \chi_j(U_p) \right] . \tag{2.54}$$

The sum goes over all irreducible representations with dimension d_j and character χ_j. Since we are interested in expectation values rather than the free energy, we dropped a constant factor (depending only on β and the lattice volume. See also [61]). For the gauge group SU(2) the explicit expressions of the expansion coefficients $a_j(\beta)$ are given by

$$a_j(\beta) = \frac{I_{2j+1}(\beta)}{I_1(\beta)} = \frac{\beta^{2j}}{2^{2j}(2j+1)!} + O(\beta^{2j+2}) , \tag{2.55}$$

Where the I_n are modified Bessel functions. For more complicated gauge groups, e.g. SU(3) the $a_j(\beta)$ cannot be written down in a closed form, see appendix A.2. If one expands the product in eq. (2.54) one generates terms that contain products of plaquettes in different, non-trivial representations

$$d_{r_{p_1}} a_{r_{p_1}} \chi_{r_{p_1}}(U_{p_1}) \cdot d_{r_{p_2}} a_{r_{p_2}} \chi_{r_{p_2}}(U_{p_2}) \cdots . \tag{2.56}$$

Plaquettes that do not appear in a particular term are in the trivial representation. Now we can think of term like the one in eq. (2.56) as a graph. In general an arbitrary graph will consist of disjoint pieces. We can decompose every such graph into connected pieces, those are called Polymers X. The contribution of such a Polymer to the effective action, after integrating out the spatial degrees of freedom, is called the activity Φ of the Polymer. In the following we will restrict ourselves to plaquettes in the fundamental representation, since higher dimensional representations contribute to a higher order in β. For simplicity we will call $a_{1/2} = u$. By using the the moment-cumulant formalism and cluster expansion one can show that the contributions to the effective action are given by the activities of clusters C which consist of a connected set of Polymers [61, 85]. The effective action then reads

$$-S_{\text{eff}} = \sum_{C=(X_l^{n_l})} a(C) \prod_l \Phi(X_l; W_j)^{n_l} , \tag{2.57}$$

$$\Phi(X_l; W_j) = \int [dU_i] \prod_{p \in X_l} d_{r_p} a_{r_p} \chi_{r_p}(U_p) .$$

The combinatorial factor $a(C)$ depends on how the polymers X_l are connected in the cluster, and is one for a single polymer [61]. Since we only integrate over spatial degrees of freedom the activities Φ still depend on the Polyakov line variables W_j. To work out, which kinds of Polymers X_l do contribute to the cluster expansion and to calculate their activities $\Phi(X_l)$ we need to perform group integrals of the type

$$\int dU \chi_{r_1}(V_1 U) \cdot \ldots \cdot \chi_{r_n}(V_n U) . \tag{2.58}$$

In principle one needs to calculate the Clebsch-Gordan decomposition of the product in the equation above. If the resulting decomposition does not contain the trivial representation the integral vanishes (for more details see appendix A.3), since:

$$\int dU \chi_r(U) = \delta_{r,0} \ . \tag{2.59}$$

Important consequences are:

1. contributing Polymers do not have spatial boundaries. If they had a spatial boundary we would have at least one link, where we had an integral of the form:

$$\int dU \chi_r(V_1 U)\chi_0(V_2 U^\dagger) = 0 \ , \tag{2.60}$$

   since any plaquette that is not part of the Polymer is regarded as a plaquette in the trivial representation. The integral vanishes, because the Clebsch-Gordan decomposition between any non-trivial and the trivial representation does not contain the trivial representation.

2. if precisely two plaquettes with representations r and r' meet in a link, we must have $r = r'$ or $r^* = r'$ depending on the plaquettes' orientations:

$$\int dU \chi_r(V_1 U)\chi_{r'}(V_2 U^\dagger) = \delta_{r,r'} \frac{1}{d_r} \chi_r(V_1 V_2) \ . \tag{2.61}$$

Leading Order Effective Action

Up to now, our discussion about the derivation of the effective action was completely general. We now specialize on the case of the gauge group SU(2), since the specific form of the effective action depends on the properties of the particular gauge group. Later on we will also show how the effective action for the gauge group G_2 will look like. Following the rules of the strong coupling expansion, and integrating over the U_i we can easily see, that the only graphs yielding a non-constant contribution are those, that close around the lattice in time direction. Graphs, that do not wind around the time direction of the lattice only produce constant terms which drop out in expectation values. The first graph with a non-trivial contribution thus is a chain of time-like plaquettes winding around the torus in time direction (Figure 2.3). The contribution from this graph is given by

$$\lambda_1 S_1 = u^{N_t} \sum_{<\vec{x}\vec{y}>} L_{\vec{x}} L_{\vec{y}} \ , \tag{2.62}$$

where the summation is over nearest neighbors. To get to this result one has to successively apply (2.61). The last step is the integration of the link at the edge of the lattice, one can use [58]:

$$\int dU U^{(r)}_{ab} (U^\dagger)^{(r)}_{cd} = \frac{1}{d_r} \delta_{a,d} \delta_{b,c} \ , \tag{2.63}$$

where $U^{(r)}$ is an SU(2) element in the representation r. Improvement of λ_1 by including graphs with decorations is a non-trivial procedure explained in the next section.

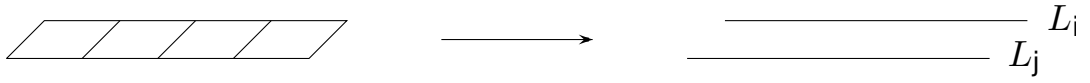

Figure 2.3.: First graph with a nontrivial contribution after spatial integration for a lattice with temporal extent $N_t = 4$. Four plaquettes in the fundamental representation lead to an interaction term involving two adjacent fundamental Polyakov loops $L_{\vec{x}}$ and $L_{\vec{y}}$.

Corrections From Decorations

At leading order we found $\lambda_1 = u^{N_t}$. However there are contributing clusters that are topologically equivalent to the leading order result, i.e. those contributions will lead to the same effective action but with additional plaquettes that will lead to a higher order in u. Clusters resulting in corrections to λ_1 will consist of one large polymer Ξ winding around the time direction of the lattice and some additional polymers X_i attached to Ξ. Clusters consisting of several large polymers lead to corrections of order β^{N_t} and will be neglected. Large polymers Ξ are constructed from the leading order diagram by adding some decorations to it. One can calculate the corrections to the LO effective action or respectively the LO λ_1 by taking the leading order diagram Ξ_0 and cutting out a connected set of plaquettes. Now take a rigid configuration of plaquettes as decoration and plug it into the hole, such that a new admissible large polymer Ξ originates [85]. The other polymers X_i of the cluster C are directly attached to Ξ. In

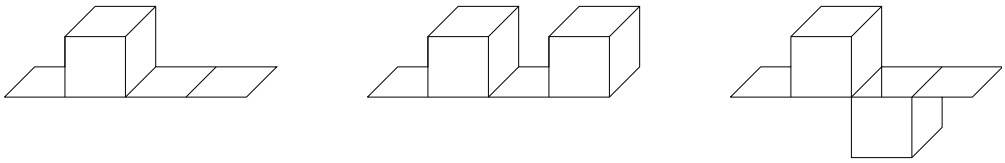

Figure 2.4.: Some polymers with decorations

order to examine, how these new clusters contribute, we shall perform a second moment-cumulant transformation. For this purpose we define two new types of polymers. We call a polymer of type X, if it is connected to Ξ and does not touch any decorations. Polymers of type Y are decorations with or without other polymers attached to them. Now the cluster C under consideration may be viewed at as composed of polymers X_i and Y_i touching a band of plaquettes Ξ_0. The product of all activities in C can be expressed as

$$\Phi(\Xi_0)\prod_i \Phi(X_i)\prod_k \Phi(Y_k)\ , \qquad \Phi(\Xi_0) = u^{N_t} L_i L_j\ , \tag{2.64}$$

with well-defined activities $\Phi(Y_k)$. As with a usual cluster expansion we write:

$$\lambda_1 S_1 = S_1 u^{N_t} \left\{ 1 + \sum_{m>0} \sum_{W_1,...,W_m} \frac{1}{m!} \langle W_1, ..., W_m \rangle \prod_i^m \Phi(W_i) \right\} , \tag{2.65}$$

where W_i is any polymer of type X or Y. The moment function $\langle W_1, ..., W_m \rangle$ is zero unless the W_i form an admissible cluster, in which case it is defined as the normal moment function (see [61]). Now the moment-cumulant transformation yields:

$$\begin{aligned} \ln(\lambda_1 S_1) =& \ln\left(u^{N_t} S_1\right) + \sum_{(W_1^{n_1},...,W_k^{n_k})} [W_1^{n_1}, ..., W_k^{n_k}] \prod_i \frac{1}{n_i!} \Phi(W_i)^{n_i} , \\ \Rightarrow \lambda_1 S_1 =& u^{N_t} S_1 \exp\left\{ \sum_{(W_1^{n_1},...,W_k^{n_k})} [W_1^{n_1}, ..., W_k^{n_k}] \prod_i \frac{1}{n_i!} \Phi(W_i)^{n_i} \right\} . \end{aligned} \tag{2.66}$$

The cumulant function [ ] has the property that it is zero unless the W_i form a connected set. A rigid object of W_i's is called a supercluster. Because of translation invariance along the band Ξ_0 the contribution of each supercluster is multiplied by N_t. Fig. 2.4 shows the most basic decorations and table 2.1 lists all decorations and additional polymers leading to corrections up to order u^8.

i	W_i	Φ	l
1	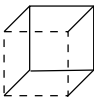	u^4	4
2	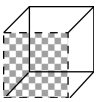	$3u^4v$	4
3	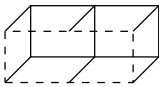	u^6	4
4	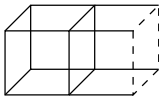	u^8	4
5	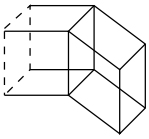	u^8	8
6	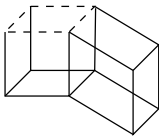	u^8	32
7	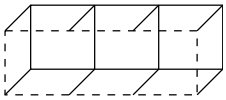	u^8	4
8	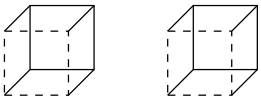	u^8	-12
9	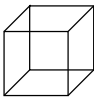	$4u^6$	4

Table 2.1.: All decorations of the LO-order graphs resulting in corrections up to order $\mathcal{O}(u^8)$.

l is the multiplicity of a particular representation, it counts how often a diagram appears per N_t. As an example take the multiplicity of W_8: Put two cubes on the original band of plaquettes. The cubes may not overlap. The number of possible arrangements is: $\frac{1}{2!}4N_t(N_t-3)+\frac{1}{2!}4N_t3(N_t-1)$. The term proportional to N_t is $l=-12$. Now what about the terms proportional to N_t^2? The terms proportional tu N_t^2 have already been counted by exponentiating W_1. So if we would include them again this would lead to over-counting of terms in higher orders of the series expansion of the exponential.

The correction W_9 is actually a cluster consisting of a cube and the LO diagram, having one plaquette in common. Therefore we get a combinatoric factor $a(C) = -1$, when adding this correction.
Further in W_2 the gray plaquette is a plaquette in the adjoint representation leading to the factor $v = a_1(\beta)$. We can use the following relation to get the right order in u of the correction:

$$v = \frac{2}{3}u^2 + \frac{2}{9}u^4 + \frac{16}{135}u^6 + ... \tag{2.67}$$

This is enough to calculate the corrections of Langelage et al. [42, 86]:

$$\begin{aligned}
\lambda_1(u,2) &= u^2 \exp\left[2\left(4u^4 - 8u^6 + \frac{134}{3}u^8 - \frac{49044}{405}u^{10}\right)\right] , \\
\lambda_1(u,3) &= u^3 \exp\left[3\left(4u^4 - 4u^6 + \frac{128}{3}u^8 - \frac{36044}{405}u^{10} + \frac{751744}{405}u^{12}\right)\right] , \\
\lambda_1(u,4) &= u^4 \exp\left[4\left(4u^4 - 4u^6 + \frac{140}{3}u^8 - \frac{37664}{405}u^{10} + \frac{3541576}{1215}u^{12}\right)\right] , \\
\lambda_1(u,N_t \geq 5) &= u^{N_t} \exp\left[N_t\left(4u^4 - 4u^6 + \frac{140}{3}u^8 - \frac{36044}{405}u^{10} + \frac{863524}{1215}u^{12}\right)\right] .
\end{aligned} \tag{2.68}$$

Higher Order Terms

There also occur terms of higher order in u that lead to a different form of the effective action, e.g. terms with a larger number of Polyakov loops involved, or an interaction of loops with distance greater than one, and loops in higher dimensional representations. The simplest higher order corrections come from Polyakov loops winding several times around the lattice. It is an easy task to sum up their contributions:

$$\sum_{<\vec{x}\vec{y}>}\left(\lambda_1 L_{\vec{x}} L_{\vec{y}} - \frac{1}{2}(\lambda_1 L_{\vec{x}} L_{\vec{y}})^2 + \frac{1}{3}(\lambda_1 L_{\vec{x}} L_{\vec{y}})^3 - ...\right) = \sum_{<\vec{x}\vec{y}>} \ln(1 + \lambda_1 L_{\vec{x}} L_{\vec{y}}) . \tag{2.69}$$

The coefficients of this series are given by the combinatorial factors $a(C)$ from (2.57). Now consider corrections coming from Polyakov loops with distance greater than one. The leading non-zero contribution comes from an L-shaped graph with a decoration of two additional plaquettes (Figure 2.5). It is given by

$$\lambda_2 S_2 = N_t(N_t - 1)u^{Nt+2} \sum_{[\vec{x}\vec{y}]} L_{\vec{x}} L_{\vec{y}} , \tag{2.70}$$

and we have to sum over all loops with a distance of $\sqrt{2}a$. Calculations by Langelage et al. [42] have shown that it is sufficient to use an effective action where we include resummation of loops winding around the lattice several times but without terms like $\lambda_2 S_2$. The partition function of our effective theory is then given by

$$Z = \int [dU_0] \prod_{<\vec{x}\vec{y}>} \left[1 + \lambda_1 L_{\vec{x}} L_{\vec{y}}\right] . \tag{2.71}$$

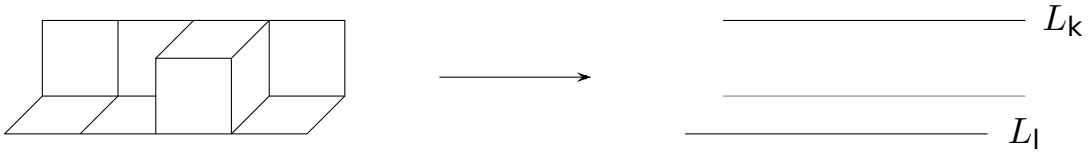

Figure 2.5.: Graph leading to a contribution with two fundamental Polyakov loops with distance $\sqrt{2}a$.

2.4.2. Heavy Fermions and Hopping Expansion

So far we only looked at SU(2) Yang-Mills theory but of course we also want to include dynamical fermions into the effective theory. We can include them by using the Hopping expansion of the quark determinant. Since the hopping expansion is an expansion for heavy quarks we will be limited to the case of fairly heavy quarks. It remains to be seen, if it is possible to use the hopping expansion to some very high order in the hopping parameter κ to get somewhat close to the physical masses of the up and down quark. In this study we use Wilson quarks where the Dirac operator reads

$$D = 1 - \kappa H \qquad with \qquad \kappa = \frac{1}{(2am + 4)} \tag{2.72}$$

$$H(x,y)_{\alpha\beta,ab} = \sum_{\mu=\pm1}^{\pm4} (1-\gamma_\mu)_{\alpha\beta} U_\mu(x)_{ab} \delta_{x+\hat{\mu},y} \ . \tag{2.73}$$

The term H collects all nearest neighbor terms and is therefore called Hopping matrix. If one considers heavy quarks the hopping parameter κ is small and we can expand the fermion determinant in orders of κ.

$$\begin{aligned} \det[D] &= \det[1-\kappa H] = \exp(\mathrm{tr}\,[\ln(1-\kappa H)]) \ , \\ &= \exp(-\sum_{i=1}^{\infty} \frac{1}{i} \kappa^i \mathrm{tr}\,[H^i]) \ . \end{aligned} \tag{2.74}$$

Here we used a well-known relation for the Determinant and expanded the logarithm in a power series in κ. Using the explicit form of the Hopping matrix one arrives at

$$\begin{aligned} \mathrm{tr}\,[H^i] = \sum_{x_1,\mu_1,\ldots,x_i,\mu_i} & \delta_{x_2,x_1+\hat{\mu}_1} \ldots \delta_{x_l,x_{l-1}+\hat{\mu}_{l-1}} \delta_{x_1,x_l+\hat{\mu}_l} \\ & \mathrm{tr}_C[U_{\mu_1}(x_1) U_{\mu_2}(x_2) \ldots U_{\mu_i}(x_i)] \mathrm{tr}_D[(1-\gamma_{\mu_1})(1-\gamma_{\mu_2})\ldots(1-\gamma_{\mu_i})] \ . \end{aligned} \tag{2.75}$$

One can easily see, that the delta functions force the arising terms to be closed loops. Loops that close around the time direction are not invariant under a center transformation. At finite temperature there are also graphs winding several times around the lattice, like the generalized Polyakov loop

$$\mathrm{tr}\, W^n(\vec{x}) = \mathrm{tr} \left(\prod_{t=0}^{N_t-1} U_0(\vec{x},t) \right)^n \ , \qquad n \in N \ . \tag{2.76}$$

We obtain the effective action from the full partition function in a way similar to pure gauge theory. First, use the hopping expansion to get a representation of fermion determinant as in (2.74). If one has the determinant in this form one can again use a cluster expansion

$$\begin{aligned} Z &= \int [dU_0][dU_i] \exp[-S_g] \det[D] = \int [dU_0] \exp[-S_{\text{eff}}] \ , \\ -S_{\text{eff}} &= \ln \int [dU_i] \exp[-S_g] \det[D] \ . \end{aligned} \tag{2.77}$$

Again similar to the cluster expansion of the pure gauge theory only graphs winding around the temporal direction of the lattice contribute to the effective action. Therefore the leading order contributions from the fermion determinant are terms containing Polyakov loops

$$-\sum_{\vec{x}} \left[(2\kappa e^{a\mu})^{N_t} L(\vec{x}) + (2\kappa e^{-a\mu})^{N_t} L(\vec{x}) \right] \ , \tag{2.78}$$

with

$$h = (2\kappa e^{a\mu})^{N_t} \ , \bar{h} = (2\kappa e^{-a\mu})^{N_t} \ . \tag{2.79}$$

The first term is a contribution from loops winding around the lattice in positive time direction while the second term comes from loops oriented in negative temporal direction. For SU(2) the only difference in those terms are the effective couplings h and $\bar{h}$ which differ in the case of non-vanishing chemical potential μ. The overall minus sign is due to the anti-periodic boundary conditions for fermions. It now is possible to sum up all generalized Polyakov loops oriented in the same direction, particularly for positive temporal direction

$$\exp\left[-2 \sum_{\vec{x}} \sum_{n=1}^{\infty} \left(\frac{(-1)^n}{n} h \, \text{tr}\,(W_{\vec{x}}^n) \right) \right] = \prod_{\vec{x}} \det\left[1 + h W_{\vec{x}}\right]^2 \ . \tag{2.80}$$

The partition function for the effective theory to leading order in strong coupling and hopping expansion reads

$$Z = \int [dU_0] \prod_{<\vec{x}\vec{y}>} \left[1 + \lambda_1 L_{\vec{x}} L_{\vec{y}}\right] \prod_{\vec{x}} \det\left[(1 + h W_{\vec{x}})(1 + \bar{h} W_{\vec{x}}^{\dagger}) \right]^2 \ . \tag{2.81}$$

We can simplify the result even more by using a simple rule for the determinant in SU(2)

$$\det[1 + CW] = 1 + C \text{tr}\,[W] + C^2 \ . \tag{2.82}$$

By changing the integration measure

$$\int \left[\prod_{t=1}^{N_t - 1} dU_0(\vec{x}, t) \right] = \int dW_{\vec{x}} = \int_{-2}^{+2} dL_{\vec{x}} \, e^{V_{\vec{x}}} \ , \ V_{\vec{x}} = \frac{1}{2} \ln(4 - L_{\vec{x}}^2) \ ,$$

our result for the partition function reads

$$Z = \int \left(\prod_{\vec{x}} dL_{\vec{x}} \; e^{V_{\vec{x}}} X_{\vec{x}}(h, \bar{h}) \right) \prod_{<\vec{x}\vec{y}>} \left[1 + \lambda_1 L_{\vec{x}} L_{\vec{y}} \right] \; , \tag{2.83}$$

and

$$X_{\vec{x}}(h, \bar{h}) = [(1 + hL_{\vec{x}} + h^2)(1 + \bar{h}L_{\vec{x}} + \bar{h}^2)]^2 \; . \tag{2.84}$$

With this result we have a dimensionally reduced effective theory that includes dynamical fermions with only SU(2) Polyakov loops as degrees of freedom.

2.4.3. Corrections to the Effective Fermion Coupling

Like in the case of pure gauge theory there are corrections to the effective fermion couplings. Those corrections will be the same for h and $\bar{h}$ since the two only differ by the sign of the chemical potential. Corrections to leading order in κ are coming from graphs that also contain spatial link variables that are integrated out. The first correction is the plaquette term with $\mathcal{O}(\kappa^4)$. Since this graph does not wind around the lattice it will not yield a correction of h but a correction in the gauge term leading to a shift in β an thus a κ dependence of u

$$\beta \to \beta + 48\kappa^4 \qquad \Rightarrow \qquad u(\beta) \to u(\beta, \kappa) \; . \tag{2.85}$$

Let us now consider corrections to the effective fermion couplings. Figure 2.6 shows graphs leading to $\mathcal{O}(\kappa^2 u^l)$ corrections after spatial integration. Here we have to include additional plaquettes from the strong coupling expansion of the gauge action, otherwise the integration over the spatial links would vanish. One can sum up all corrections coming from decorations with $1 \leq l \leq N_t - 1$ additional plaquettes

$$(2\kappa e^{a\mu})^{N_t} 6 N_t \kappa^2 \sum_{l=1}^{Nt-1} u^l = (2\kappa e^{a\mu})^{N_t} 6 N_t \kappa^2 \frac{u - u^{N_t}}{1 - u} \; . \tag{2.86}$$

Again, successive decorations lead to exponentiation. Therefore, including all corrections up to $\mathcal{O}(u^n \kappa^m)$, with $n + m = 7$, we obtain

$$\begin{aligned} h(u, \kappa, N_t \geq 4) = (2\kappa e^{a\mu})^{N_t} \exp \Bigg[6 N_t \kappa^2 u \Bigg(& \frac{1 - u^{N_t - 1}}{1 - u} \\ & + 4u^4 - 8\kappa^2 + 9\kappa^2 u + 4\kappa^2 u^2 \Bigg) \Bigg] \; . \end{aligned} \tag{2.87}$$

It is possible to show, that for free quarks in leading order hopping expansion the quark mass, extracted from the pole of the propagator is $am = -\log(2\kappa)$. Therefore we can interpret h as

$$h = \exp\left(\frac{\mu - m}{T} \right) \; , \tag{2.88}$$

Figure 2.6.: Graphs reducing to Polyakov loops after spatial link integration resulting in $\mathcal{O}(\kappa^2 u^l)$corrections, with $1 \leq l \leq N_t - 1$

and the corrections from decorations correspond to corrections to the quark mass

$$am = -\log(2\kappa) - 6N_t\kappa^2 u \left(\frac{1-u^{N_t-1}}{1-u} + 4u^4 - 8\kappa^2 + 9\kappa^2 u + 4\kappa^2 u^2 \right) . \tag{2.89}$$

This form of the effective fermion coupling has an important consequence on the validity of the effective theory. In eq. (2.80) we have resummed all multiple winding loops to a log. The radius of convergence for this series is $|r| < 1$. As the operator norm of the Polyakov line is $||W|| = 1$, the effective theory is only valid for $h < 1$, or respectively $\mu < m_q$. Let us state that the hopping expansion is convergent for any μ, it is just the resummation of the multiple winding loops that diverges for $\mu \geq m_q$. However we can still use the resummed effective theory for $\mu > m_q$ in the sense of an analytic continuation and we will see that we get resonable results.

2.4.4. Fermions beyond Leading Order

So far, we only considered the so-called static quark determinant with corrections to the effective fermion coupling. To go beyond this approximation, we will define the kinetic quark determinant

$$\begin{aligned} \det[D] &= \det[1 - T^+ - T^- - S^+ - S^-] \, , \\ &= \det[1 - T^+ - T^-] \det[1 - (1-T)^{-1}(S^+ + S^-)] \\ &= \det[D_{\text{stat}}] \det[D_{\text{kin}}] \, , \end{aligned} \tag{2.90}$$

here, $T^\pm$ and $S^\pm$ denote hops in $\pm$ temporal or spatial directions. We already computed $\det[D_{\text{stat}}]$ in our LO analysis. We further split the kinetic determinant into parts describing quarks moving in positive and negative spatial directions, $P = \sum_k P_k$ and $M = \sum_k M_k$. Since the trace in (2.90) is also a trace in coordinate space only closed loops contribute and we need the same number of Ps and Ms.

$$\begin{aligned} \det[D_{\text{kin}}] &= \det[1 - (1-T)^{-1}(S^+ + S^-)] \, , \\ &= \det[1 - P - M] \, , \\ &= \exp[\text{tr } \log(1 - P - M)] \end{aligned} \tag{2.91}$$

To order $\mathcal{O}(\kappa^4)$ we have

$$\begin{aligned} \det[D_{\text{kin}}] &= \exp\left[-\text{tr}\, PM - \text{tr}\, PPMM - \frac{1}{2}\text{tr}\, PMPM \right] [1 + \mathcal{O}(\kappa^6)] \, , \\ &= \left[1 - \text{tr}\, PM - \text{tr}\, PPMM - \frac{1}{2}\text{tr}\, PMPM + \frac{1}{2}(\text{tr}\, PM)^2 \right] [1 + \mathcal{O}(\kappa^6)] \, . \end{aligned} \tag{2.92}$$

Now we need to make the directions of the hops visible. Again, P's and M's need to come in pairs for every direction

$$\sum_{ij} \mathrm{tr}\, P_i M_j = \sum_i \mathrm{tr}\, P_i M_i \ , \tag{2.93}$$

$$\sum_{ijkl} \mathrm{tr}\, P_i P_j M_k M_l = \sum_i \mathrm{tr}\, P_i P_i M_i M_i + \sum_{i\neq j} \mathrm{tr}\, P_i P_j M_i M_j + \sum_{i\neq j} \mathrm{tr}\, P_i P_j M_j M_i \ , \tag{2.94}$$

$$\frac{1}{2}\sum_{ijkl} \mathrm{tr}\, P_i M_j P_k M_l = \frac{1}{2}\sum_i \mathrm{tr}\, P_i M_i P_i M_i + \frac{1}{2}\sum_{i\neq j} \mathrm{tr}\, P_i M_i P_j M_j + \frac{1}{2}\sum_{i\neq j} \mathrm{tr}\, P_i M_j P_i M_j \ , \tag{2.95}$$

$$\frac{1}{2}\sum_{ijkl} \mathrm{tr}\, P_i M_j \mathrm{tr}\, P_k M_l = \frac{1}{2}\sum_{i,j} \mathrm{tr}\, P_i M_i \mathrm{tr}\, P_j M_j \ . \tag{2.96}$$

Now let us shed some more light on the static quark propagator $(1-T)^{-1}$ that appears in equation (2.91). From $(1+\gamma_\mu)(1-\gamma_\mu) = 0$ we can immediately see, that hops in positive and negative time-direction do not mix and we therefore get

$$(D_{\mathrm{stat}})^{-1} = (D^+_{\mathrm{stat}})^{-1} + (D^-_{\mathrm{stat}})^{-1} - 1 \ . \tag{2.97}$$

We can now use a series expansion for the hops in positive time-direction

$$(D^+_{\mathrm{stat}})^{-1} = (1-T^+)^{-1} = \sum_{n=0}^{\infty} (T^+)^n \ . \tag{2.98}$$

We then find

$$(D^+_{\mathrm{stat}})^{-1}_{t_1,t_2} = \delta_{t_1,t_2}(1 - q z^{N_t} W) + q z^{t_2-t_1} W(t_2,t_1)\left[\theta(t_2-t_1) - z^{N_t}\theta(t_1-t_2)\right] \ , \tag{2.99}$$

$$q = \frac{1}{2}(1+\gamma_0)(1+z^{N_t}W)^{-1} \ , \qquad z = 2\kappa e^{a\mu} \ . \tag{2.100}$$

$W(t_2,t_1)$ is a temporal Wilson line and for $t_1 = t_2$ we have a Polyakov line $W(t_1,t_1) = W$. The contribution to the propagator in negative time direction is obtained analogously:

$$(D^-_{\mathrm{stat}})^{-1}_{t_1,t_2} = \delta_{t_1,t_2}(1 - \bar{q}\bar{z}^{N_t} W^\dagger) + \bar{q}\bar{z}^{t_1-t_2} W^\dagger(t_1,t_2)\left[\theta(t_1-t_2) - \bar{z}^{N_t}\theta(t_2-t_1)\right] \ , \tag{2.101}$$

$$\bar{q} = \frac{1}{2}(1+\gamma_0)(1+\bar{z}^{N_t}W^\dagger)^{-1} \ , \qquad \bar{z} = 2\kappa e^{-a\mu} \ . \tag{2.102}$$

It will be convenient, to split the propagator in propagation direction as well as in Dirac space:

$$
\begin{aligned}
(D_{\text{stat}})^{-1} &= A + \gamma_0 B = A^+\gamma_0 B^+ + A^- - \gamma_0 B^- \ , \qquad (2.103)\\
A^+_{xy} &= \frac{1}{2}\left[1 - \frac{hW}{1+hW}\right]\delta_{xy} + \frac{1}{2} z^{t_y - t_x}\frac{W(t_x,t_y)}{1+hW}\left[\theta(t_y-t_x) - h\theta(t_x-t_y)\right]\delta_{\vec{x}\vec{y}} \ ,\\
B^+_{xy} &= -\frac{1}{2}\frac{hW}{1+hW}\delta_{xy} + \frac{1}{2} z^{t_y - t_x}\frac{W(t_x,t_y)}{1+hW}\left[\theta(t_y-t_x) - h\theta(t_x-t_y)\right]\delta_{\vec{x}\vec{y}} \ ,\\
A^-_{xy} &= \frac{1}{2}\left[1 - \frac{\bar{h}W^\dagger}{1+\bar{h}W^\dagger}\right]\delta_{xy} + \frac{1}{2} \bar{z}^{t_x - t_y}\frac{W^\dagger(t_x,t_y)}{1+\bar{h}W^\dagger}\left[\theta(t_x-t_y) - \bar{h}\theta(t_x-t_y)\right]\delta_{\vec{x}\vec{y}} \ ,\\
B^-_{xy} &= -\frac{1}{2}\frac{\bar{h}W^\dagger}{1+\bar{h}W^\dagger} + \frac{1}{2} \bar{z}^{t_x - t_y}\frac{W^\dagger(t_x,t_y)}{1+\bar{h}W^\dagger}\left[\theta(t_x-t_y) - \bar{h}\theta(t_y-t_x)\right]\delta_{\vec{x}\vec{y}} \ .
\end{aligned}
$$

Note, that the coordinates without vector arrows are space-time coordinates, and that we already included corrections from spatial hops by replacing z^{N_t} with h from (2.87). It is very important to realize that this form of the static propagator is also valid for $h < 1$, due to the convergence criterion for the geometric series. We will now collect all the terms, take the trace in Dirac and position space and perform the group integration.

Taking Traces

When we deal with more than one combination of $\operatorname{tr} P_i M_i$, it will also be necessary to explicitly display the spatial coordinates. We will distinguish between terms, coupling two, three or even four spatial coordinates and we will call those term n-point interactions.

Two-Point Interactions

Up to order κ^4 we find three terms involving two-point interactions

$$
e^{-S_{\text{f}}} = \int [dU_k] \left[-\sum_i \operatorname{tr} P_i M_i - \frac{1}{2}\sum_i \operatorname{tr} P_i M_i P_i M_i + \frac{1}{2}\sum_{\vec{x},i} \operatorname{tr} P_{\vec{x},i} M_{\vec{x},i} \operatorname{tr} P_{\vec{x},i} M_{\vec{x},i} \right] \ .
$$

The first contribution is of order κ^2:

$$
\begin{aligned}
-\int [dU_k] \sum_i \operatorname{tr} P_i M_i &= -\sum_i \int [dU_k] \operatorname{tr}\left[D^{-1}_{\text{stat}} S^+_i D^{-1}_{\text{stat}} S^-_i \right] \ , \qquad (2.104)\\
&= -\frac{8\kappa^2}{N_c}\sum_{u,i} \operatorname{tr} B_{u,u} \operatorname{tr} B_{u+i,u+i} \ ,\\
&= -2\frac{\kappa^2 N_t}{N_c}\sum_{\vec{x},i}\left[\left(\operatorname{tr}\frac{hW_{\vec{x}}}{1+hW_{\vec{x}}} - \operatorname{tr}\frac{\bar{h}W^\dagger_{\vec{x}}}{1+\bar{h}W^\dagger_{\vec{x}}} \right)\left(\operatorname{tr}\frac{hW_{\vec{x}+i}}{1+hW_{\vec{x}+i}} - \operatorname{tr}\frac{\bar{h}W^\dagger_{\vec{x}+i}}{1+\bar{h}W^\dagger_{\vec{x}+i}} \right)\right] \ .
\end{aligned}
$$

Group integration was performed using eq. (2.63). This forces the link variables to be at the same position. Therefore the two temporal traces only result in a factor of N_t not

N_t^2. The next contribution to the two-point interaction is of the order κ^4. For this term we will show the derivation of the final result in great detail. The reader should then in principle be able to reproduce the calculations for all other terms:

$$
\begin{aligned}
&-\frac{1}{2}\int [dU_k] \sum_i \mathrm{tr}\, P_i M_i P_i M_i = , \\
&-\frac{1}{2}\sum_i \int [dU_k] \mathrm{tr}\, [D^{-1}_{\mathrm{stat}} S^+ D^{-1}_{\mathrm{stat}} S^- D^{-1}_{\mathrm{stat}} S^+ D^{-1}_{\mathrm{stat}} S^-] \, , \\
&= -\frac{1}{2}\sum_i \int [dU_k] \mathrm{tr}\, \Big[(A+\gamma_0 B)\kappa(1+\gamma_i) U_i (A+\gamma_0 B)\kappa(1-\gamma_i) U_i^\dagger \\
&\qquad\qquad (A+\gamma_0 B)\kappa(1+\gamma_i) U_i (A+\gamma_0 B)\kappa(1-\gamma_i) U_i^\dagger \Big] \, .
\end{aligned}
\tag{2.105}
$$

Now we take a closer look on the trace in Dirac space:

$$
\mathrm{tr}_{\,D}\, [(A+\gamma_0 B)(1+\gamma_i)(A+\gamma_0 B)(1-\gamma_i)(A+\gamma_0 B)(1+\gamma_i)(A+\gamma_0 B)(1-\gamma_i)] \, .
$$

It is easy to see that all terms containing an A will vanish, since for those terms we always have an $(1+\gamma_i)(1-\gamma_i) = 0$. We then find

$$
\begin{aligned}
&\mathrm{tr}_{\,D}\, [\gamma_0 B(1+\gamma_i)\gamma_0 B(1-\gamma_i)\gamma_0 B(1+\gamma_i)\gamma_0 B(1-\gamma_i)] = , \\
&\mathrm{tr}_{\,D}\, [B(1-\gamma_i)B(1-\gamma_i)B(1-\gamma_i)B(1-\gamma_i)] \, , \\
&= \mathrm{tr}_{\,D} [B^4 (1-\gamma_i)^4] = 32 B^4 \, .
\end{aligned}
\tag{2.106}
$$

When we plug this result back into eq. (2.105) we arrive at

$$
\begin{aligned}
&-\frac{1}{2}\int [dU_k] \sum_i \mathrm{tr}\, P_i M_i P_i M_i = , \\
&-16\kappa^4 \sum_{\vec{x},i,t_{[\xi]}} \int [dU_k] B_{ab}(\vec{x}, t_\alpha, t_\beta) U_{bc}(\vec{x}, t_\beta, i) B_{cd}(\vec{x}+i, t_\beta, t_\gamma) U^\dagger_{de}(\vec{x}+i, t_\gamma, i) \\
&\qquad\qquad B_{ef}(\vec{x}, t_\gamma, t_\delta) U_{fg}(\vec{x}, t_\delta, i) B_{gh}(\vec{x}+i, t_\delta, t_\alpha) U^\dagger_{ha}(\vec{x}+i, t_\alpha, i) \, .
\end{aligned}
\tag{2.107}
$$

Here we made all indices and coordinates explicit, latin indices denote color indices. Because of the overall trace we have to have a closed loop in space-time and we have to have a trace in color-space. Now we have to perform the group integral. There are only three combinations of the U's and $U^\dagger$'s where the group integral does not vanish:

- There are one U and one $U^\dagger$ per link: use eq. (2.63) as integration rule
- All U and $U^\dagger$ occupy the same link [87]:

$$
\begin{aligned}
\int dU U_{i_1 j_1} U_{i_2 j_2} U^\dagger_{k_1 l_1} U^\dagger_{k_2 l_2} =& \frac{1}{N_c^2-1} (\delta_{i_1 l_1}\delta_{i_2 l_2}\delta_{j_1 k_1}\delta_{j_2 k_2} + \delta_{i_1 l_2}\delta_{i_2 l_1}\delta_{j_1 k_2}\delta_{j_2 k_1}) \\
&- \frac{1}{N_c(N_c^2-1)} (\delta_{i_1 l_2}\delta_{i_2 l_1}\delta_{j_1 k_1}\delta_{j_2 k_2} + \delta_{i_1 l_1}\delta_{i_2 l_2}\delta_{j_1 k_2}\delta_{j_2 k_1}) \, ,
\end{aligned}
\tag{2.108}
$$

We will also end up with Kronecker deltas for the time coordinates, since pairs of time coordinates or even all coordinates have to be the same. Then we arrive at

$$
\begin{aligned}
&-\frac{1}{2}\int[dU_k]\sum_i \mathrm{tr}\, P_iM_iP_iM_i = \\
&-\frac{16\kappa^4}{N_c^2}\sum_{\vec{x},t_1\neq t_2,i}\big[\mathrm{tr}\, B(\vec{x},t_1,t_2)B(\vec{x},t_2,t_1)(\mathrm{tr}\, B(\vec{x}+i,t_1,t_1))^2 \\
&\qquad\qquad + (\mathrm{tr}\, B(\vec{x},t_1,t_1))^2\mathrm{tr}\, B(\vec{x}+i,t_1,t_2)B(\vec{x}+i,t_2,t_1)\big] \\
&-\frac{16\kappa^4}{N_c^2-1}\sum_{\vec{x},t,i}\{\mathrm{tr}\, B(\vec{x},t,t)B(\vec{x},t,t)(\mathrm{tr}\, B(\vec{x}+i,t,t))^2 + (\mathrm{tr}\, B(\vec{x},t,t))^2\mathrm{tr}\, B(\vec{x}+i,t,t)B(\vec{x}+i,t,t) \\
&-\frac{1}{N_c}[\mathrm{tr}\, B(\vec{x},t,t)B(\vec{x},t,t)\mathrm{tr}\, B(\vec{x}+i,t,t)B(\vec{x}+i,t,t) + (\mathrm{tr}\, B(\vec{x},t,t))^2(\mathrm{tr}\, B(\vec{x}+i,t,t))^2]\}\ ,
\end{aligned}
\tag{2.109}
$$

or in a more compact form with the 4-vectors u, v:

$$
\begin{aligned}
&-\frac{1}{2}\int[dU_k]\sum_i \mathrm{tr}\, P_iM_iP_iM_i = \\
&-\frac{16\kappa^4}{N_c^2}\sum_{u\neq v,i}\big[\mathrm{tr}\, B_{u,v}B_{v,u}(\mathrm{tr}\, B_{u+i,u+i})^2 + (\mathrm{tr}\, B_{u,u})^2\mathrm{tr}\, B_{u+i,v+i}B_{v+i,u+i}\big] \\
&-\frac{16\kappa^4}{N_c^2-1}\sum_{u,i}\{\mathrm{tr}\, B_{u,u}B_{u,u}(\mathrm{tr}\, B_{u+i,u+i})^2 + (\mathrm{tr}\, B_{u,u})^2\mathrm{tr}\, B_{u+i,u+i}B_{u+i,u+i} \\
&-\frac{1}{N_c}[\mathrm{tr}\, B_{u,u}B_{u,u}\mathrm{tr}\, B_{u+i,u+i}B_{u+i,u+i} + (\mathrm{tr}\, B_{u,u})^2(\mathrm{tr}\, B_{u+i,u+i})^2]\}\ .
\end{aligned}
\tag{2.110}
$$

When we now use the definition for B from eq. (2.103) and perform the sum over the time indices we arrive at

$$
\begin{aligned}
&-\frac{1}{2}\int[dU_k]\sum_{\vec{x},i}\mathrm{Tr}P_{\vec{x},i}M_{\vec{x},i}P_{\vec{x},i}M_{\vec{x},i} = \qquad (2.111)\\
&\frac{\kappa^4 N_t(N_t-1)}{N_c^2}\sum_{\vec{x},i}\Big\{\mathrm{Tr}\Big(\frac{hW_{\vec{x}}}{(1+hW_{\vec{x}})^2}+\frac{\bar{h}W^\dagger_{\vec{x}}}{(1+\bar{h}W^\dagger_{\vec{x}})^2}+2\frac{\frac{1}{N_t-1}\sum_{t=1}^{N_t-1}(2\kappa)^{2t}}{(1+hW_{\vec{x}})(1+\bar{h}W^\dagger_{\vec{x}})}\Big)\\
&\qquad\Big(\mathrm{Tr}\frac{hW_{\vec{x}+i}}{1+hW_{\vec{x}+i}}-\mathrm{Tr}\frac{\bar{h}W^\dagger_{\vec{x}+i}}{1+\bar{h}W^\dagger_{\vec{x}+i}}\Big)^2+\Big(\mathrm{Tr}\frac{hW_{\vec{x}}}{1+hW_{\vec{x}}}-\mathrm{Tr}\frac{\bar{h}W^\dagger_{\vec{x}}}{1+\bar{h}W^\dagger_{\vec{x}}}\Big)^2\\
&\qquad\mathrm{Tr}\Big(\frac{hW_{\vec{x}+i}}{(1+hW_{\vec{x}+i})^2}+\frac{\bar{h}W^\dagger_{\vec{x}+i}}{(1+\bar{h}W^\dagger_{\vec{x}+i})^2}+2\frac{\frac{1}{N_t-1}\sum_{t=1}^{N_t-1}(2\kappa)^{2t}}{(1+hW_{\vec{x}+i})(1+\bar{h}W^\dagger_{\vec{x}+i})}\Big)\Big\}\\
&-\frac{\kappa^4 N_t}{N_c^2-1}\sum_{\vec{x},i}\Big\{\mathrm{Tr}\Big(\frac{hW_{\vec{x}}}{1+hW_{\vec{x}}}-\frac{\bar{h}W^\dagger_{\vec{x}}}{1+\bar{h}W^\dagger_{\vec{x}}}\Big)^2\Big(\mathrm{Tr}\frac{hW_{\vec{x}+i}}{1+hW_{\vec{x}+i}}-\mathrm{Tr}\frac{\bar{h}W^\dagger_{\vec{x}+i}}{1+\bar{h}W^\dagger_{\vec{x}+i}}\Big)^2\\
&\qquad+\Big(\mathrm{Tr}\frac{hW_{\vec{x}}}{1+hW_{\vec{x}}}-\mathrm{Tr}\frac{\bar{h}W^\dagger_{\vec{x}}}{1+\bar{h}W^\dagger_{\vec{x}}}\Big)^2\mathrm{Tr}\Big(\frac{hW_{\vec{x}+i}}{1+hW_{\vec{x}+i}}-\frac{\bar{h}W^\dagger_{\vec{x}+i}}{1+\bar{h}W^\dagger_{\vec{x}+i}}\Big)^2\Big\}\\
&+\frac{\kappa^4 N_t}{N_c^3-N_c}\sum_{\vec{x},i}\Big\{\mathrm{Tr}\Big(\frac{hW_{\vec{x}}}{1+hW_{\vec{x}}}-\frac{\bar{h}W^\dagger_{\vec{x}}}{1+\bar{h}W^\dagger_{\vec{x}}}\Big)^2\mathrm{Tr}\Big(\frac{hW_{\vec{x}+i}}{1+hW_{\vec{x}+i}}-\frac{\bar{h}W^\dagger_{\vec{x}+i}}{1+\bar{h}W^\dagger_{\vec{x}+i}}\Big)^2\\
&\qquad+\Big(\mathrm{Tr}\frac{hW_{\vec{x}}}{1+hW_{\vec{x}}}-\mathrm{Tr}\frac{\bar{h}W^\dagger_{\vec{x}}}{1+\bar{h}W^\dagger_{\vec{x}}}\Big)^2\Big(\mathrm{Tr}\frac{hW_{\vec{x}+i}}{1+hW_{\vec{x}+i}}-\mathrm{Tr}\frac{\bar{h}W^\dagger_{\vec{x}+i}}{1+\bar{h}W^\dagger_{\vec{x}+i}}\Big)^2\Big\}\,.
\end{aligned}
$$

Again we have replaced all factors z^{N_t} with h, to include corrections from spatial hops, and since we want to apply our model in the cold and dense regime, we drop all terms that are subleading in N_t and have $\bar{h}\sim e^{-a\mu N_t}\to 0$. In this limit the expression above reduces to

$$
\begin{aligned}
&-\frac{1}{2}\int[dU_k]\sum_i \mathrm{tr}\,P_iM_iP_iM_i =\\
&\frac{\kappa^4 N_t^2}{N_c^2}\sum_{\vec{x},i}\mathrm{tr}\,\frac{hW_{\vec{x}}}{(1+hW_{\vec{x}})^2}\Big[\Big(\mathrm{tr}\,\frac{hW_{\vec{x}+i}}{1+hW_{\vec{x}+i}}\Big)^2+\Big(\mathrm{tr}\,\frac{hW_{\vec{x}-i}}{1+hW_{\vec{x}-i}}\Big)^2\Big]\,, \qquad (2.112)
\end{aligned}
$$

where we have relabeled the summation indices of the second term. Also, the next contribution to the two-point interactions is of order κ^4:

$$\begin{aligned}
&\frac{1}{2}\int [dU_k] \sum_{\vec{x},i} \mathrm{tr}\ P_{\vec{x},i} M_{\vec{x},i} \mathrm{tr}\ P_{\vec{x},i} M_{\vec{x},i} \qquad (2.113)\\
= \ & \frac{32\kappa^4}{N_c^2} \sum_{u\neq v,i} \left[\Big(\mathrm{tr}\ B_{u,u}\Big)^2 \Big(\mathrm{tr}\ B_{v+\hat{\imath},v+\hat{\imath}}\Big)^2 + \mathrm{tr}\ B_{u,v}B_{v,u} \mathrm{tr}\ B_{u+\hat{\imath},v+\hat{\imath}} B_{v+\hat{\imath},u+\hat{\imath}} \right] \\
& + \frac{32\kappa^4}{N_c^2-1} \sum_{u,i} \left\{ \Big(\mathrm{tr}\ B_{u,u}\Big)^2 \Big(\mathrm{tr}\ B_{u+\hat{\imath},u+\hat{\imath}}\Big)^2 + \mathrm{tr}\ B_{u,u}B_{u,u} \mathrm{tr}\ B_{u+\hat{\imath},u+\hat{\imath}} B_{u+\hat{\imath},u+\hat{\imath}} \right. \\
& \left. - \frac{1}{N_c} \left[\mathrm{tr}\ B_{u,u}B_{u,u} \Big(\mathrm{tr}\ B_{u+\hat{\imath},u+\hat{\imath}}\Big)^2 + \Big(\mathrm{tr}\ B_{u,u}\Big)^2 \mathrm{tr}\ B_{u+\hat{\imath},u+\hat{\imath}} B_{u+\hat{\imath},u+\hat{\imath}} \right] \right\} .
\end{aligned}$$

These are all two-point interactions that one finds in general, other corrections to the two-point interaction start with $\mathcal{O}(\kappa^6)$. However, for the special case of SU(2), there are additional two-point interactions coming from dynamic diquark contributions. In the terms:

$$-\frac{1}{2}\int dU \sum_i \mathrm{tr}\, P_i M_i P_i M_i \ ,$$
$$\frac{1}{2}\int dU \sum_i \mathrm{tr}\, P_i M_i \mathrm{tr}\, P_i M_i \ ,$$

we find further non-vanishing combinations of the U's and $U^\dagger$' from the group integration rule for SU(2)

$$\int dU U_{ij} U_{kl} = \frac{1}{2}\epsilon_{ik}\epsilon_{jl} \ . \qquad (2.114)$$

With this rule we can calculate the contributions from the dynamic diquarks to be

$$-\frac{1}{2}\int dU \sum_i \mathrm{tr}\, P_i M_i P_i M_i = -8\kappa^4 \sum_{u\neq v} \det[B_{u,v}] \det[B_{v+i,u+i}] \ ,$$
$$\frac{1}{2}\int dU \sum_i \mathrm{tr}\, P_i M_i \mathrm{tr}\, P_i M_i = 16\kappa^4 \sum_{u\neq v} \det[B_{u,v}] \det[B_{v+i,u+i}] \ ,$$

leading to an overall diquark contribution of

$$\begin{aligned}
-S_{\mathrm{diquark}} &= 8\kappa^4 \sum_{u\neq v} \det[B_{u,v}] \det[B_{v+i,u+i}] \ , \\
&= 2\kappa^4 N_t^2 \sum_{x,i} \det \frac{h}{(1+hW_x)(1+hW_{x+i})} \\
&= 2\kappa^4 N_t^2 \sum_{x,i} \frac{h^2}{(1+hL_x+h^2)(1+hL_{x+i}+h^2)} \qquad (2.115)
\end{aligned}$$

Three-Point Interactions

Interactions connecting three spatial indices start at $\mathcal{O}(\kappa^4)$

$$e^{-S_3^f} \equiv \int [dU_k] \Big[-\sum_i \text{tr } P_i P_i M_i M_i - \sum_{i\neq j} \text{tr } P_i P_j M_j M_i \tag{2.116}$$
$$-\frac{1}{2}\sum_{i\neq j} \text{tr } P_i M_i P_j M_j - \frac{1}{2}\sum_{i\neq j} \text{tr } P_i M_j P_j M_i + \frac{1}{2}\sum_{\vec{x},\vec{y},i,j} \text{tr } P_{\vec{x},i} M_{\vec{x},i} \text{tr } P_{\vec{y},j} M_{\vec{y},j} \Big] .$$

The different contributions are evaluated to be

$$-\int [dU_k] \sum_i \text{tr } P_i P_i M_i M_i =$$
$$-\frac{32\kappa^4}{N_c^2} \sum_{u,v,i} \text{tr } B_{u,u} \text{tr } A_{u+\hat{\imath},v+\hat{\imath}} A_{v+\hat{\imath},u+\hat{\imath}} \text{tr } B_{u+2\hat{\imath},u+2\hat{\imath}} , \tag{2.117}$$

$$-\int [dU_k] \sum_{i\neq j} \text{tr } P_i P_j M_j M_i =$$
$$-\frac{16\kappa^4}{N_c^2} \sum_{u,v,i\neq j} \text{tr } B_{u-\hat{\imath},u-\hat{\imath}} \Big[\text{tr } A_{u,v} A_{v,u} + \text{tr } B_{u,v} B_{v,u} \Big] \text{tr } B_{u+\hat{\jmath},u+\hat{\jmath}} , \tag{2.118}$$

$$-\frac{1}{2}\int [dU_k] \sum_{i\neq j} \text{tr } P_i M_i P_j M_j =$$
$$-\frac{8\kappa^4}{N_c^2} \sum_{u,v,i\neq j} \text{tr } B_{u+\hat{\imath},u+\hat{\imath}} \Big[\text{tr } A_{u,v} A_{v,u} + \text{tr } B_{u,v} B_{v,u} \Big] \text{tr } B_{u+\hat{\jmath},u+\hat{\jmath}} , \tag{2.119}$$

$$-\frac{1}{2}\int [dU_k] \sum_{i\neq j} \text{tr } P_i M_j P_j M_i =$$
$$-\frac{8\kappa^4}{N_c^2} \sum_{u,v,i\neq j} \text{tr } B_{u-\hat{\imath},u-\hat{\imath}} \Big[\text{tr } A_{u,v} A_{v,u} + \text{tr } B_{u,v} B_{v,u} \Big] \text{tr } B_{u-\hat{\jmath},u-\hat{\jmath}} , \tag{2.120}$$

$$\frac{1}{2}\int [dU_k] \sum_{\vec{x},\vec{y},i,j} \text{tr } P_{\vec{x},i} M_{\vec{x},i} \text{tr } P_{\vec{y},j} M_{\vec{y},j} =$$
$$\frac{32\kappa^4}{N_c^2} \sum_{u,v,i,j} \text{tr } B_{u,u} \text{tr } B_{u+\hat{\imath},u+\hat{\imath}} \text{tr } B_{v,v} \text{tr } B_{v+\hat{\jmath},v+\hat{\jmath}} , \tag{2.121}$$

where the sum is only over terms where the two traces share one spatial point.

Four-point Interactions

There are only two four-point interactions to order κ^4

$$e^{-S_4^f} \equiv \int [dU_k] \Big[- \sum_{i \neq j} \text{tr } P_i P_j M_i M_j + \frac{1}{2} \sum_{\vec{x},\vec{y},i,j} \text{tr } P_{\vec{x},i} M_{\vec{x},i} \text{tr } P_{\vec{y},j} M_{\vec{y},j} \Big] \,. \tag{2.122}$$

After integration the first contribution vanishes in the strong coupling limit and only gives a non-zero contribution if a plaquette is inserted into the fermionic loop:

$$\int [dU_k] \sum_{i \neq j} \text{tr } P_i P_j M_i M_j \quad = \quad \mathcal{O}(\kappa^4 u) \,. \tag{2.123}$$

Since we only calculate the action to order $\kappa^m u^n$ with $m + n = 4$ we neglect this term. The second contribution is

$$\begin{aligned} \frac{1}{2} \int [dU_k] \sum_{\vec{x},\vec{y},i,j} \text{tr } P_{\vec{x},i} M_{\vec{x},i} \text{tr } P_{\vec{y},j} M_{\vec{y},j} \quad &= \quad \frac{32\kappa^4}{N_c^2} \sum_{u,v,i,j} \quad \text{tr } B_{u,u} \text{tr } B_{u+\hat{\imath},u+\hat{\imath}} \text{tr } B_{v,v} \text{tr } B_{v+\hat{\jmath},v+\hat{\jmath}} \,, \end{aligned} \tag{2.124}$$

where the sum is only over terms where the traces share no common spatial point.

2.4.5. Resummation

Remember that we had to expand the exponential in the kinetic part of the fermion determinant to be able to perform the group integrations

$$\begin{aligned} \det[D_{\text{kin}}] &= \exp \big[- \text{tr } PM - \text{tr } PPMM - \frac{1}{2} \text{tr } PMPM \big] \,, \\ &= 1 - \text{tr } PM - \text{tr } PPMM - \frac{1}{2} \text{tr } PMPM + \frac{1}{2} (\text{tr } PM)^2 + \mathcal{O}(\kappa^6) \,. \end{aligned} \tag{2.125}$$

Now, we have all those terms after integration. Our goal is now to resum the resulting terms back into an exponential to improve convergence and take as many terms of the original exponential into account as we can. The resummation for the κ^2 term looks like

$$\begin{aligned} \int [dU_k] e^{-\sum_i \text{tr } P_i M_i} = 1 \quad &- \quad \frac{8\kappa^2}{N_c} \sum_{u,i} \text{tr } B_{u,u} \text{tr } B_{u+\hat{\imath},u+\hat{\imath}} \\ &+ \quad \frac{32\kappa^4}{N_c^2} \sum_{u,v,i,j} \text{tr } B_{u,u} \text{tr } B_{u+\hat{\imath},u+\hat{\imath}} \text{tr } B_{v,v} \text{tr } B_{v+\hat{\jmath},v+\hat{\jmath}} \\ = \quad & e^{-\frac{8\kappa^2}{N_c} \sum_{u,i} \text{tr } B_{u,u} \text{tr } B_{u+\hat{\imath},u+\hat{\imath}}} + \mathcal{O}(\kappa^6) \,. \end{aligned} \tag{2.126}$$

The form of the higher order terms indicates, that this procedure should always be valid. However the higher orders in eq. (2.126) have to be excluded from the appropriate orders in κ to avoid over counting.

2.4.6. Effective Action for the Cold and Dense Regime

We now have all the ingredients to write down the effective action for the cold and dense regime. We have to add up and resum all the terms we have evaluated in the last section. One has to be a little careful as there are some terms that can lead to double counting in the resummation, however in general this procedure is straightforward. As already mentioned above, we will neglect all terms proportional to $\bar{h}$ and all terms subleading in N_t, which is reasonable for $\mu > 0$ and $T \to 0$. Further, we find that the effective gauge coupling λ becomes negligible $\lambda(\beta = 2.5, N_t = 200) \sim 1 \cdot 10^{-15}$. Therefore, we will completely drop the effective gauge action of our theory. Yet, there are still remnants of the Yang-Mills part in our effective theory. As mentioned in section 2.4.3, there are gauge corrections to the effective fermion coupling h, see eq. (2.87). The effective action for the cold and dense regime for one flavor reads

$$\begin{aligned}
-S_{\text{eff}} &= \sum_{\vec{x}} \log(1 + hL_i + h^2)^2 - 2h_2 \sum_{\vec{x},i} \operatorname{tr} \frac{hW_{\vec{x}}}{1 + hW_{\vec{x}}} \operatorname{tr} \frac{hW_{\vec{x}+i}}{1 + hW_{\vec{x}+i}} \\
&+ 2\frac{\kappa^4 N_t^2}{N_c^2} \sum_{\vec{x},i} \operatorname{tr} \frac{hW_{\vec{x}}}{(1 + hW_{\vec{x}})^2} \operatorname{tr} \frac{hW_{\vec{x}+i}}{(1 + hW_{\vec{x}+i})^2} \\
&+ \frac{\kappa^4 N_t^2}{N_c^2} \sum_{\vec{x},i,j} \operatorname{tr} \frac{hW_{\vec{x}}}{(1 + hW_{\vec{x}})^2} \operatorname{tr} \frac{hW_{\vec{x}-i}}{1 + hW_{\vec{x}-i}} \operatorname{tr} \frac{hW_{\vec{x}-j}}{1 + hW_{\vec{x}-j}} \\
&+ 2\frac{\kappa^4 N_t^2}{N_c^2} \sum_{\vec{x},i,j} \operatorname{tr} \frac{hW_{\vec{x}}}{(1 + hW_{\vec{x}})^2} \operatorname{tr} \frac{hW_{\vec{x}-i}}{1 + hW_{\vec{x}-i}} \operatorname{tr} \frac{hW_{\vec{x}+j}}{1 + hW_{\vec{x}+j}} \\
&+ \frac{\kappa^4 N_t^2}{N_c^2} \sum_{\vec{x},i,j} \operatorname{tr} \frac{hW_{\vec{x}}}{(1 + hW_{\vec{x}})^2} \operatorname{tr} \frac{hW_{\vec{x}+i}}{1 + hW_{\vec{x}+i}} \operatorname{tr} \frac{hW_{\vec{x}+j}}{1 + hW_{\vec{x}+j}} \\
&- 2\kappa^4 N_t^2 \sum_{x,i} \frac{h}{(1 + hL_x + h^2)(1 + hL_{x+i} + h^2)} \, .
\end{aligned} \tag{2.127}$$

We have introduced a new coupling h_2, which also results from gauge corrections to the $\mathcal{O}(\kappa^2)$ coupling

$$h_2 = \frac{\kappa^2 N_t}{N_c} \left[1 + 2\frac{u - u^{N_t}}{1 - u} + \dots \right] \, . \tag{2.128}$$

The gauge corrections to this coupling do not seem to exponentiate [84]. One should also remember, that the last term of eq. (2.127) is only there in two- color QCD. In general SU(N) gauge theories similar terms will start to emerge in order κ^{2N}.

2.4.7. Effective Action for N_f Flavors

We will now discuss how to extend the effective model to more than one quark flavor. When we take all flavors to be degenerate, the partition function is modified to

$$Z = \int dU e^{-S_g} \det[D]^{N_f} \, , \tag{2.129}$$

where we just get additional fermion determinants from each flavor. Again, we can split up the fermion determinants in terms of static and kinetic parts and expand the kinetic part in powers of the hopping parameter. We now find

$$\begin{aligned}
\det[D]^{N_f} &= (\det[D_{\text{stat}}]\det[D_{\text{kin}}])^{N_f} \ , \\
&= \det[D_{\text{stat}}]^{N_f} \exp\Big[- N_f \ \text{tr}\, PM - N_f \ \text{tr}\, PPMM \\
&\qquad\qquad - \frac{N_f}{2} \ \text{tr}\, PMPM \Big] \left[1 + \mathcal{O}(k^6)\right] \ , \\
&= \det[D_{\text{stat}}]^{N_f} \Big[1 - N_f \ \text{tr}\, PM - N_f \ \text{tr}\, PPMM - \frac{N_f}{2} \ \text{tr}\, PMPM \\
&\qquad\qquad + \frac{{N_f}^2}{2} \ (\text{tr}\, PM)^2 \Big] \left[1 + \mathcal{O}(k^6)\right] \ .
\end{aligned}$$

When we compare this result with the one from eq. (2.92) we can conclude that the effective action for the N_f-flavor case will consist of the same terms as for $N_f = 1$ with different prefactors. The effective action for N_f flavors of degenerate quarks reads

$$\begin{aligned}
-S_{\text{eff}} &= N_f \sum_{\vec{x}} \log(1 + hL_i + h^2)^2 - 2N_f h_2 \sum_{\vec{x},i} \text{tr}\, \frac{hW_{\vec{x}}}{1 + hW_{\vec{x}}} \text{tr}\, \frac{hW_{\vec{x}+i}}{1 + hW_{\vec{x}+i}} \\
&+ 2N_f^2 \frac{\kappa^4 N_t^2}{N_c^2} \sum_{\vec{x},i} \text{tr}\, \frac{hW_{\vec{x}}}{(1 + hW_{\vec{x}})^2} \text{tr}\, \frac{hW_{\vec{x}+i}}{(1 + hW_{\vec{x}+i})^2} \\
&+ N_f \frac{\kappa^4 N_t^2}{N_c^2} \sum_{\vec{x},i,j} \text{tr}\, \frac{hW_{\vec{x}}}{(1 + hW_{\vec{x}})^2} \text{tr}\, \frac{hW_{\vec{x}-i}}{1 + hW_{\vec{x}-i}} \text{tr}\, \frac{hW_{\vec{x}-j}}{1 + hW_{\vec{x}-j}} \\
&+ 2N_f \frac{\kappa^4 N_t^2}{N_c^2} \sum_{\vec{x},i,j} \text{tr}\, \frac{hW_{\vec{x}}}{(1 + hW_{\vec{x}})^2} \text{tr}\, \frac{hW_{\vec{x}-i}}{1 + hW_{\vec{x}-i}} \text{tr}\, \frac{hW_{\vec{x}+j}}{1 + hW_{\vec{x}+j}} \\
&+ N_f \frac{\kappa^4 N_t^2}{N_c^2} \sum_{\vec{x},i,j} \text{tr}\, \frac{hW_{\vec{x}}}{(1 + hW_{\vec{x}})^2} \text{tr}\, \frac{hW_{\vec{x}+i}}{1 + hW_{\vec{x}+i}} \text{tr}\, \frac{hW_{\vec{x}+j}}{1 + hW_{\vec{x}+j}} \\
&- 2(2N_f^2 - N_f)\kappa^4 N_t^2 \sum_{x,i} \frac{h^2}{(1 + hL_x + h^2)(1 + hL_{x+i} + h^2)} \ .
\end{aligned} \tag{2.130}$$

2.4.8. Mass Scale

In order to establish a reference scale for our simulations at finite density, we calculate the diquark or respectively the pion mass in the vacuum in the hopping expansion. We extract the mass from the exponential decay of the following pion correlator

$$am(\pi) = \lim_{t\to\infty} \frac{1}{t} \ln\langle \pi(0)\overline{\pi}(t)\rangle \ , \tag{2.131}$$

where we have to sum over space-like indices in order to have mass eigenstates [88]

$$\pi(t) = \sum_{\vec{x}} \pi(\vec{x}, t) \ . \tag{2.132}$$

The pion correlator is of the form

$$\langle \pi(0)\overline{\pi}(t)\rangle = \langle \overline{d}(0)\gamma_5 u(0)\overline{u}(t)\gamma_5 d(t)\rangle \ . \tag{2.133}$$

Applying the Wick theorem and keeping in mind that one can only contract fermion fields with equal flavor (also in the case of degenerate quark masses), we arrive at

$$\langle \pi(0)\overline{\pi}(t)\rangle = -\langle \mathrm{tr}\left[\gamma_5 D^{-1}(0,t)\gamma_5 D^{-1}(t,0)\right]\rangle_{QCD} \tag{2.134}$$

Now, hopping expand the pion propagator up to order $\mathcal{O}(\kappa^2)$. The index QCD of the expectation value means, that up to now we cannot integrate out the spatial links but have to use the full theory. Only after expanding the quark propagator we can integrate over the spatial links. Remember, nly diagrams that give non-vanishing contributions to the link integration will show up in the pion propagator.
To LO, these are just two anti-parallel temporal gauge-link chains running between 0 and t. The computation of their contribution is analogous to the LO hopping expansion of the fermion determinant

$$\langle \pi(0)\overline{\pi}(t)\rangle^{LO} \propto (2\kappa)^{(2t)} \tag{2.135}$$

To order $\mathcal{O}(\kappa^2)$ we have five different contributions, one without and four with attached gauge plaquettes. Figure 2.7 shows all diagrams to order $\mathcal{O}(\kappa^2)$. The $\mathcal{O}(\kappa^2)$ decorations are (in the limit of large t)

$$6t\kappa^2 + 24t\kappa^2 \frac{u-u^{t+1}}{1-u} \ . \tag{2.136}$$

In the order $\mathcal{O}(\kappa^4 u^0)$ we have only anti-parallel gauge-link chains, each with two hops in spatial direction. We get $6t \cdot 6(t-1)$ diagrams with hops at different temporal coordinates and $6 \cdot 5t$ diagrams with two hops at the same temporal coordinate. Again, we would count the terms proportional to t^2 twice when exponentiating repeating contributions, leading to the $\mathcal{O}(\kappa^4 u^0)$ contribution

$$(-36t + 30t)\kappa^4 = -6t\kappa^4 \ , \tag{2.137}$$

As in the hopping expansion of the fermion determinant, repeating corrections lead to exponentiation and the pion propagator becomes

$$\langle \pi(0)\overline{\pi}(t)\rangle^{NLO} \propto (2\kappa)^{(2t)} \exp\left[6t\kappa^2 + 24t\kappa^2 \frac{u-u^{t+1}}{1-u} - 6t\kappa^4\right] \ . \tag{2.138}$$

By plugging this result into (2.131) we get the mass of the pion

$$am(\pi) = -2\ln(2\kappa) - 6\kappa^2 - 24\kappa^2 \frac{u}{1-u} + 6\kappa^4 + \mathcal{O}(\kappa^4 u^2, \kappa^2 u^5) \ . \tag{2.139}$$

We can even improve this result by using the pion mass for a free theory from [89], which includes the meson propagator to all orders in κ, together with our string coupling corrections. There are still corrections from the hopping expansion of the effective action, but they will only start to give contributions at $\mathcal{O}(\kappa^6)$. The pion mass is then given by

$$am(\pi) = \mathrm{arcosh}\left(1 + \frac{(1-16\kappa^2)(1-4\kappa^2)}{8\kappa^2(1-6\kappa^2)}\right) - 24\kappa^2 \frac{u}{1-u} + \mathcal{O}(\kappa^4 u^2, \kappa^2 u^5, \kappa^6) \ . \tag{2.140}$$

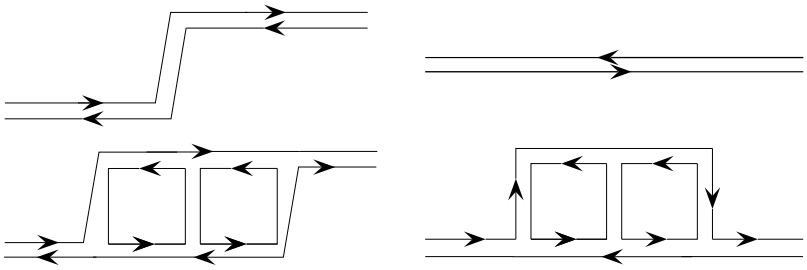

Figure 2.7.: Graphs contributing to the pion propagator in $\mathcal{O}(\kappa^2)$ hopping expansion. Each of the lower graphs has to be counted twice, since it is a difference, which propagator stands of the up and the down quark.

2.5. Effective Polyakov-Loop Theory for G_2

In this section we will discuss the derivation of an effective Polyakov-loop theory for G_2-QCD. In principle most of the steps will be completely equivalent to the derivation for two-color QCD. The only differences are the coefficients of the character expansion a_j (compare to eq. (2.55)) and the group integrals. The two points are of course related to each other since we need to integrate over the gauge group if we want to compute the a_j.

2.5.1. Effective Theory for the G_2 Yang-Mills Action

We have computed all the necessary expansion parameters to retrace all the steps in section 2.4. The explicit relations can be found in appendix B. There will be additional corrections from decorations that yield vanishing contributions in SU(2) but the general procedure is completely analogous. Therefore we can also conclude that the effective action will have exactly the same form as for the SU(2) case:

$$-S_{\text{eff}} = \sum_{<ij>} \ln(1 + \lambda L_i L_j) \; . \tag{2.141}$$

In the literature one finds also Polyakov loop models where we have a nearest-neighbor term with loops in the 14 dimensional fundamental representation. However, one can show that also these terms, as all other terms, are parametrically suppressed. We have calculated the corrections to λ up to order u^6. Again as, in the case of SU(2), the corrections exponentiate and we find λ to be

$$\lambda(u, N_t) = u^{N_t} \exp[N_t(4u^4 + 28u^5 + \frac{82}{3}u^6 + \mathcal{O}(u^7))] \; . \tag{2.142}$$

The u^5 correction comes from a decoration like the one on the left of fig. 2.4, where we have an additional plaquette on the bottom of the cube. In this case we find two links where three plaquettes in the fundamental representation meet. This would lead to a vanishing group integral in SU(2), in G_2 we have

$$(7) \otimes (7) \otimes (7) = (1) \oplus 4 \cdot (7) \oplus 2 \cdot (14) \oplus 3 \cdot (27) \oplus 2 \cdot (64) \oplus (77) \; , \tag{2.143}$$

and the trivial representation in the Clebsch-Gordon series leads to a non-vanishing group integral of the form:

$$\int dU\ U_{ab}U_{cd}U_{ef} = \frac{1}{14}c_{ace}c_{bdf}\ ,$$
$$c_{ace} = \frac{1}{\sqrt{3}}\psi_{ace}\ , \qquad a,c,e \in \{1,2,\ldots,7\}\ , \tag{2.144}$$

where ψ_{ace} is the totally antisymmetric octonionic tensor defined by [72]

$$\psi_{123} = \psi_{147} = \psi_{165} = \psi_{246} = \psi_{257} = \psi_{354} = \psi_{367} = 1\ . \tag{2.145}$$

Also, there is a similar, additional diagram contributing to order $\mathcal{O}(u^6)$. Here, we have a plaquette in the adjoint representation at the bottom of the cube. The higher the order in u, the harder it gets to calculate the contributions from decorations as there are a lot of combinations of plaquettes in various representations that give non-vanishing contributions.

2.5.2. Leading Order Heavy Fermions for G_2

Our strategy to include dynamical fermions into the effective theory is described in detail in section 2.4.2. The general procedure stays the same. And we again arrive at the partition function from eq. (2.81):

$$Z = \int [dU_0] \prod_{<ij>} [1+\lambda_1 L_i L_j] \prod_{\vec{x}} \det\left[(1+hW_{\vec{x}})(1+\bar{h}W_{\vec{x}}^T)\right]^2\ ,$$
$$= \int [dU_0] \prod_{<ij>} [1+\lambda_1 L_i L_j] \prod_{\vec{x}} \det\left[(1+hW_{\vec{x}})(1+\bar{h}W_{\vec{x}})\right]^2\ .$$

For SU(2) we were able to simplify this expression by rewriting the determinant as a characteristic polynomial and expand in invariants of tensors

$$p_W(\lambda) = \sum_{k=0}^{n} (-1)^k \lambda^{n-k} \mathrm{tr}\,(\Lambda^k W)\ , \tag{2.146}$$

where $\mathrm{tr}\,(\Lambda^k W)$ is the trace of the k-th exterior power, or respectively one of the k tensor invariants. The idea behind this expansion is to express the determinant in terms of traces, so we do not have to sample over the full gauge group in the Monte-Carlo simulation, but only over the class angles. SU(2) has rank 1 and there is exactly one invariant $\mathrm{tr}\,W$. For SU(3) with rank 2 we have one more invariant which can be chosen to be $\mathrm{tr}\,W^\dagger$. Elements of G_2 are represented by 7x7 matrices. For a 7x7 matrix we generally find seven tensor invariants, however because of the structure of G_2 they are not independent [72], but the relations are more involved than in the simple cases of SU(2) or SU(3). We do not need this expression in our simulations as it will not lead to a algorithmic speed up but will use the eigenvalues of W. However, as for the case of

SU(2), one can use this expression to get e.g. insight into the spectrum of the effective theory.
Getting the G_2 equivalent of eq. (2.82) is more challenging as it is for SU(2) oder SU(3). However, if we use the fact that the determinant is a class function, it is sufficient to use elements t from the maximal torus T of G_2 (see appendix C). Examining t a little closer, we see that we can write

$$t = \begin{pmatrix} u & & \\ & u^* & \\ & & 1 \end{pmatrix} \qquad \text{with} \quad u = \begin{pmatrix} e^{i\varphi} & & \\ & e^{i\vartheta} & \\ & & e^{-i(\varphi+\vartheta)} \end{pmatrix} , \tag{2.147}$$

where u is an element of the maximal torus of SU(3) and $\varphi, \vartheta \in [0, 2\pi]$. So we can split up the G_2 determinant in two SU(3) determinants with an additional factor

$$\det\left[1 + hW_{G_2}\right] = \Big[\det(1 + hu_{SU(3)}) \det(1 + hu^\dagger_{SU(3)})(1 + h)\Big] \ . \tag{2.148}$$

Now we can use the SU(3) equivalent of (2.82)

$$\det[1 + hu_{SU(3)}] = 1 + hL + h^2L^* + h^3 \qquad \text{with} \quad L = \operatorname{tr} u_{SU(3)} \ , \tag{2.149}$$

to rewrite the SU(3) determinants and arrive at

$$\det\left[1 + hW_{G_2}\right] = \left[(1 + hL + h^2L^* + h^3)(1 + hL^* + h^2L + h^3)(1 + h)\right] \ . \tag{2.150}$$

We now have the LO fermion content in terms of SU(3) Polyakov loops. However, we still have to perform the G_2 group integral. Although, one can measure the SU(3) Polyakov loop in a G_2 lattice simulation, it is not exactly clear what its physical meaning is. So we would like to transform this awkward expression into one with G_2 Polyakov loops, since we know that G_2 has rank 2, we expect to need two different tensor invariants. The first two candidates that come to mind are the Polyakov loops in the two fundamental representations χ_7 and χ_{14}. It is now straight forward to expand eq. (2.150), plug in the SU(3) Polyakov loops in terms of the class angles, look at χ_7 and χ_{14}, again in terms of class angles, and find the result by equating coefficients:

$$\begin{aligned} \det\left[1 + hW_{G_2}\right] = 1 &+ (h + h^6)\chi_7 + (h^2 + h^5)(\chi_7 + \chi_{14}) \\ &+ (h^3 + h^4)(\chi_7^2 - \chi_{14}) + h^7 \ . \end{aligned} \tag{2.151}$$

Thus the LO fermion contribution is given by

$$\begin{aligned} \det\left[1 + hW_{G_2}\right]^2 = 1 &+ (h + h^{13})(2\chi_7) + (h^2 + h^{12})(2\chi_{14} + 2\chi_7^2 + 2\chi_7) \\ &+ (h^3 + h^{11})(4\chi_7^2 + 2\chi_{14}\chi_7 - 2\chi_{14}) + (h^4 + h^{10})(3\chi_7^3 + \chi_{14}^2 + 3\chi_7^2 - 2\chi_{14}) \\ &+ (h^5 + h^9)(4\chi_7^3 + 2\chi_{14}\chi_7^2 - 2\chi_{14}^2 - 4\chi_{14}\chi_7 + 2\chi_{14} + 2\chi_7) \\ &+ (h^6 + h^8)(\chi_7^4 + 2\chi_7^3 - \chi_{14}^2 + 2\chi_7^2 + 2\chi_7)] \\ &+ h^7(2 + 2\chi_7^4 - 4\chi_7^2\chi_{14} + 4\chi_{14}^2 + 4\chi_{14}\chi_7) + h^{14} \ . \end{aligned} \tag{2.152}$$

Also different is h, since the derivation of h also involves group integrals. The effective fermion coupling for G_2 is given by

$$h(u,\kappa,N_t) = (2\kappa e^{a\mu})^{N_t} \exp\Big[6N_t\kappa^2 u\Big(\frac{1-u^{N_t-1}}{1-u} + 4u^4 - 28\kappa^2 + 9\kappa^2 u + 4\kappa^2 u^2\Big)\Big] \,. \tag{2.153}$$

2.5.3. Kinetic Fermion Determinant for G_2

We reevaluate all terms in section 2.4.4, this time with gauge group G_2. The basic group integrals for G_2 is the same as in SU(N). We can even recycle the integration rule for a link occupied by $UU^\dagger UU^\dagger$ in eq. (2.108). There is one additional non-vanishing group integral. Since G_2 is a real subgroup of SO(7) we can evaluate it with the help of the basic integration rule

$$\int dU\; U_{ab}U_{cd} = \int dU\; U_{ab}U^{-1}_{dc} = \frac{1}{7}\delta_{ac}\delta_{bd} \,. \tag{2.154}$$

This again leads to additional terms in the two-point interaction

$$-\frac{1}{2}\int dU \sum_i \mathrm{tr}\, P_i M_i P_i M_i \,,$$
$$\frac{1}{2}\int dU \sum_i \mathrm{tr}\, P_i M_i \mathrm{tr}\, P_i M_i \,,$$

similar to the dynamic diquark contributions in the effective theory for two-color QCD. However for G_2 it can be easily shown that those additional terms only result in a term independent of temporal gauge links, so we can omit it when calculating expectation values. The effective action for the cold and dense regime of one-flavor G_2-QCD then reads

$$\begin{aligned}
-S_{\text{eff}} &= \sum_{\vec{x}} \log\det(1+hW_{\vec{x}})^2 - 2h_2 \sum_{\vec{x},i} \mathrm{tr}\,\frac{hW_{\vec{x}}}{1+hW_{\vec{x}}}\mathrm{tr}\,\frac{hW_{\vec{x}+i}}{1+hW_{\vec{x}+i}} \\
&+ 2\frac{\kappa^4 N_t^2}{N_c^2}\sum_{\vec{x},i} \mathrm{tr}\,\frac{hW_{\vec{x}}}{(1+hW_{\vec{x}})^2}\mathrm{tr}\,\frac{hW_{\vec{x}+i}}{(1+hW_{\vec{x}+i})^2} \\
&+ \frac{\kappa^4 N_t^2}{N_c^2}\sum_{\vec{x},i,j} \mathrm{tr}\,\frac{hW_{\vec{x}}}{(1+hW_{\vec{x}})^2}\mathrm{tr}\,\frac{hW_{\vec{x}-i}}{1+hW_{\vec{x}-i}}\mathrm{tr}\,\frac{hW_{\vec{x}-j}}{1+hW_{\vec{x}-j}} \\
&+ 2\frac{\kappa^4 N_t^2}{N_c^2}\sum_{\vec{x},i,j} \mathrm{tr}\,\frac{hW_{\vec{x}}}{(1+hW_{\vec{x}})^2}\mathrm{tr}\,\frac{hW_{\vec{x}-i}}{1+hW_{\vec{x}-i}}\mathrm{tr}\,\frac{hW_{\vec{x}+j}}{1+hW_{\vec{x}+j}} \\
&+ \frac{\kappa^4 N_t^2}{N_c^2}\sum_{\vec{x},i,j} \mathrm{tr}\,\frac{hW_{\vec{x}}}{(1+hW_{\vec{x}})^2}\mathrm{tr}\,\frac{hW_{\vec{x}+i}}{1+hW_{\vec{x}+i}}\mathrm{tr}\,\frac{hW_{\vec{x}+j}}{1+hW_{\vec{x}+j}}
\end{aligned} \tag{2.155}$$

where h_2 is defined as in eq. (2.128).

3
Results at Finite Temperature

Before turning to results in the phase diagram at finite baryon density, let us start by giving some results from the effective theory at finite temperature but vanishing baryon density. This serves to be an introduction to the finite temperature effects in our effective theory and, since there are plenty of results for both effective theories and full theories at finite temperature, to test whether our implementation of the effective theory is correct.

3.1. Effective Polyakov-Loop Theory for SU(2)

We start by discussing results for the effective theories at finite temperature for SU(2) Yang-Mills theory. Later we will also show results from the effective theory with dynamical quarks.
There are many studies on the finite temperature properties of SU(2) Yang-Mills and two-color QCD on the lattice, e.g. [45, 65, 75, 90–92] in the literature. There is also extensive work on effective Polyakov-loop theories for finite temperature SU(2) Yang-Mills theory [42, 44, 74, 81, 83]. Determining the critical effective coupling λ_c, $\beta_c(\lambda_c, N_t)$ and the order of the phase transition and then comparing this to existing results is an excellent way to test the code for our numerical simulations.

3.1.1. Critical Coupling and Order of the Transition for SU(2)

Already in the early 80s, it was conjectured that a $d+1$ dimensional SU(2) Yang-Mills theory has the same universal behavior as the d dimensional Ising model [74] and therefore has a 2nd order deconfinement phase transition. This was later confirmed by lattice simulations with high accuracy (e.g. [45, 75]). From all these studies we expect our effective theory for SU(2) Yang-Mills theory with the partition function in eq. (2.71) to have a 2nd order phase transition with the universal properties of the 3d Ising model.

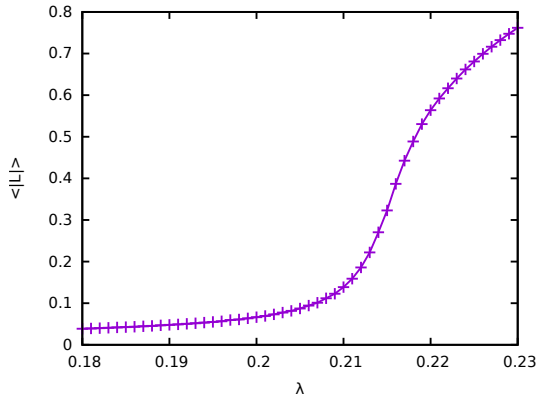

Figure 3.1.: Polyakov loop $\langle|L|\rangle$ as a function of the effective coupling λ for $N_s = 16$.

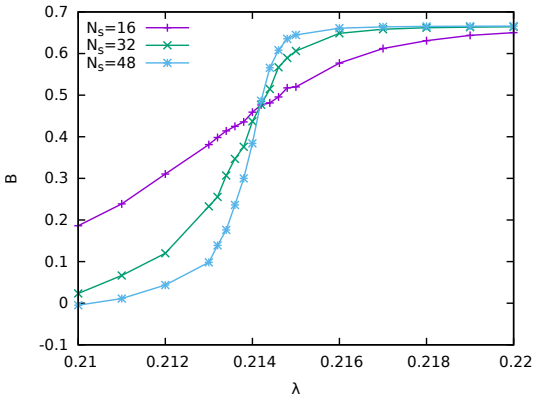

Figure 3.2.: Binder cumulant $B(|L|)$ as a function of the effective coupling λ for various lattices sizes.

Fig. 3.1 shows the Polyakov loop $\langle|L|\rangle$ as a function of the effective coupling. The plot shows the typical signs for a system with a second order phase transition in the thermodynamic limit. To check whether this is really the case and to determine the universality class and the critical coupling λ_c of the system one has to perform a finite size scaling analysis. We will do this by using the 4th order Binder cumulant

$$B(|L|) = 1 - \frac{\langle|L|^4\rangle}{3\langle|L|^2\rangle^2} \,. \tag{3.1}$$

The use of the Binder cumulant has the advantage that finite size effects are much reduced compared to analyzing the peak location and height in the susceptibilities. The Binder cumulant for our system has the following properties

- confined phase: $B(|L|) = -\frac{1}{3} + \mathcal{O}(\frac{1}{V})$ as $V \to \infty$
- deconfined phase: $B(|L|) + \frac{2}{3} + \mathcal{O}(\frac{1}{V})$ as $V \to \infty$
- at λ_c: $B(|L|)$ tends towards a universal value B^*

Fig. 3.2 shows the Binder cumulant for three different lattice sizes. The lines intersect at $\lambda = 0.21417(3)$ and $B = 0.471(5)$, which we will take as the values for the critical coupling and the universal value for the Binder cumulant[9]. Our value for λ_c is in very good agreement with the critical coupling $\lambda_c = 0.21423(70)$ found by Langelage et al. [42] and the universal values for the Binder cumulant of the 3d Ising model $B^* = 0.470(5)$ and $B^* = 0.46575(11)$ [75].
Since we now have the critical effective coupling λ_c we can use eqs. (2.69) to calculate the

[9] This is a little sloppy, as the the value of the Binder cumulant in the vicinity of the critical coupling scales like $B \sim B^* + aN_s^{-a_1}$. However, since the finite volume dependence of the crossing point is very small this will be sufficient for our purposes.

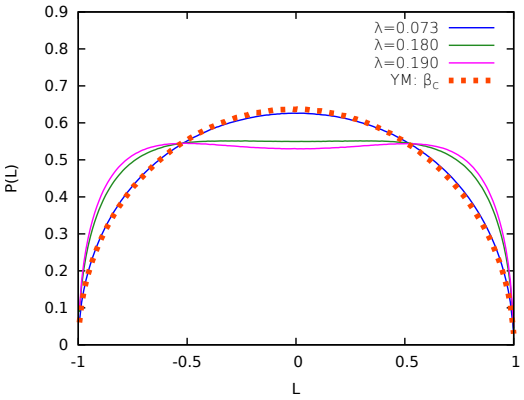

Figure 3.3.: Polyakov loop distributions $P(L)$ for a naive Polyakov loop model and several effective couplings λ compared to the distribution from a 4d lattice simulation at the critical coupling β_c at $N_t = 4$.

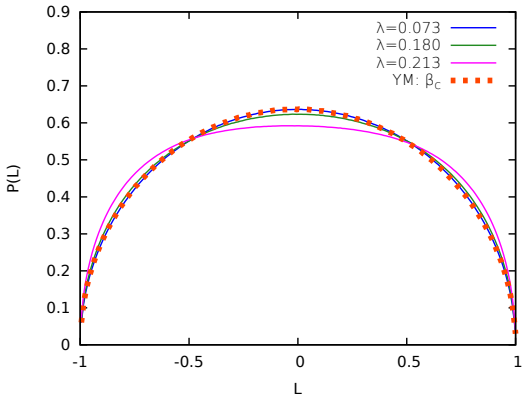

Figure 3.4.: Polyakov loop distributions $P(L)$ for the resummed Polyakov loop model and several effective couplings λ compared to the distribution from a 4d lattice simulation at the critical coupling β_c at $N_t = 4$.

critical lattice coupling β_c to a given N_t. For $N_t = 4$, $\lambda_c = 0.21423(70)$ corresponds to $\beta_c = 2.3102(08)$. Compared to the critical $\beta_c = 2.2991(2)$ from a full 4d lattice analysis [75] we have an accuracy of better than 1 %. At $N_t = 16$, λ_c leads to a critical coupling $\beta_c = 2.5582(02)$ while the 4d analysis from [93] finds $\beta_c = 2.7310(20)$, corresponding to an accuracy of about 6 %.

3.1.2. Comparison of Different Action

The amazing agreement of the critical coupling β_c from full 4d simulations and from the effective theory comes as a result of the resummations of the Polyakov loops with higher winding numbers together with the order $\mathcal{O}(u^{12})$ corrections to the effective coupling λ. Already the resummation of the multiple-winding loops leads to a dramatic improvement of the effective theory. A quantity that shows this improvement is the per-site Polyakov loop probability distribution $P(L)$ defined by

$$\langle L \rangle = \int dL\, L\, P(L)\ . \tag{3.2}$$

The Polyakov loop distribution can be measured by histograming the local Polyakov loop variable on the spatial lattice and aggregating over the whole ensemble. Full 4d lattice simulations have shown that the Polyakov loop distribution is given by the gauge group's Vandermonde potential and remains unchanged up to the critical coupling β_c [92, 94]. In the case of SU(2) the distribution is given by

$$P(L) = \frac{1}{2\pi}\sqrt{4 - L^2}\ . \tag{3.3}$$

Only if the coupling is increased further, the distributions are skewed and get asymmetric resulting in a non-zero expectation value for the Polyakov loop $\langle L \rangle$. We can now compare Polyakov loop distributions from full 4d lattice calculations in the confined phase to distributions from effective Polyakov loop models, also in the confined phase. Fig. 3.3 shows the comparison of a distribution from a naive Polyakov loop model with nearest neighbor interaction

$$S_{\text{eff}} = -\lambda \sum_{\langle ij \rangle} L_i L_j \ , \tag{3.4}$$

with a distribution from a 4d lattice simulation at the critical coupling β_c at $N_t = 4$. Note, that due to the different form of the effective action, the critical coupling for this kind of model is $\lambda_c = 0.18$ [81]. We see that the distributions match only for very small values of the effective coupling λ. For values close to the critical coupling $\lambda_c = 0.18$ we find that the distributions from the naive effective theory are massively distorted and for values $\lambda \approx \lambda_c$ we see some kind of double peak structure emerging. The Polyakov loop distributions from our model with the resummed action

$$S_{\text{eff}} = -\sum_{\langle ij \rangle} \log(1 + \lambda L_i L_j) \ , \tag{3.5}$$

are shown in Fig. 3.4. The critical coupling in this case is $\lambda_c = 0.21417(3)$ and the distributions match the distribution given by the Vandermonde determinant for almost all subcritical λ. We only see some minor deformations of the distributions close to λ_c. To see the effect of the corrections coming from decorations to the effective coupling λ we can compare the critical 4d coupling β_c to the critical lattice coupling calculated by inversion of the LO strong coupling result from eq. (2.62)

$$\lambda_c = u(\tilde{\beta}_c)^{N_t} \ . \tag{3.6}$$

For $N_t = 4$ this leads to $\tilde{\beta}_c = 4.3225$ which is almost twice the known value $\beta_c = 2.2991$. This gets even worse for bigger N_t as more decorations fit onto the lattice. For $N_t = 16$ the critical beta from inversion of eq. (3.6) would be $\tilde{\beta}_c = 16.0678$ compared to $\beta_c = 2.7310$. However, by including corrections from decorations up to order $\mathcal{O}(u^{12})$ we are able to restrict the errors in β_c to about 6%.

3.1.3. Including Dynamical Fermions

Dynamical fermions in the fundamental representation of the gauge group break center symmetry explicitly. Therefore we expect the second order deconfinement phase transition of the pure gauge theory to turn into an analytic crossover. Fig. 3.5 shows the Polyakov loop $\langle |L| \rangle$ as a function of the effective gauge coupling λ for $N_s = 16$, with dynamical quarks and effective fermion coupling $h = 0.004$. Since we only want to show the effect of the explicit breaking of center symmetry we only included the static part of the fermion determinant. If we compare this to fig. 3.1 we see that the phase transition turns into a broad crossover, as expected.

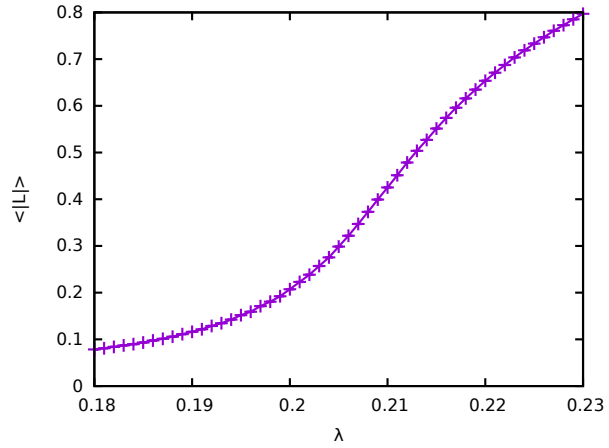

Figure 3.5.: Polyakov loop $\langle|L|\rangle$ as a function of the effective gauge coupling λ for $N_s = 16$, with dynamical quarks and effective fermion coupling $h = 0.004$.

3.2. Effective Polyakov-Loop Theory for G_2 QCD

We now turn our attention to the effective theory for the gauge group G_2. Again we start with analyzing the effective theory in the case of pure gauge theory. Studies of G_2 Yang-Mills and effective Polyakov-loop theories have found a 1st order deconfinement phase transition [50, 95]. First, we have to check if our effective theory is applicable in the case of G_2 Yang-Mills theory.

Complex action problem and non-analyticity of the partition function

In principle our effective theory shows a complex action problem for large couplings λ independent of the gauge group. Consider the leading-order partition function

$$Z = \int [dW] \sum_{<ij>} (1 + \lambda L_i L_j) \,, \tag{3.7}$$

it is easy to see that for couplings above a certain threshold $\lambda \geq \lambda_T$ some configurations will yield negative contributions to the partition function, or equivalently, have a complex action. The partition function may receive negative contributions for

$$\lambda \geq \frac{1}{|\min(L_i L_j)|} \,. \tag{3.8}$$

In the case of SU(2) negative contributions to the partition function start to appear at $\lambda > 0.25$,[10] for G_2 the negative contributions start to kick in at $\lambda > \frac{1}{14}$. However for G_2 it turns out to be even worse when we look into the origin of the complex action problem.

[10] This is not a big problem, as the critical coupling for the effective theory in SU(2) is $\lambda_c = 0.214123 < 0.25$. For SU(3) one also finds $\lambda_c < \lambda_T$.

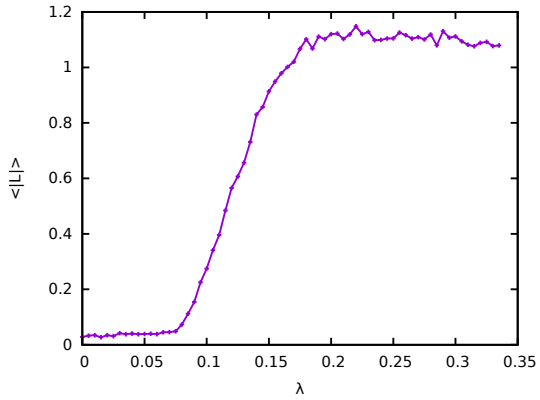

Figure 3.6.: Polyakov loop $\langle |L| \rangle$ as a function of the effective coupling λ for $N_s = 16$.

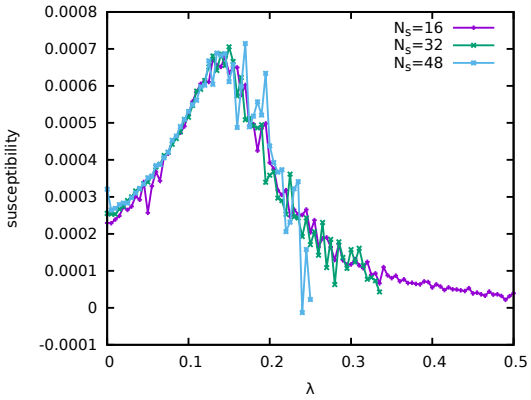

Figure 3.7.: Polyakov loop susceptibility as a function of the effective coupling λ for various lattices sizes.

Normally, a complex action problem is caused by imaginary parts of the action, e.g. in real time MC simulations, by including quark chemical potential or a topological term. This is not a flaw in the theory, we just have no suitable algorithm to perform the path integral as Monte-Carlo methods break down in this case. The sign problem here is different, it is not caused by some physical feature but appears due to our resummation scheme. When we derived the effective action for the Yang-Mills theory in eq. (2.69), we used the following relation

$$x - \frac{1}{2}x^2 + \frac{1}{3}x^3 + \cdots = \sum_{n=1}^{\infty} (-1)^{n+1} \frac{x^n}{n} = \log(1+x) \,, \tag{3.9}$$

with $x = \lambda L_i L_j$ to resum terms with multiple windings. What we ignored so far is that the power series on the left hand side of the equation has a finite radius of convergence, namely $|x| < 1$. Our complex action problem is just a result from using the power series outside its region of convergence. For G_2 the situation is much more malign than we orignialy thought, as we have $\max(LL) = 7^2$. This means we start to run into problems already at $\lambda \geq \frac{1}{49}$, here the logarithm is of course real and positiv but the power series on the left hand side of eq. (3.9) diverges. This would not be a problem if the critical coupling for the deconfinement transition λ_c would be less than λ_T, however this is not the case. In fact if we use the resummed effective action we do not see a true phase transition at all. Fig. 3.6 shows that the resummed model does not contain a 1st order deconfinement transition. The Polyakov loop starts to rise continuously at $\lambda \sim 0.08 > \lambda_T \gg \frac{1}{49}$. Fig. 3.7 shows that the deconfinement transition is a smooth crossover as the susceptibility does not diverge with the volume of the system. Thus, the resummed model can not be used to describe the phase structure of of G_2 Yang-Mills theory. Even if we treat the right hand side of eq. (3.9) as an analytic continuation above $\lambda > \frac{1}{49}$ the negative contributions to the partition function set in at $\lambda = 1/14 < 0.08$. One should note that the strong coupling expansion is still valid for all gauge groups and

for all couplings β, as the power series of an exponential function has an infinitely large radius of convergence. What does break down in this case is this particular resummation scheme we have chosen, to take Polyakov loops with multiple winding numbers into account.

3.2.1. Effective Theory for G_2 Yang-Mills Theory

In the last paragraphs we showed that we are not able to use the resummed model as an effective theory for G_2 Yang-Mills theory so we turn back to the effective action without resummation of multiple-winding loops

$$S_{\text{eff}} = -\lambda \sum_{<ij>} L_i L_j \ , \tag{3.10}$$

as an effective theory of the thermodynamics of pure G_2 gauge theory. As we said above, we expect the theory to exhibit a first order phase transition and indeed, this is what we find. Fig. 3.8 shows the Polyakov loop as a function of the effective coupling λ, where we find a jump at $\lambda = 0.0988(50)$. We have also looked at the distribution of the Polyakov loop around λ_c and found a double peak structure, which is the smoking gun for a 1st order phase transition. The histogram is shown in Fig. 3.9. Even though the fundamental domain of G_2 is asymmetric, there is an approximate Z_3 center symmetry [96]. Therefore, one should in principle be able to observe a three peak structure in the Polyakov loop histograms. However, it is quite challenging to actually observe this also in a full 4d simulation.
We have also tried to extract the critical lattice coupling β_c from our simulations by using eq. (2.142). Unfortunately there are only few publications on critical lattice couplings for G_2. This is due to the fact that for small N_t the topological bulk transition is very close to the deconfinement transition and for large N_t numerical simulations become very expensive. The only established value for the critical coupling in the literature is for $N_t = 6$, here one finds $\beta_c/N_c = 1.395$ [97]. By using $\lambda_c = 0.0988$ and inverting eq. (2.142) we find

$$\frac{\beta_c}{N_c} = 1.57514 \ . \tag{3.11}$$

This is a deviation of 12% from the actual result. This is due to the fact that our equation for $\lambda(N_t, \beta)$ only takes corrections of up to order $\mathcal{O}(u^6)$ into account and we do not resum multiple-winding loops. We can try to take partial resummations of multiple windings into account, e.g. by summing up loops that wind up to three times around the lattice. However this only leads to minor changes, the critical effective coupling λ_c shifts down to $\lambda_c = 0.068(1)$ from which we can extract $\beta_c/N_c = 1.54945$. Since including winding loops has little effect on β_c, let us again take a look at the expression for $\lambda(N_t, \beta)$. When we try to extract the critical β for SU(2) Yang-Mills theory from a effective coupling with corrections up to order $\mathcal{O}(u^6)$ for $N_t = 6$ we find a deviation of 27% for β_c. So it does not come as a surprise that our extracted β_c for G_2 Yang-Mills theory is off by 12%. Still, this is very unfortunate when we want to use our effective theory in a fixed scale approach. In a fixed scale approach the lattice coupling β is left

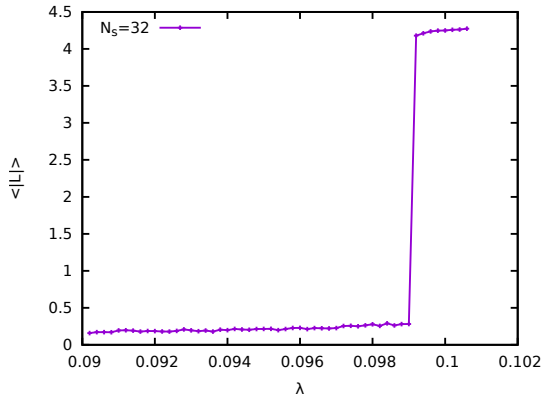

Figure 3.8.: Polyakov loop as a function of the effective coupling λ for a $N_s = 32$ lattice with the action (3.10), without resummation. The error bars are hidden inside the points

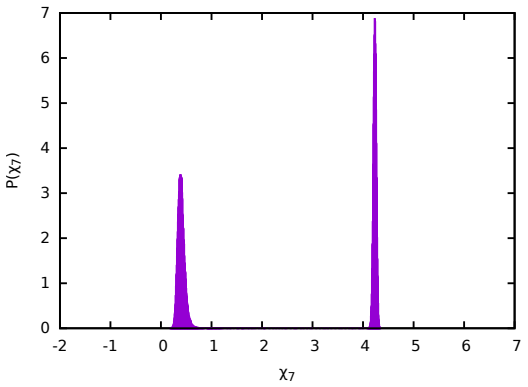

Figure 3.9.: Polyakov loop histogram in the vicinity of the critical coupling λ_c. The double peak structure is an evidence for a first order phase transition.

constant, the only parameter left to tune the temperature is N_t. The 12% deviation in β_c has a dramatic effect for the critical N_t when working at a fixed scale. When choosing $\beta/N_c = 1.395$, corresponding to the critical coupling at $N_t = 6$, the critical N_t from $\lambda_c(\beta, N_t)$ lies between $N_t = 2 - 3$. To correct this effect we can try to include the higher u corrections in the effective coupling λ by using an ansatz of the form

$$\lambda_1(u, N_t, \theta) = u^{N_t} \exp[N_t(4u^4 + 28u^5 + \frac{82}{3}u^6 + \theta u^7)] \, . \tag{3.12}$$

We now fix the unknown parameter θ such that

$$\lambda_1(u(\beta_c(N_t = 6)), N_t = 6, \theta = 608.547) = \lambda_c \, . \tag{3.13}$$

Unfortunately, there are no reliable results for β_c at $N_t \neq 6$ from G_2 Yang-Mills simulations, so we are not able to check if our ansatz is indeed reasonable. We can however check, if it is for the case of SU(2) Yang-Mills theory. When we use an ansatz of this form to fix θ at $N_t = 4$ we find that in the range of $N_t = 3 - 16$ the critical β_c is reproduced with better than 5% deviation.

With eq. (3.12) we are now able to make predictions about the critical couplings for different N_t in G_2 Yang-Mills theory. These predictions are summarized in table 3.1.

3.2.2. Dynamical Fermions and Critical κ

We can now include dynamical fermions into our simulations. In the case of two-color QCD we saw a drastic change in the features of our theory when we included dynamical fermions. Here, the case is somewhat different: center symmetry can not be broken explicitly, as there is no center of G_2. Still, there is an approximate Z_3 symmetry

N_t	β_c/N_c
4	1.348
6	1.395
8	1.416
12	1.436
16	1.4457

Table 3.1.: Predictions from the effective theory for the critical couplings β_c/N_c of G_2 Yang-Mills theory.

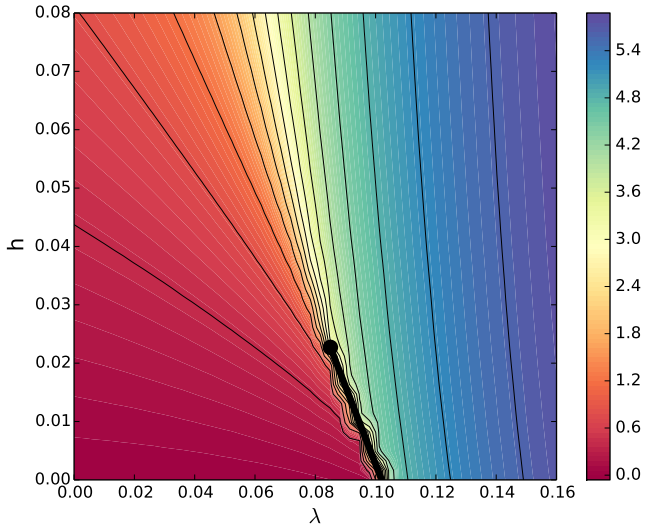

Figure 3.10.: Contour plot of the Polyakov loop in the $\lambda - h$-plane of the phase diagram for $N_s = 24$. The critical 1st order line and the critical point are indicated by the black line and point.

but on the other hand dynamical fermions act like an external magnetic field, breaking this approximate symmetry explicitly. However, first order phase transitions are stable against weak external fields, but only up to some critical value. As a consequence we expect the deconfinement phase transition to weaken with decreasing quark mass until it becomes a second order phase transition at a critical point. From there on the transition should be an analytic crossover. Fig. 3.10 shows a contour plot of the Polyakov loop in the $\lambda - h$-plane of the phase diagram. We can see that, according to our assumptions, there is a first order phase transition that ends in a critical point. The critical point is located at

$$\lambda_c = 0.0850(5) \quad \text{and} \quad h_c = 0.0227(5)\ . \tag{3.14}$$

Now we can use eq. (2.153) to extract a critical hopping parameter κ_c at a given N_t. For $N_t = 6$ the critical hopping parameter is $\kappa_c = 0.230(2)$, which is relatively large

compared to the critical values for heavy QCD [41]. Unfortunately, there is no data from full 4d G_2-QCD simulations for the critical κ_c. However, G_2-QCD simulations at $\kappa = 0.1565$ in [98] seem to indicate that we have a cross-over at this value of κ [99]. We conclude that our equation for the effective fermion coupling $h(\kappa, \beta, N_t)$ is not valid for hopping parameters in this range or we need to include additional spatial hopping terms in the effective action to accurately determine κ_c. In sec. 4.2 we find evidence that additional spatial hopping terms have to be taken into account to reach convergence of the hopping series for $\kappa \approx 0.06$ and $N_t = 6$.

4
Results at Finite Density

Now, we will turn to the application of the effective theory to the cold and dense part of the phase diagram of QCD-like theories. We will start with results from the effective theory for two-color QCD and then discuss results from the effective theory for G_2-QCD.

Numerical Details

All our simulations were preformed on NIVIDIA GPUs. Since the effective action is quite complicated we have used the Metropolis algorithm for the update sweeps in our simulations. For the effective theory for two-color QCD we explicitly made measurements of the autocorrelations in the density and the Polyakov loop, for that purpose we have generated 10 000 configurations. Especially in the transition region between the two exponential regimes that we are interested in here we find basically no autocorrelations. Only as we approach lattice saturation for $\mu \geq m_q$, see below, we observe some non-negligible autocorrelations in our data. However, for locating the diquark onset and the pseudo-critical values for the Polyakov loop we only use data points at values for the chemical potential of $\mu \leq 9.995$ GeV where the autocorrelations are negligible. To be completely safe we nevertheless use only every tenth configuration for the measurements of the observables, yielding 1000 uncorrelated measurements.

To these measurements we have applied a standard jackknife analysis for the statical mean and error of our data. The resulting errorbars are included in Fig. 4.1. Because in linear plots they are always smaller than the symbols, we have omitted them in most of the other figures with the exception of Fig. 4.9 where we show an example of the transition region in close-up with errorbars. In the logarithmic plots the observed scatter of the data at extremely small values of the density or the Polyakov loop serves as an indication of these residual small relative errors from the independent measurements.

In the effective theory for G_2-QCD we did not determine the autocorrelations in our

data, as we expect them to be small when the lattice is not saturated. Still, we used only every tenth configuration for the measurements of observables. Again, we omitted the error bars in the plots, as they are not visible in a linear scale.

4.1. Effective Theory for Two-Color QCD in the Cold and Dense Regime

We now turn our attention to the investigation of the cold and dense regime of the two-color QCD phase diagram. Similar to the nuclear liquid-gas transition in QCD there should be a phase transition at low temperature and finite baryon chemical potential to a phase with finite baryon density. In the case of two-color QCD this should be a phase transition to a Bose-Einstein condensate of scalar diquarks, where a non-vanishing diquark condensate $\langle qq \rangle \neq 0$ spontaneously breaks the baryon $U(1)_B$. In contrast to QCD where we have a 1st order liquid-gas phase transition, the phase transition to the Bose-Einstein condensate is of 2nd order and continuous. Therefore at $T = 0$ the transition must occur at $\mu_B = m_d$, i.e. $\mu_c = m_d/2 = m_\pi/2$. The BEC is not a self-bound liquid. Thus, the transition happens exactly, when the chemical potential is equal to half the diquark mass unlike for the nuclear matter liquid-gas transition, where the critical μ_c is shifted by a binding energy $\mu_c = m_B - \epsilon$.

Leading-order mean-field density

Let us start by analyzing the partion function in the strong coupling limit $\lambda = \beta = 0$, where we can solve the integrals for the static part of the fermion determinant analytically. This gives us aditional insight into the model and the effective degrees of freedom. In the strong coupling limit, the partition function factorizes,

$$Z(\beta = 0) = \left(\int dL \, [1 + hL + h^2]^{2N_f} \times [1 + \bar{h}L + \bar{h}^2]^{2N_f} \right)^{N_s^3} . \tag{4.1}$$

For $T \to 0$ at a finite chemical Potential μ we have $\bar{h} \to 0$. We can now solve the gauge integrals analytically, in the case of $N_f = 1$ we find

$$\begin{aligned} Z(\beta = 0) &= \left(\int dW \, [1 + 2h^2 + h^4 + 2hL + 2h^3 L + h^2 L^2] \right)^{N_s^3} , \\ &= \left(1 + 3h^2 + h^4\right)^{N_s^3} . \end{aligned} \tag{4.2}$$

We see that for $N_f = 1$ and $T \to 0$, $\mu > 0$ the contributions to the partition function at each point in space come from diquarks and states consisting of 4 quarks. The Prefactors can be identified as spin degeneracies, i.e. we have a vector diquark and a scalar 4 quark state. This shows us that for $N_f = 1$ we do not have a scalar diquark and therefore no Bose-Einstein condensate of scalar diquarks as the groundstate for $\mu \geq m_d/2$. For

N_f=2 the partition function in the strong coupling limit reads

$$\begin{aligned} Z(\beta=0) &= \left(\int dL \, [1 + h_u L + h_u^2]^2 \times [1 + h_d L + h_d^2]^2 \right)^{N_s^3} \\ &= \Big(1 + 3(h_u^2 + h_d^2) + h_u^4 + h_d^4 + 4h_u h_d + 4(h_u^3 h_d + h_d^3 h_u) + 3(h_u^4 h_d^2 + h_d^4 h_u^2) \\ &\quad + 10 h_u^2 h_d^2 + 4 h_u^3 h_d^3 + h_u^4 h_d^4 \Big)^{N_s^3} . \end{aligned} \tag{4.3}$$

We can identify the contributions to Z as diquarks and their composites. In particular we find vector diquarks for all isospin values and an additional scalar diquark in the isopin zero sector. Since we took the trace in Dirac space we can no longer distinguish between different parity states but they are degenerate. However from analyzing correlators in full two-color QCD we know the theory contains a scalar and a pseudo scalar diquark. Therefore the $N_f = 2$ theory may have a scalar Bose-Einstein condensate as groundstate for $\mu \geq m_d/2$. Further, we observe an explicit symmetry between flavors and also between states with $4 \pm n$ quarks. This second symmetry leads to a particle-hole symmetry around the half-filling point of the lattice.

Since all our simulations are done on a lattice with a finite size we will always encounter a finite expectation value of the Polyakov loop. To include this finite volume artifact we will use eq. (4.1) with mean-field description for the Polyakov loop. At $T \to 0$, $\mu > 0$ the partition functions reads

$$Z = [1 + 2h\tilde{L} + h^2]^{2N_f N_s^3} , \tag{4.4}$$

where a factor of two was inserted because the mean-field Polyakov loop $\tilde{L}$ here is normalized to assume values within $[-1, 1]$. The quark number density then follows as

$$\begin{aligned} n &= \frac{T}{V} \frac{\partial}{\partial \mu} \ln Z , \\ a^3 n &= 4N_f \frac{1 + \tilde{L} e^{\frac{m_q - \mu}{T}}}{1 + 2\tilde{L} e^{\frac{m_q - \mu}{T}} + e^{\frac{2(m_q - \mu)}{T}}} . \end{aligned} \tag{4.5}$$

The same expression can be derived from a Polyakov-Quark-Meson-Diquark model [53] for very heavy quarks where the quark mass is larger than the UV cutoff Λ. For $\tilde{L} = 1$ it simply reduces to the zero-momentum occupation number of the Fermi-Dirac distribution since the momentum is negligible compared to the mass $m^2 \gg p^2$. In the deconfined phase it thus describes a free gas of heavy quarks. In the confined phase with $\tilde{L} = 0$ statistical confinement rules out single quark states and we only find states with integer baryon numbers. We will see below that for small but finite Polyakov-loop expectation values $\tilde{L} > 0$, and small T, Eq. (4.5) due to imperfect confinement behaves as a quark gas, suppressed by $\tilde{L}$, up to some critical chemical potential $\mu_c(T)$ where it starts to reflect the behavior of a diquark gas with $m_d = 2m_q$ at this leading-order. By considering $\mu < m_q$ and hence $x \equiv \exp\{(m_q - \mu)/T\} > 1$, we can then distinguish two regimes:

$$\frac{a^3 n}{4N_f} \to \begin{cases} e^{(\mu_B - m_d)/T} , & \tilde{L}\, x \ll 1 , \\ \tilde{L}\, e^{(\mu - m_q)/T} , & \tilde{L}\, x \gg 1 . \end{cases} \tag{4.6}$$

The transition occurs at around $\tilde{L}\,x \sim 1$ or respectively $\mu_c \sim m_q + T \ln \tilde{L}$.

Scale Setting and Units

Of course we could state all our results in terms of the lattice spacing a. However to have a more intuitive view on the results we will set a scale and give our results in natural units. The first thing to do is to set a scale. We will assume that quarks as heavy as those used here only have a negligible influence on the running of the coupling, therefore we use the non-perturbative SU(2) Yang-Mills β-function from [92]

$$\frac{1}{a\sqrt{\sigma}} = \exp\left(\frac{\beta - d}{b}\right) , \tag{4.7}$$

with the parameters

$$d = 1.98(1) , \qquad b = 0.305(6) . \tag{4.8}$$

In lack of phenomenological input we somewhat arbitrarily use the typical $\sqrt{\sigma} = 440$ MeV from QCD also for the string tension of two-color QCD. With Eqs. (4.7) and (2.131) we are then able to assign a physical scale to our systems. In all our simulations the diquark mass from Eq. (2.131) is adjusted in this way to $m_d = 20$ GeV, and the temperatures range between $T = 3.454$ MeV and 9 MeV. On our finest lattice with $\beta = 2.5$, corresponding to $a = 0.0810$ fm, this amounts to $\kappa = 0.00802123$ and N_t values between 269 and 700. The parameters for the coarser lattices with β values down to 2.4 lead to even smaller values for the expansion parameter.

Convergence of the hopping series

In order to assess the range of validity of the effective theory we need to test the convergence properties of the hopping series for various parameter choices. As can be seen from Equation (2.127) the relevant expansion parameter for the effective theory is $\kappa^2 N_t/N_c$. Because we are interested in very low temperatures $T = 1/aN_t$, we need lattices of large extend N_t in the temporal direction, especially as we go to smaller lattice spacings a. Therefore our hopping parameter κ needs to be sufficiently small. This implies that one can reach smaller quark masses at higher temperatures and vice versa. To check the convergence of the hopping expansion we compare expectation values for the densities $a^3 n$ from simulations including corrections up to $\mathcal{O}(\kappa^2)$ and $\mathcal{O}(\kappa^4)$ for different values of the expansion parameter $\frac{\kappa^2 N_t}{N_c}$. By taking a closer look at the effective action (2.127) one recognizes that the convergence properties of the hopping series change with chemical potential μ. For small chemical potentials we have $h \to 0$ and all $\mathcal{O}(\kappa^2 N_t/N_c)$ corrections become negligible. For large chemical potentials we have $h \to \infty$ and all all $\mathcal{O}(\kappa^2 N_t/N_c)$ corrections become zero or constant and therefore also negligible. The effect of the corrections is most prominent when h is of order 1 or respectively $\mu = m_d/2$, which is where we should check the convergence properties of the hopping series. Figure 4.1 shows a plot of the two densities for $\mu = m_d/2$ at $\beta = 2.5$, including gauge corrections. The two agree reasonably well for all values of $\kappa^2 N_t/2$ up to slightly above 0.02. Our N_t range of 269 to 700 is chosen such that $\kappa^2 N_t/2$ lies within 0.0087 and 0.0225, and hence within

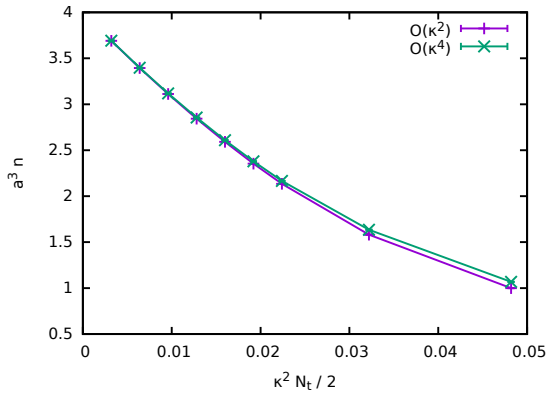

Figure 4.1.: Comparison of quark densities evaluated at the orders κ^2 and κ^4, both for $\kappa = 0.00802$, $\beta = 2.5$, $\mu = m_d/2$ and N_t ranging between 100 and 2400, including gauge corrections.

the range of validity of the hopping expansion, cf. Fig. 4.1.
Another matter of convergence is the convergence of the resummations of multiple-winding loops we used. Strictly speaking, our approach is only valid at $\mu < m_q$. However, we will also analytically continue the effective action, derived at $\mu < m_q$, to larger μ and find the expected behavior.

4.1.1. Results for $N_f = 1$

In this subsection we first present our numerical results for the Polyakov loop and the quark density in the effective theory at low temperatures with one quark flavor, $N_f = 1$. Even though it is not quite clear what the physical meaning of the Polyakov loop at finite density is, we will take it as an indication of deconfinement at high density and low temperature. We plot the the Polyakov-loop expectation value in Fig. 4.2, where $\langle|L|\rangle$ stands for the usual expectation value of the modulus of the volume averaged Polyakov loop

$$L \equiv \frac{1}{V}\sum_{\vec{x}} L_{\vec{x}} \,. \tag{4.9}$$

Because of the presence of dynamical quarks, even for vanishing net-baryon density, the Polyakov loop will have a small but nonzero expectation value $\langle|L|\rangle > 0$. For the parameters of Fig. 4.2 its $\mu = 0$ value is $\langle|L|\rangle = 0.012$. For aspect ratios as the one considered here, with $N_t/N_s \approx 30$ in this example, this value is determined by the finite spatial volume. It is therefore basically temperature independent. It furthermore also remains constant in μ until just below the onset of the density near $m_d/2$ because the temperature of $T = 5$ MeV here is so low that no baryonic degrees of freedom are being excited as long as the baryon chemical potential 2μ stays well below the gap in the baryon spectrum. From Fig. 4.2 it appears however that $\langle|L|\rangle$ starts to rise from its $\mu = 0$ value before the onset of the density so that we can not distinguish baryon density

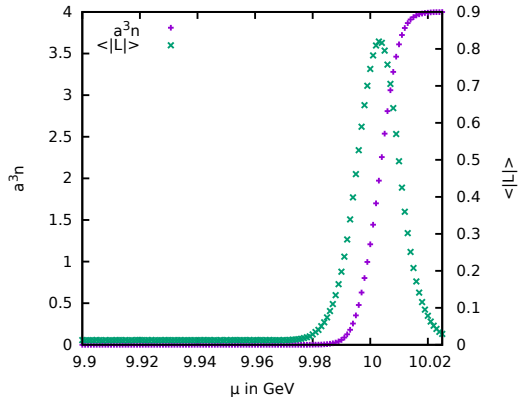

Figure 4.2.: Quark density a^3n in lattice units and Polyakov-loop expectation value $\langle|L|\rangle$, both over μ, with simulation parameters $\beta = 2.5$, $\kappa = 0.00802$, leading to $m_d = 20$ GeV, $N_s = 16$, $N_t = 484$, corresponding to $T = 5$ MeV, and $N_f = 1$.

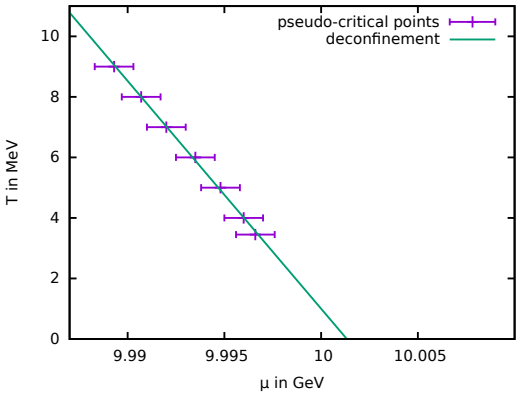

Figure 4.3.: The pseudo-critical line for the deconfinement transition from simulations with the same parameters as in Fig. 4.2 except for different N_t, corresponding to $T = 9, 8, \ldots 4$ MeV and 3.454 MeV, with a linear extrapolation to $T = 0$.

from quark density here. As we will discuss in the next subsection, however, there is a very small diquark contribution in the density above $\mu_c \approx 9.96$ GeV at this temperature which is not visible on the linear scale of Fig. 4.2 but where the Polyakov loop still has its zero-density expectation value. We will provide some evidence that this diquark-density onset might stay below the deconfinement transition when we extrapolate both to $T = 0$ for $N_f = 2$ with scalar diquarks below.

At larger values of the chemical potential the quark density saturates at $a^3n = 2N_cN_f$. This is the maximum number of quarks per site due to the Pauli principle, as in the effective theory for heavy quarks in $SU(3)$ [40]. This behavior which is a lattice artifact has previously also been observed in finite density simulations of two-color [47] and G_2-QCD [98]. This saturation leads to an effective quenching of the quarks and hence the Polyakov loop decreases again as it is approached. We also analyzed the Polyakov-loop susceptibility and found no increase of its rather broad maximum with the lattice volume hence indicating a smooth cross-over behavior rather than a deconfinement phase transition in the infinite volume limit. The pseudo-critical chemical potential μ_{pc} from the inflection point of $\langle|L|\rangle$ along the μ axis is shown in Fig. 4.3. It coincides with the point where $\langle|L|\rangle$ reaches half its maximum value. By determining this μ_{pc} for different temperatures we obtain a pseudo-critical line for the deconfiment transition at low temperature which can be extrapolated to $T = 0$ as shown in Fig. 4.3. We can see that the pseudo-critical line terminates at μ_{pc} slightly above 10 GeV which corresponds to half the scalar-diquark mass from eq. (2.140) with the parameters used here.

We conclude this subsection by discussing in some more detail the quark-number

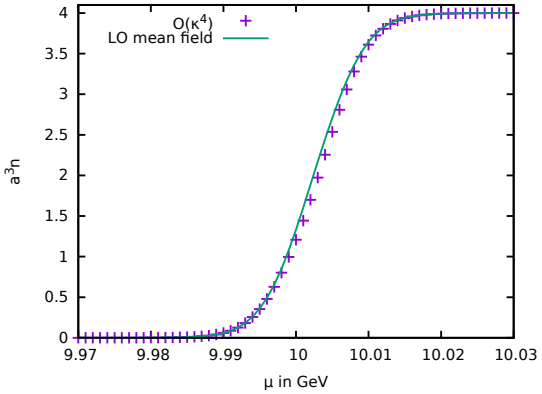

Figure 4.4.: Comparison of the quark density at order κ^4 from Fig. 4.2 to the leading-order formula in Eq. (4.5) with $\tilde{L}$ replaced by the corresponding data for $\langle|L|\rangle/2$ from Fig. 4.2, $T = 5$ MeV.

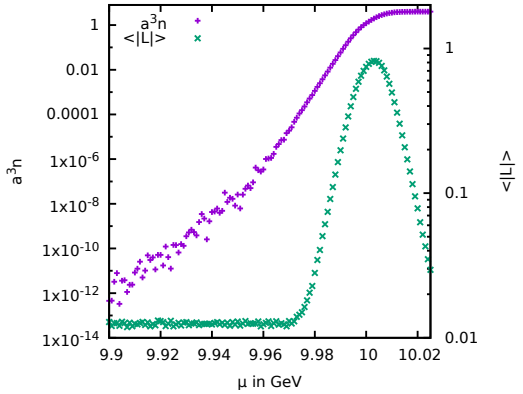

Figure 4.5.: Logarithmic plot of the density in lattice units a^3n and the Polyakov loop $\langle|L|\rangle$ as a function of μ in physical units at $T = 5$ MeV with the same parameters as in Fig. 4.2.

density n defined by

$$n = \frac{T}{V}\frac{\partial}{\partial\mu}\ln Z\ . \tag{4.10}$$

As mentioned above, Fig. 4.2 shows the strong increase in the density in lattice units a^3n at a value of the quark chemical potential around $\mu = m_d/2$, from where on it rapidly grows to its saturation value with each lattice site fully occupied by $2N_cN_f = 4$ quarks. This transition is described qualitatively well by the leading-order mean-field formula in Eq. (4.5). This can be seen in Fig. 4.4 where we compare the data for the quark density at order κ^4 from Fig. 4.2 to the leading-order form in Eq. (4.5) with the corresponding $am_q = -\ln(2\kappa)$ for the strong-coupling limit, and with $\tilde{L}$ replaced by $\langle|L|\rangle/2$, i.e., using the μ-dependent data for the Polyakov-loop expectation value of Fig. 4.2 in the mean-field approximation. To resolve the differences we need to have a closer look at the behavior of the chemical potential and temperature dependence of the quark density, especially in the region where $\tilde{L}\,x \sim 1$ with $x = \exp\{(m_q - \mu)/T\}$ as defined in Sec. 4.1 above. Fig. 4.5 shows a logarithmic plot of the density and the Polyakov loop of Fig. 4.2. We observe two different regimes of exponential increase before the density approaches its saturation value. They are separated by a kink in the logarithmic plot, here at $\mu_c \approx 9.96$ GeV, where the Polyakov-loop still is constant at its $\mu = 0$ expectation value, $\langle|L|\rangle/2 \approx 0.006$.

The two regimes correspond to the two limits in eq. (4.6) of the leading-order mean-field density, Eq. (4.5). This is demonstrated in Fig. 4.6 where we compare the density to two corresponding fits:

When we fit the data in the region of the second exponential increase, for μ values between 9.96 GeV and 9.99 GeV, to

$$a^3n = 4N_f \exp\{(2\mu - m_{\text{fit}})/T\} \tag{4.11}$$

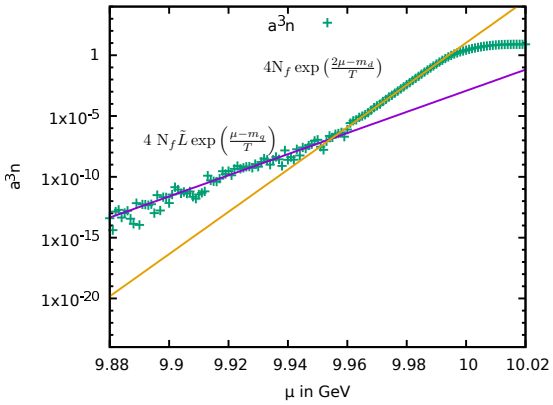

Figure 4.6.: Logarithmic plot of the density in lattice units a^3n at $T = 5$ MeV compared to one-parameter fits using $\tilde{L}$ for $\mu < 9.96$ GeV and m_d for $\mu > 9.96$ GeV, see text.

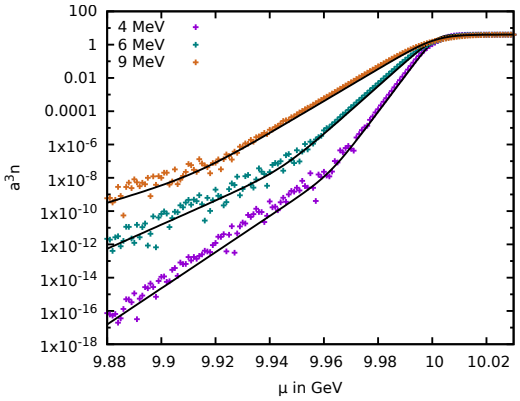

Figure 4.7.: Comparison of the measured density with the leading-order mean-field density with $\tilde{L} = \langle L_{\vec{x}} \rangle / 2$ at $m_d = 20$ GeV, $\beta = 2.5$, $\kappa = 0.00802$, and different temperatures.

with a single parameter $m_{\rm fit}$ we obtain for $N_f = 1$,

$$m_{\rm fit} = 20.0045(5)\,\text{GeV}\,. \tag{4.12}$$

For comparison, with the same lattice parameters the quark mass from Eq. (2.89) becomes $m_q^{(0)} = 10.0024$ GeV at the leading-order $n + m = 0$, $m_q^{(4)} = 10.0014$ GeV at the order $n + m = 4$, and $m_q^{(7)} = 10.0013$ GeV at the order $n + m = 7$. Therefore, the fit parameter $m_{\rm fit}$ is consistent with $2m_q^{(0)}$ but slightly larger than $2m_q = 20.0028(2)$ at the same order $n + m = 4$ (with an error of the size of the higher-order corrections up to $n + m = 7$ as given explicitly in Eq. (2.89)). It is larger than the corresponding scalar diquark mass, $m_d = 20$ GeV from Eq. (2.140), which might simply reflect the fact that scalar diquarks do not exist for $N_f = 1$. A daring interpretation would be that we see a heavier diquark mass here, such as that of an axial-vector diquark which can exist also for $N_f = 1$.

To test this, we have done the same analysis with the same parameters also for two flavors (see the next subsection). The same fit to the form in (4.11) then yields for $N_f = 2$,

$$m_{\rm fit} = 19.9986(10)\,\text{GeV}\,, \tag{4.13}$$

which is now indeed very close to the scalar diquark mass m_d and significantly smaller than $2m_q$. In order to quantitatively describe this regime of exponential increase we therefore have to replace $2m_q$ by m_d in the leading-order mean-field formula for the density in Eq. (4.5). This indicates that matter on this side of the kink consists of diquark excitations.

The first exponential increase, for the μ values below 9.96 GeV, is described by

$$a^3 n = 4N_f\,\tilde{L}\,\exp\{(\mu - m_q)/T\}\,. \tag{4.14}$$

In this case we use $m_q = 10.0014$ GeV for the quark mass at this order and fit the data via $\tilde{L}$ as the free parameter. For the one-flavor data of Fig. 4.6 this leads to $\tilde{L}$ of the order of 10^{-4}, however, with a very large uncertainty. It determines the precise value of the onset μ_c of the diquark density, by the intersection point of the two different exponential fits (4.11) and (4.14), as

$$\tilde{L} = \exp\{(\mu_c - m_d + m_q)/T\} \; . \tag{4.15}$$

With $m_d = m_{\text{fit}}$ from (4.12) for the $N_f = 1$ data in Fig. 4.6, for example, this leads to values between $\tilde{L} = 8 \cdot 10^{-5}$ for $\mu_c = 9.956$ GeV and $\tilde{L} = 1.2 \cdot 10^{-4}$ for $\mu_c = 9.958$ GeV. In any case, it is much smaller than the zero-density value of $\langle|L|\rangle/2 \approx 0.006$. Instead we observe that it is more consistent with the expectation value of the local Polyakov loop $L_{\vec{x}}$. Its expectation value is extracted from the per-site probability distribution $P(L_{\vec{x}})$ which we obtain by histograming the local Polyakov-loop variable $L_{\vec{x}}$ as in [92]. At $T = 5$ MeV, with $\beta = 2.5$ and $\kappa = 0.00802$, we obtain for this observable a zero-density value of about $\langle L_{\vec{x}}\rangle \sim 10^{-4}$ instead of $\langle|L|\rangle \approx 0.012$ for the modulus of the volume-averaged Polyakov loop. This suggests that one should use the local Polyakov-loop expectation value $\langle L_{\vec{x}}\rangle$ in mean-field approximations as Eq (4.5). The reason behind this can be found by analyzing values of the local Polyakov loop: since the probability distribution of the local Polyakov loops stays symmetric around zero up to μ_{pc} we will always have some negative Polyakov loops. A quick look at eq. (4.5) shows that a negative local Polyakov loop induces negative local particle numbers. Now the expectation value $\langle L_{\vec{x}}\rangle$ stays positiv but using $\langle|L|\rangle$ as mean-field Polyakov loop value completly ignores the negative contributions and therefore overestimates the density. Like $\langle|L|\rangle$, $\langle L_{\vec{x}}\rangle$ is independent of the chemical potential below the deconfinement crossover at μ_{pc}. And as soon as the Polyakov-loop starts to rise from its constant zero-density expectation value the two agree well within the errors. It is only the residual small value at vanishing net-baryon density due to imperfect confinement in a finite volume in which the two differ simply because it takes longer for the modulus to vanish than the local Polyakov loop in the infinite-volume limit for $\mu < \mu_{pc}$. This difference is only relevant at densities in lattice units below 10^{-4} and hence not visible on the linear scale of Fig. 4.4 above.

In fact, using the local Polyakov-loop expectation value $\langle L_{\vec{x}}\rangle$ for various temperatures in the leading-order mean-field formula for the quark density, Eq. (4.5), describes the data especially also in the low-density region around the diquark-density onset at μ_c very well as can be seen in Fig. 4.7. These are not fits. We simply use Eq. (4.5) with $\tilde{L} = \langle L_{\vec{x}}\rangle/2$ here to describe the quark density over the whole range of temperatures we have investigated. It describes the imperfect statistical confinement of quarks for μ below $\mu_c = m_d - m_q + T\ln(\langle L_{\vec{x}}\rangle/2)$, an ensemble of diquarks above μ_c, and quark matter with lattice saturation for μ larger than μ_{pc} where $2\tilde{L} = \langle L_{\vec{x}}\rangle = \langle|L|\rangle$ as in Fig. 4.4, all at the same time.

4.1.2. Results for $N_f = 2$

In this subsection we discuss the results from the effective theory with $N_f = 2$ degenerate quark flavors in somewhat more detail. In particular, we describe how well the onset of

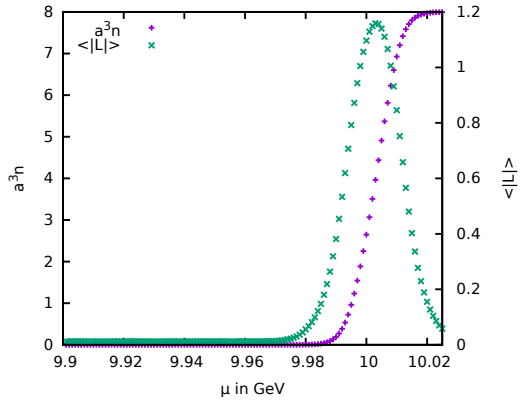

Figure 4.8.: Quark density in lattice units and Polyakov-loop expectation value $\langle|L|\rangle$, both over μ, with the same simulation parameters as in Fig. 4.2, but for $N_f = 2$ here.

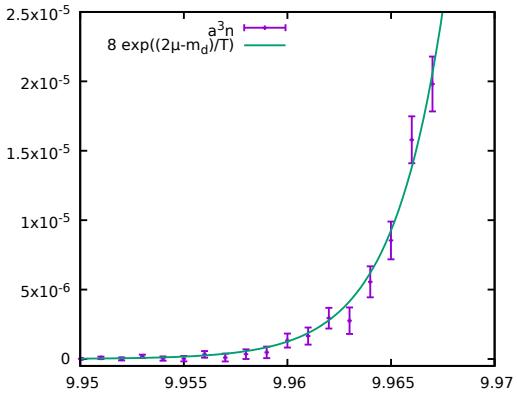

Figure 4.9.: Zoom-in of Fig. 4.8 on the region of the diquark onset. Also shown is the fit to the LO mean-field formula for the second exponential increase from Eq. (4.11).

the diquark density at $\mu = \mu_c$ agrees with the scalar diquark mass m_d from Eq. (2.140) which we know exists for $N_f = 2$.

As a first example in Fig. 4.8 we present the $N_f = 2$ results for the quark density and the Polyakov loop on our finest lattice, with $\beta = 2.5$, $\kappa = 0.00802123$, $N_s = 16$ and $N_t = 484$. This set of parameters corresponds to $m_d = 20$ GeV and $T = 5$ MeV at a lattice spacing of $a = 0.081$ fm as in the previous subsection for the one-flavor case. Both observables show the same qualitative behavior as for $N_f = 1$ before.

The most obvious differences between $N_f = 1$ and 2 are the different saturation densities given by $a^3 n_{\rm sat} = 2N_c N_f$ and the maximum value of the Polyakov loop $\langle|L|\rangle$ which is a bit higher for $N_f = 2$. The direct comparison of the Polyakov-loop expectation values in Fig. 4.10 shows that the deconfinement crossover tends to start at somewhat smaller values of μ for $N_f = 2$, and gets quenched later, likewise.

The difference between the normalized quark-number densities $n/n_{\rm sat}$ for $N_f = 2$ and $N_f = 1$ is shown in Fig. 4.11. We can see a deviation around $\mu = 10$ GeV. This is in line with the observation that the deconfinement transition happens earlier for $N_f = 2$ as well. As described for $N_f = 1$ above, we follow the same procedure with $N_f = 2$ for various temperatures from 9 MeV down to 3.454 MeV. That is, for each temperature we determine the intersection point of the two exponential regimes in the quark density (for $N_f = 2$ their μ-values are consistently about $1 - 2$ MeV lower than those for $N_f = 1$). Since the mass-parameter in the second exponential for $N_f = 2$, see Eq. (4.13), agrees well with the scalar diquark mass, $m_d = 20$ GeV from Eq. (2.140), we now take the intersection of the lines in logarithmic plots analogous to Fig. 4.6 as the onset of baryonic diquark matter and extrapolate the corresponding onset chemical potentials μ_c to $T = 0$. The result for the $N_s = 16$ lattice is shown in Fig. 4.12. Using a linear extrapolation as in the figure, which is consistent with a temperature independent $\tilde{L} \approx \langle L\rangle/2$, the

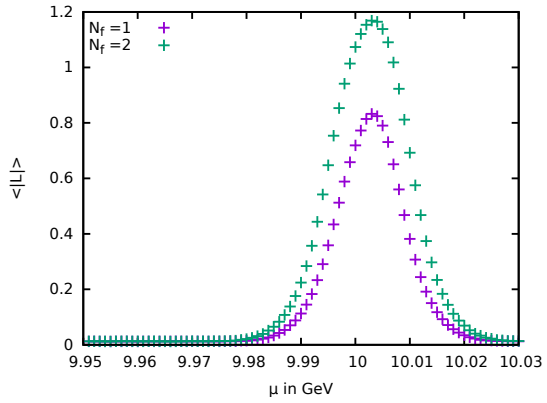

Figure 4.10.: Comparison of the Polyakov loop $\langle |L| \rangle$ for $N_f = 1$ and 2 at $T = 5$ MeV with parameters as in Figs. 4.2 and 4.8.

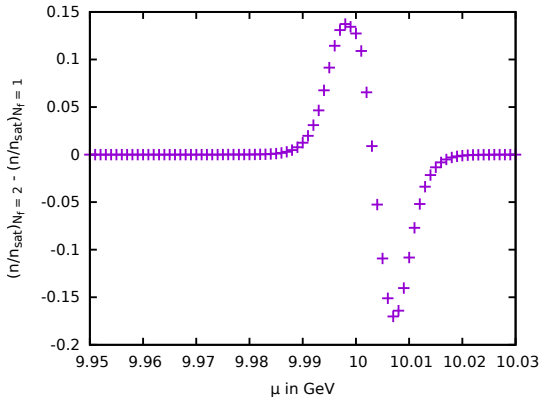

Figure 4.11.: Difference between the normalized quark number densities for $N_f = 2$ and $N_f = 1$ at $T = 5$ MeV.

result for the $T = 0$ diquark onset on the $N_s = 16$ lattice is $\mu_c = 9.9994(18)$ GeV and hence includes $m_d/2 = 10$ GeV within the error. Larger lattices lead to smaller values of $\tilde{L}$ and hence a smaller slope $\ln \tilde{L}$ in the linear extrapolation, but the extrapolated μ_c remains the same. For comparison, the same analysis was also done on a $N_s = 48$ lattice with the result that $\mu_c = 9.9998(9)$ GeV as also shown in Fig. 4.6. The extrapolation of the diquark onset to $T = 0$ is dominated by its value at $T = 3.454$ MeV. To obtain an estimate for the systmatic error of the fit to the exponentials we have used three different fit intervals for the onsets at $T = 3.454$ MeV and took the average. Than we used the combination of the corresponding error with the error of the extrapolation to calculate the total error of the critical chemical potential μ_c at $T = 0$.

In order to test the scaling of this onset we have performed the same analysis also for 7 different lattice couplings β between 2.4 and 2.5, corresponding to lattice spacings between $a = 0.1124$ fm and 0.0810 fm with κ values adjusted so that m_d from Eq. (2.140) remains fixed at 20 GeV as before. Again, for each β we extract the corresponding intersection points of the two exponential regimes in the quark density at the same 7 temperatures between 9 MeV and 3.454 MeV. The extrapolated $N_f = 2$ results for the zero-temperature diquark-density onsets from these intersection points are collected in Fig. 4.13. Within the errors, these extrapolated values for μ_c basically all agree. Assuming that μ_c is thus independent of the lattice spacing in this parameter regime we simply use their average as our final overall estimate of

$$\mu_c = 9.9999(7) \tag{4.16}$$

from the data in Fig. 4.13 as indicated by the horizontal line with the gray error band. This overall estimate thus confirms that $\mu_c = m_d/2$ with rather high precision.

This agrees with the corresponding onset of isospin density at $m_\pi/2$ in the effective theory for heavy quarks in QCD [84], and it shows that there is no "Silver Blaze" problem [100] in the effective lattice theory for two-color QCD with heavy quarks either.

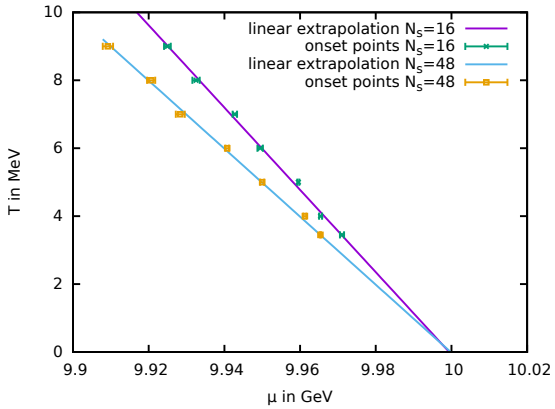

Figure 4.12.: Section of the $N_f = 2$ phase diagram with a linear extrapolation of the diquark-density onset to $T = 0$ at $\beta = 2.5$ or $a = 0.081$ fm with $N_s = 16$ and $N_s = 48$.

In contrast to the effective theory for heavy quarks in QCD [84] where there is some evidence of a finite binding energy per nucleon ϵ, shifting the nuclear-matter transition to $3\mu_c = m_B - \epsilon$, there is no such evidence of a shift of the onset μ_c by a non-zero ϵ in the effective theory for heavy two-color QCD. This is consistent with the generally expected difference between a first-order liquid-gas transition in QCD and Bose-Einstein condensation of diquarks in a second-order transition in two-color QCD. At the same time, however, the diquark densities obtained here are far from reflecting any sign of Bose-Einstein condensation. Quarks and diquarks are way too heavy to interpret the latter as deeply bound dimers. With our parameters for the $\beta = 2.5$ lattice the 20 GeV diquarks are only bound by about 2.8 MeV. If it wasn't for confinement, the transition temperature of the diquark-condensation phase by pair breaking should roughly be of the same order. All we can observe here is an essentially free heavy-diquark gas behavior in the small window between $\mu = \mu_c(T)$ and the beginning deconfinement crossover followed by lattice saturation. The only reason we can observe this diquark gas at temperatures above 4 MeV is probably statistical confinement. Unfortunately, the region where one might find a superfluid diquark-condensation phase is currently still beyond reach within the convergence region of the hopping series. Nevertheless, we can attempt to give a very rough first estimate of a region where such a diquark superfluid might be found, if we were able to further reduce the temperature, as follows:

Since the pseudo-critical chemical potentials for deconfinement at the available temperatures are also all below $m_d/2$, we compare their zero-temperature extrapolation to that of the diquark-density onset in Fig. 4.14. The difference between the extrapolated $\mu_c = m_d/2$ and μ_{pc} is small but significant. As seen in the figure, the deconfinement crossover then hits the $T = 0$ axis of the phase diagram just above $m_q = 10.0014$ GeV. Therefore, a small window for a potential superfluid diquark-condensation phase at sufficiently low temperatures remains. The region where this might occur is indicated by the shaded red triangle in Fig. 4.14. This region starts at a chemical potential slightly below $\mu = m_d/2 = 10$ GeV, i.e. at the lower limit given by the extrapolation error of the

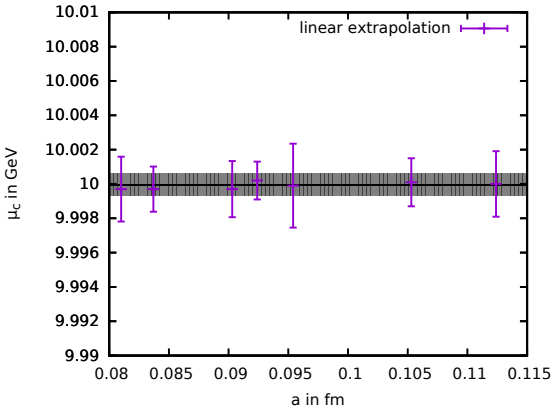

Figure 4.13.: Critical chemical potentials μ_c for the diquark-density onset at $T = 0$ from linear extrapolations for different lattice spacings between $a = 0.0810$ fm and 0.1124 fm corresponding to lattice couplings between $\beta = 2.5$ and 2.4.

diquark-density onset for the $\beta = 2.5$ data used here. We use this lower limit instead of $m_d/2$ because there are also some truncation errors in our equations for the diquark mass m_d, Eq. (2.140), and the effective fermion couplings h and h_2 in Eqs. (2.87) and (2.128). The deconfinement transition temperature at this lower limit is then of roughly the same order as the diquark-binding energy and hence of the naive estimate of the transition temperature of a possible diquark-condensation phase.

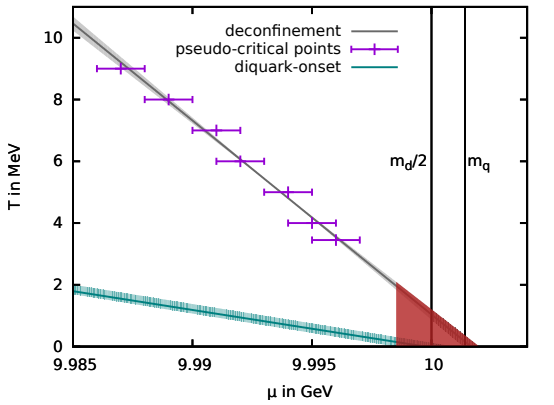

Figure 4.14.: Extrapolation of the deconfinement transition compared to the extrapolated diquark-density onset from Fig. 4.12. The region where one might hope to find a superfluid diquark-condensation phase is marked by the shaded red triangle. Half the diquark mass, $m_d/2 = 10$ GeV, and the quark mass $m_q = 10.0014$ GeV are indicated by vertical lines.

4.2. Effective Theory for G_2 QCD at Finite Density

We now apply the effective theory to the cold and dense region of the phase diagram of G_2-QCD. This is particularly interesting because we do not only expect to find a Bose-Einstein condensate of diquarks, like in two-color QCD, at sufficiently low temperatures but also a liquid-gas transition as we know it from QCD. This is due to the fact that the spectrum of G_2 QCD contains bosonic diquarks as well as fermionic baryons, i.e. nucleons or deltas. The effective theory should in principle be able to show all these phenomena.

Leading-order strong coupling limit

Let us again start by analyzing the leading-order of the effective theory in the strong coupling limit to identify the relevant degrees of freedom of the effective theory. The leading-order partition function for one quark flavor in the strong coupling limit reads

$$\begin{aligned} Z &= \left(\int d\mu_{\text{red}} \det[1+hW]^2 \right)^{N_s^3} , \\ &= \Big(\int d\mu_{\text{red}} \big[1 + (h+h^{13})(2\chi_7) + (h^2+h^{12})(2\chi_{14} + 2\chi_7^2 + 2\chi_7) \\ &+ (h^3+h^{11})(4\chi_7^2 + 2\chi_{14}\chi_7 - 2\chi_{14}) + (h^4+h^{10})(3\chi_7^3 + \chi_{14}^2 + 3\chi_7^2 - 2\chi_{14}) \\ &+ (h^5+h^9)(4\chi_7^3 + 2\chi_{14}\chi_7^2 - 2\chi_{14}^2 - 4\chi_{14}\chi_7 + 2\chi_{14} + 2\chi_7) \\ &+ (h^6+h^8)(\chi_7^4 + 2\chi_7^3 - \chi_{14}^2 + 2\chi_7^2 + 2\chi_7) \\ &+ h^7(2 + 2\chi_7^4 - 4\chi_7^2\chi_{14} + 4\chi_{14}^2 + 4\chi_{14}\chi_7) + h^{14} \big] \Big)^{N_s^3} , \end{aligned} \tag{4.17}$$

where $d\mu_{\text{red}}$ is the reduced Haar measure of G_2 (for details, see appendix C) and χ_7 and χ_{14} are the Polyakov loops in the 7 and 14 dimensional representation. After integration over the group manifold we arrive at

$$\begin{aligned} Z = \big(&1 + 2(h^2+h^{12}) + 4(h^3+h^{11}) + 7(h^4+h^{10}) \\ &+ 4(h^5+h^9) + 7(h^6+h^8) + 10h^7 + h^{14} \big)^{N_s^3} . \end{aligned} \tag{4.18}$$

The partition function is made up of gauge invariant states build from up to 14 quarks including 2 diquark states, one of which is a scalar, and 4 three quark states, corresponding to a spin 3/2 delta baryon. Our partition function does not include gauge invariant 1 quark states, like hybrid states made from e.g. one quark and three gluons in full 4d G_2-QCD because gluonic degrees of freedom are absent in the strong coupling limit.
To get to a leading-order mean-field description of the quark number density we again replace all Polyakov loop variables with a mean-field value.

Convergence of the hopping series

Before we analyze the cold and dense region of the G_2-QCD phase diagram we have to check the range of validity of the effective theory. As our effective expansion parameter

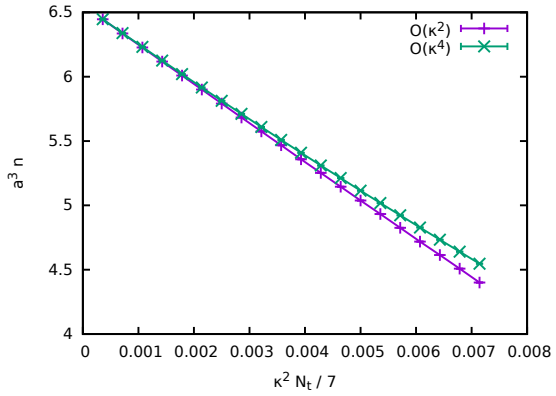

Figure 4.15.: Comparison of quark densities evaluated at the orders κ^2 and κ^4, both for $\kappa = 0.005$, $\beta/N_c = 1.39$, $\mu = m_d/2$ and N_t ranging between 100 and 2000, including gauge corrections.

is $\kappa^2 N_t/N_c$, we will vary this parameter and compare results of simulations including corrections up to order $\mathcal{O}(\kappa^2)$ and $\mathcal{O}(\kappa^4)$. This way we can check the convergence of the hopping series. The effects of the corrections are largest when h is of order one. Fig. 4.15 shows a plot of the two quark number densities for $\beta/N_c = 1.39$, $\mu = m_d/2$, including gauge corrections. The two curves agree up to $\kappa^2 N_t/N_c \approx 0.003$. If we compare this to the results for the effective action for two-color QCD in Fig. 4.1, we see that the convergence region for the effective theory for G_2 is much smaller. Even for small values of N_t, we have to choose κ very small to ensure convergence.

4.2.1. Results

Let us start by discussing results for the Polyakov loop and quark number density for low temperatures and one quark flavor. We choose our parameters such that we are certain to stay in the convergence region of the hopping expansion. Fig. 4.16 shows the quark number density and the Polyakov loop expectation value of the fundamental representations for the parameter set: $\beta/N_c = 1.39$, $\kappa = 0.005$, leading to $am_d = 9.210$, $N_t = 100$ and $N_f = 1$. In this case, the effective expansion parameter is $\kappa^2 N_t/N_c = 3.6 \cdot 10^{-4}$ and thus well inside the convergence region. We again see that the quark number density and the Polyakov-loop stay almost zero and independent of μ until the chemical potential approaches half the diquark mass $\mu \approx m_d/2$. Beyond that point we see a sharp increase in the quark number density until it saturates at $2 \cdot N_c = 14$, as expected. The Polyakov-loop also starts to rise as μ is approaching $m_d/2$, it reaches a maximum approximately at the half-filling point of the lattice. For even larger chemical potentials it starts to drop back to its $\mu = 0$ value because of the effective quenching of the dynamical quarks due to lattice saturation. Again the density onset is well described by the leading-order mean-field formula. The comparison of the data from the $\mathcal{O}(\kappa^4)$ simulation with the leading-order mean-field model is shown in Fig. 4.17. If we plot the quark number den-

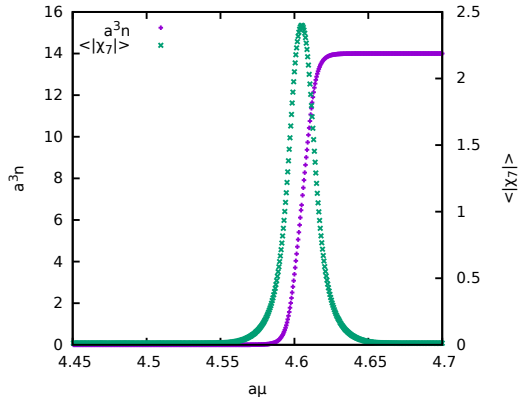

Figure 4.16.: Quark density a^3n and Polyakov-loop expectation value in the 7 dimensional representation $\langle|\chi_7|\rangle$, both over $a\mu$, with simulation parameters $\beta/N_c = 1.39$, $\kappa = 0.005$, leading to $am_d = 9.210$, $N_t = 100$ and $N_f = 1$.

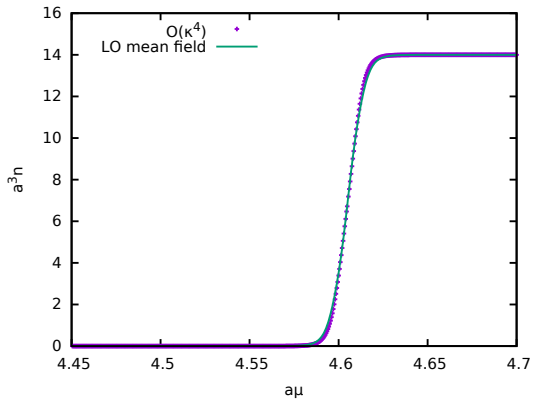

Figure 4.17.: Comparison of the quark density at order κ^4 from Fig. 4.16 to the leading-order formula for G_2.

sity logarithmically over the chemical potential we may now distinguish three different regions with different exponential increase. The exponential increase is proportional to

$$a^3n \sim \exp\left(x\,\frac{\mu - m_q}{T}\right)\,, \qquad x = 1, 2, 3\,. \tag{4.19}$$

Logarithmic plots of the quark density and the expectation values of the Polyakov-loop in the 7 and 14 dimensional representations are shown in Fig. 4.18. The transition to the second exponential region $\sim \exp\left(2\frac{\mu-m_q}{T}\right)$ happens where the expectation values of the Polyakov-loop in the fundamental representations are still constant at their $\mu = 0$ value. As this is the same situation we encountered with the effective theory for two-color QCD, we will again interpret the two different regions as thermal excitations of a quark gas, suppressed by the expectation value of the Polyakov loop and a thermal gas consisting of two-quark states. In contrast to the effective theory for two-color QCD, we also find a third exponential region $\sim \exp\left(3\frac{\mu-m_q}{T}\right)$ corresponding to a thermal gas of three-quark states. Fig. 4.19 shows the three different exponential regions in the quark number density indicated by black lines. The interpretation of the different thermal gases is somewhat more complicated as in the effective theory for two-color QCD. The strong-coupling partition function (4.17) shows that the two- and three-quark states are mixtures of color singlet baryons and non-singlet contributions. As our numerical simulations on a finite lattice will always lead to small but finite values of $\langle\chi_7\rangle$ and $\langle\chi_{14}\rangle$, we will also have finite contributions of color non-singlets to our two and three-quark states. Because of the non-trivial dependence of the expectations values of $\langle\chi_7\rangle$ and $\langle\chi_{14}\rangle$ of non-singlet contributions we were not able to determine the diquark or delta mass from fits to the quark number density as we did in two-color QCD (see section

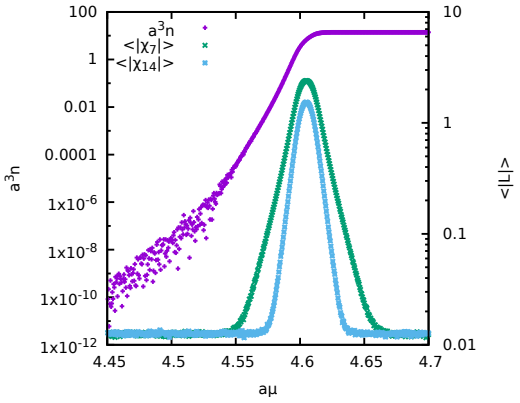

Figure 4.18.: Logarithmic plot of the quark density a^3n, Polyakov-loop expectation value in the 7 dimensional representation $\langle|\chi_7|\rangle$ and 14 dimensional representation $\langle|\chi_{14}|\rangle$ for the same parameters as in Fig. 4.16.

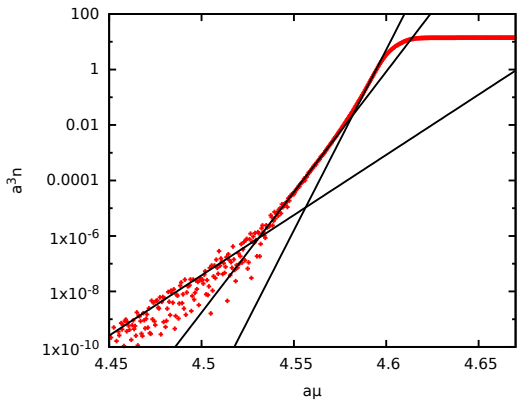

Figure 4.19.: Logarithmic plot of the quark density a^3n, same as in Fig. 4.18. The black lines indicate different exponential regions, the corresponding slopes are μ, 2μ and 3μ.

4.1.1). We still interpret the main contribution of the two and three-quark states as thermal gases of color singlet diquarks and deltas, as we found a (lightly) bound diquark in the effective theory of two-color QCD and the G_2 strong coupling partition function also includes these states as color singlets. Analyzing the partition function one would expect to find also exponential regions corresponding to four and five quark states, even up to 14 quark states, setting in one after another. However, we are not able to observe these onsets, probably because the saturation of the lattice is suppressing these regions. For the parameter region, where the hopping expansion converges, all the onsets and transitions we are able to find are analytic. From this, we conclude that to find the phase-transitions to a BEC and the nuclear liquid-gas transition we have to lower temperatures, i.e. larger N_t. To go to sufficiently small temperatures we will have to leave the region of convergence.

4.2.2. Results outside the Region of Convergence

In the previous sections, the accessible quark masses in the convergence region of the hopping expansion of the effective theory are too large to realize the liquid-gas phase transition or the transition to a diquark BEC (or respectively, the temperatures are to high). On the other hand, one of our main goals is to compare results from the effective theory to results from full 4d G_2-QCD simulations. Also for reaching that goal we have to lower the quarks masses to satisfy algorithmic requirements in the full 4d G_2-QCD simulations [99]. We will now increase the hopping parameter to reduce the quark mass to compare to results from full 4d simulations. To stay at least close to the region of convergence and due to the fact that large temporal extends are numerically not feasible

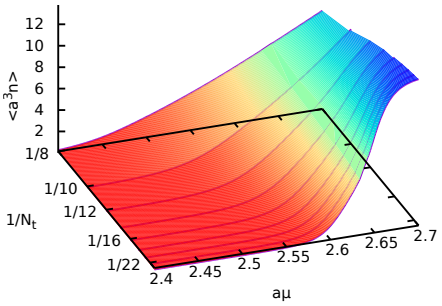

Figure 4.20.: Quark number density over N_t and $a\mu$ for the parameters $\beta/N_c = 1.4$, $\kappa = 0.0357$ and $N_s = 16$. The region of numerical instability is marked by the small irregularity in color.

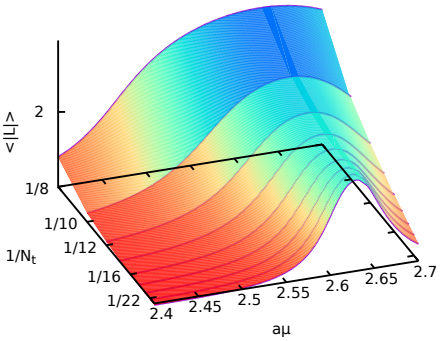

Figure 4.21.: Polyakov loop in the 7 dimensional representation over N_t and $a\mu$ for the parameters $\beta/N_c = 1.4$, $\kappa = 0.0357$ and $N_s = 16$.

in 4d G_2-QCD simulations we can lower N_t. Fig.'s 4.20 and 4.21 show the quark number density a^3n and the Polyakov loop in the 7 dimensional representation over N_t and $a\mu$ for $\beta/N_c = 1.4$, $\kappa = 0.0357$ and $N_s = 16$. The diquark mass for this parameter set is $am_d = 5.32058$. The effective expansion parameter for the chosen parameter set and $N_t = 24$ is $\kappa^2 N_t/N_c = 0.00437$, comparing this to Fig. 4.15 we are just outside out of the convergence region of the hopping expansion. As a result we find a numerical instability for $h \approx 1$ in our data. This numerical instability is a result of the breakdown of the resummation procedure for multiple winding Polyakov loops in the fermion action (see discussion in sec. 2.4.3). Strictly speaking the instability is there for every parameter set as $h \to 1$, also in the effective theory for two-color QCD. As we are in the region of convergence of the hopping series we simply do not see the instability because our resolution in μ is not good enough to approach $h = 1$ close enough. As we increase the effective expansion parameter and move outside the region of convergence, the μ range in which the numerical instability occurs grows larger. Still, outside the instability region we find the expected results: density is almost zero until a^3n starts to rise as μ approaches $m_d/2$. For even higher chemical potential the density goes into saturation at $2N_c = 14$. The Polyakov loop also starts to rise from its $\mu = 0$ value as $\mu \to m_d/2$, takes a maximum at approximately half-filling of the lattice and goes down again for even larger μ because of lattice saturation. As N_t grows, we also recognize that density and Polyakov loop are suppressed and the onsets of density and Polyakov loop get sharper, again in agreement with the Silver Blaze property.

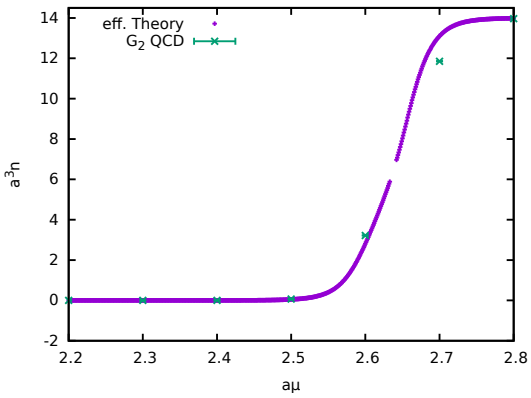

Figure 4.22.: Comparison of the quark number density from the effective theory and full G_2-QCD simulations.

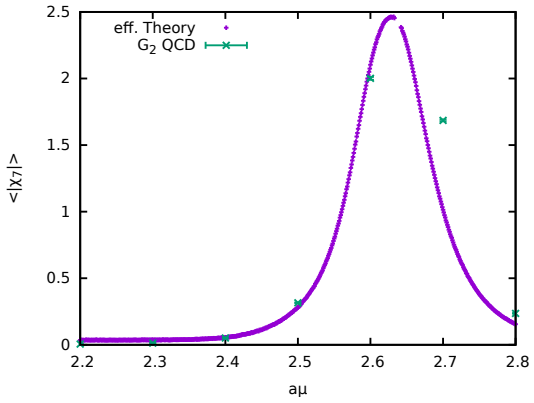

Figure 4.23.: Comparison of the Polyakov loop expectation value in the 7 dimensional representation from the effective theory and full G_2-QCD simulations.

Comparison to G_2-QCD Results

We will now compare our data from the effective theory to data from full 4d G_2-QCD simulations. In general it is not easy to find parameter sets where the effective theory and the full theory can be compared. In the derivation of the effective action for the cold and dense regime we neglected all terms subleading in N_t. If we choose N_t too small, this approximation is not valid anymore. On the other hand, large temporal extends of the 4d lattice are difficult because they require a lot of computer time. The parameter set we found optimal to compare our data is $\beta/N_c = 1.4$, $\kappa = 0.0357$ now on a $N_s = 8$ lattice. The temporal extend of the 4d lattice is $N_t = 18$. With this parameter set were on the edge of the hopping series' convergence region. Fig. 4.22 shows a comparison of the quark number density a^3n from the effective theory to full G_2-QCD simulations. The errorbars are hidden inside the points. The missing datapoints lie inside the region of numerical instability. Comparing the results from the effective theory to the results from the full theory, we see that the agreement is very good up to the region of instability. Beyond the region where the effective theory is unstable the effective theory seems to overestimate the density until it goes into saturation. However, at these values of the quark number density we expect lattice artifacts to become important anyway. Also the datapoint from the full theory at $a\mu = 2.2$ seems to deviate from the results of the effective theory. Here, the effective theory underestimates the density, predicted by G_2-QCD, yet this deviation is not visible on a linear scale. If this deviation at small μ is connected to the sub-leading terms we neglected in the derivation of the effective theory (see sect. 2.4.6) or due to different behavior of finite size effects is not yet clear and we have to do more work to figure out which is the case. Fig. 4.23 shows the expectation value of the Polyakov loop in the 7 dimensional representation $\langle|\chi_7|\rangle$ from the effective and the full theory. We see a good match of the effective theory's results and the results

from the full theory up until $a\mu = 2.6$. In the region, where the Polyakov loop drops down again due to lattice saturation, we see clear deviations. At small values of the chemical potential the effective theory seems to overestimate the Polyakov loop when compared to G_2-QCD. Again, it is not clear, if this comes from simplifications of the effective action or if it is a consequence of the theories' different finite volume behavior. Overall the comparison of the results of the effective theory and full G_2-QCD is satisfactory, still a lot is to be done on both sides to make reliable conclusions about the range of validity of the effective theory and quantitative comparisons. E.g. we would like to have more datapoints of the effective theory in Fig. 4.22, especially around $\mu \approx m_d/2$. Further, we would like to check the effects of different values of β, N_t, κ and N_s on the matching of the results from both theories. Ideally we would like to start deep in the convergence region of the hopping expansion, with heavy quarks but low temperature and gradually go to smaller quark masses and/or move closer to the continuum limit. This would take careful choice of the simulation parameters, to make simulations of both, the effective theory and full G_2-QCD, feasible and and would require a huge amount of computer time.

4.2.3. On the Nuclear Liquid-Gas Transition and Bose-Einstein Condensation

In all our simulations of an effective theory for G_2-QCD we were not able to observe evidence for Bose-Einstein condensation of diquarks or a nuclear liquid-gas transition. Similar to the effective theory for two-color QCD our quarks are simply much too heavy. One of the main reasons to explore the effective theory outside the hopping expansion's region of convergence was to find possible evidence for a phase transition at low temperatures. The effective theory for QCD does indeed show signs for the nuclear liquid-gas transition, when going outside of the convergence region [84]. We expected to find similar behavior for the effective theory for G_2-QCD, as the nuclear liquid-gas transition is an established feature of G_2-QCD [101]. However even for values of $\kappa^2 N_t/N_c$ extremely far outside the region of convergence we did not find any hints towards a phase transition. One possible reason, why we do not find at least the nuclear liquid-gas transition is that the additional presence of the thermal diquark gas in G_2-QCD somehow covers the effects of the phase transition as diquark and nucleon onsets are very close to each other $m_d/2 \approx m_\Delta/3$ in the heavy quark limit and it is difficult to separate between the two scales.

4.2.4. Results for 2 Dimensional G_2-QCD

Since full 4d G_2-QCD simulations require a lot of computational resources the Gießen group, simulating G_2-QCD at finite density, now also does simulations in 1+1 dimensions to reduce computational efforts. Since it is not much work to modify the effective theory for 3+1 dimensional space-time to arrive at an effective theory for 1+1 dimensions we will show the first steps towards comparing the effective theory to a 1+1 dimensional QCD-like theory. One of the main questions of the comparison will be, if one can compare the theories at all. In the case of a 1+1 dimensional underlying theory, the effective theory will be 1 dimensional. Usually one argues that 1 dimensional systems can not undergo a phase transition, this is known as the van Hove theorem [102]. However, the van Hove theorem is only applicable, if certain requirements are given, one of them being the absence of external fields. Since dynamical quarks in the fundamental representation of the gauge group act like external magnetic fields (in the language of spin systems) the van Hove theorem does not exclude a phase transition in our effective 1d theory. In fact there a plenty of 1d models in the literature that undergo phase transitions [102, 103]. What is forbidden, is the Bose-Einstein condensation of diquarks. The Mermin-Wagner theorem rules out phase transitions connected to th spontaneous breaking of continuous symmetries in two or less dimensions [104]. The liquid-gas transition is again not affected by this theorem however, because it is not connected to the spontaneous breakdown of a continuous symmetry.
Now, let us start the discussion with stating the effective action in the case of one dimension. The effective action for the Yang-Mills part is

$$-S_{\text{eff}}^{g} = u^{N_t} \sum_x L_x L_{x+1} \,, \tag{4.20}$$

the effective coupling λ reduces to its LO expression since in 1+1 dimensions there is no room for decorations to be attached to the LO diagrams. In the cold and dense regime the effective action reduces to

$$\begin{aligned}
-S_{\text{eff}} &= \sum_x \log\det(1+hW_x) - 2h_2 \sum_x \operatorname{tr}\frac{hW_x}{1+hW_x}\operatorname{tr}\frac{hW_{\vec{x}+1}}{1+hW_{\vec{x}+1}} \\
&+ 2\frac{\kappa^4 N_t^2}{N_c^2}\sum_x \operatorname{tr}\frac{hW_x}{(1+hW_x)^2}\operatorname{tr}\frac{hW_{\vec{x}+1}}{(1+hW_{\vec{x}+1})^2} \\
&+ \frac{\kappa^4 N_t^2}{N_c^2}\sum_x \operatorname{tr}\frac{hW_x}{(1+hW_x)^2}\left(\operatorname{tr}\frac{hW_{x+1}}{1+hW_{x+1}}\right)^2 \\
&+ 2\frac{\kappa^4 N_t^2}{N_c^2}\sum_x \operatorname{tr}\frac{hW_x}{(1+hW_x)^2}\operatorname{tr}\frac{hW_{x-1}}{1+hW_{x-1}}\operatorname{tr}\frac{hW_{x+1}}{1+hW_{x+1}} \,.
\end{aligned} \tag{4.21}$$

Where we also have to adjust the effective coupling

$$h = (2\kappa e^{a\mu})^{N_t} \exp\left[2N_t\kappa^2 u\left(\frac{1-u^{N_t-1}}{1-u} - 4\kappa^2 + 3\kappa^2 u\right)\right] \,. \tag{4.22}$$

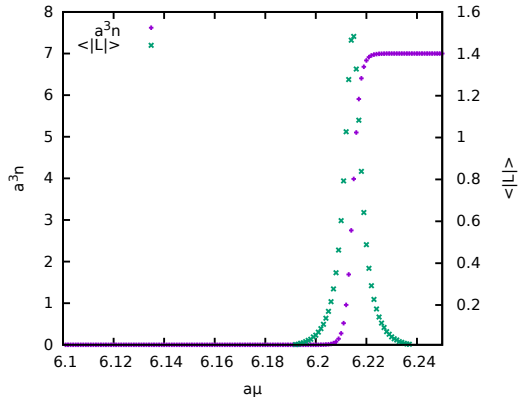

Figure 4.24.: Linear plot of the quark number density and Polyakov loop in the 7 dimensional representation over $a\mu$ for the parameters $\beta/N_c = 1.39$, $\kappa = 0.001$, $N_t = 200$ and $N_s = 32768$.

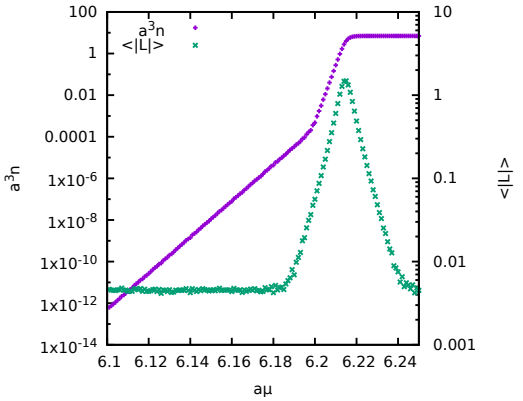

Figure 4.25.: Logarithmic plot of the quark number density and Polyakov loop in the 7 dimensional representation over $a\mu$ for the parameters $\beta/N_c = 1.39$, $\kappa = 0.001$, $N_t = 200$ and $N_s = 32768$.

The most important difference to the effective theory for 4 space-time dimensions is the missing power of two in the LO term in eq. (4.21). This is due to the fact that in 1+1 dimensions one looses the classification in 'spin up' and 'spin down'. One important consequence becomes visible in the strong coupling partition function

$$\begin{aligned} Z(\beta = 0) &= \Big[\int dW (1 + (h + h^6)\chi_7 + (h^2 + h^5)(\chi_7 + \chi_{14}) \\ &\quad + (h^3 + h^4)(\chi_7^2 - \chi_{14}) + h^7) \Big]^{N_s^3} , \\ &= [1 + h^3 + h^4 + h^7]^{N_s^3} . \end{aligned} \tag{4.23}$$

The partition function of the effective theory does not contain color singlet states, made up of two-quarks. Fig. 4.24 shows the density and the Polyakov loop in the 7 dimensional representation from a simulation with the effective action in eq. (4.21) and the parameters $\beta/N_c = 1.39$, $\kappa = 0.001$, $N_t = 200$ and $N_s = 32768$. The plot looks similar to the 4d case, hovever the density saturates at $N_c = 7$ again because we lost the spin degrees of freedom. Fig. 4.25 shows a logarithmic plot of the density and the Polyakov loop in the 7 dimensional representation for the same parameters as before. In contrast to the results from the effective theory for 4d G_2-QCD we only see two exponential regimes. The slopes in the two regimes are given by μ and 3μ. As predicted by the LO strong coupling result, we do not find a diquark in the effective theory. First results [99] from 1+1d G_2-QCD simulations indicate that the theory contains bound diquarks. However the mass ordering is quite unusual, e.g. the scalar diquark is heavier than the axial vector diquark. This and further evidence seem to indicate that the diquarks consist of two quarks with some relative momentum between each other. In the effective theory, two quarks, forming a diquark, have to live on one site or neighboring sites, thus it is

not possible for the quarks to carry relative momentum and we do not expect to find the diquarks from the full theory in our effective theory. Retrospectively the absence of an exponential region corresponding to 2μ, though we find color non-singlet two-quark states in the partition function, is a confirmation of our assumption for the effective theory for 4d G_2-QCD. Here we made the assumption, that the exponential region corresponding to 2μ was mainly there due to color singlet diquarks. Like in the results from the effective theory for 4d G_2-QCD, the onset of the three quark state happens beyond the point where the Polyakov loop in the seven dimensional representation starts to rise. Now it is not clear, what relevance the Polyakov loop at finite density has, in connection with deconfinement. Yet, if we choose to interpret this thermal three quark state as a thermal gas of fermionic baryons, the rise of the Polyakov loop might be interpreted as a screening effect from the presence of G_2-QCD matter in the system rather than deconfinement. However, the interplay between the onset of baryonic matter, the rise of the Polyakov loop and deconfiment at finite density needs more in-depth investigations that we are not able to give here.

5
Summary and Outlook

In this work we have investigated the cold and dense region of the phase diagram of two different QCD-like theories: two-color QCD and G_2-QCD. In order to perform this investigation we made use of effective theories in terms of Polyakov loops. To calculate the effective action we have adapted a method, originally developed for QCD. In particular, we determined the effective Polyakov-loop theory by combining a strong coupling and hopping expansion and integrating out spatial gauge degrees of freedom. Using the strong coupling and hopping expansions in the process, the effective theory is valid for heavy quarks, and away from the continuum limit. However, the advantage of this effective theory is that it is systematically improvable order-by-order and therefore allows for a good control over the systematic errors in our approach.
We first applied the effective theory to pure SU(2) gauge theory to crosscheck with earlier results from effective Polyakov-loop theories and full 4d Yang-Mills results. We showed that our implementation reproduced the known results. Further, we were able to show that resummations of generalized Polyakov loops in the effective action considerably improve the behavior of the local Polyakov loop distribution near the critical temperature. This is an important feature, e.g. for determining the effective Polyakov loop potential from the effective theory.
Trying to reproduce the deconfinement phase transition of pure G_2 gauge theory in the effective theory, we saw that resummation of generalized Polyakov loops is not possible in this case. This is due to the fact that the resummation of multiple-winding Polyakov loops does not converge around T_c. We determined the effective coupling constant $\lambda(u(\beta), N_t)$ up to sixth order in the expansion coefficient of the 7 dimensional representation $u(\beta)$. By finding the critical coupling in the effective theory λ_c and using the analytic relationship between the effective and 4d lattice coupling, we tried to determine the critical β_c. However, by comparing our value of β_c to the known value for $N_t = 6$ we found a deviation of about 12%. Including higher orders of $u(\beta)$ in the

effective coupling turned out to be extremely difficult, as for G_2 many group integrals, including plaquettes in different representations, do not vanish but give additional, non-trivial contributions to the effective coupling λ. We therefore tried to include higher orders in $u(\beta)$ effectively, by fixing λ at one particular N_t to produce the right value for β_c. We checked this procedure for SU(2) Yang-Mills theory where it produces reasonable results, which hence allows us to make predictions for the critical lattice coupling β_c for various N_t in pure G_2 gauge theory as well.
We further included dynamical quarks by using the hopping expansion. In the case of G_2-QCD we found the first order deconfinement transition to be stable against the introduction of heavy quarks. We mapped the G_2-QCD phase diagram in the plane of the effective couplings $\lambda - h$ where h is the effective fermion coupling. Decreasing the quark mass, lead to a weakening of the first order phase transition until it ended in a 2nd order critical point. From the location of the critical point in the $\lambda - h$ phase diagram we were able to extract the critical hopping parameter κ_c. The extracted value turned out to be too large when compared to 4d G_2-QCD simulations, as the extracted κ_c lies outside the convergence region of the hopping series.
When we applied the effective theory to the cold and dense region of the two-color QCD phase diagram we were able to map out the pseudo-critical line of the deconfinement crossover at small temperatures. At these low temperatures the Polyakov loop expectation value $\langle L \rangle$ stays at its constant zero net-baryon density value, which is dominated by the finite size of the lattice. Only when we raise the quark chemical potential up to the deconfinement crossover around μ_{pc} the Polyakov loop starts to rise. Within the constant regime of the Polyakov loop we were able to identify a kink in the logarithmic plot of the quark-number density, where the finite temperature behavior of the system changes from a Polyakov loop suppressed gas of heavy quarks, existing due to imperfect statistical confinement, to a thermal gas of free, heavy diquarks. For chemical potentials above the quark mass $\mu > m_q$ the density describes quark matter going into saturation as the lattice gets filled with the maximum number of quarks per site as allowed by the Pauli principle.
We were able to describe the density of the system by a analytic leading-order formula, with a mean-field description for the Polyakov loop. To describe the Polyakov loop suppressed quark gas it turned out to be important to use the expectation value of the Polyakov loop $\langle L \rangle$, determined from probability distributions of the local Polyakov loop, as mean-field Polyakov loop value. This local Polyakov loop expectation value is about two orders of magnitude smaller than the expectation value of the modulus of its volume average $\langle |L| \rangle$, usually used as order parameter in lattice studies. This is due to the fact, that negative values of the local Polyakov loop induce negative local quark numbers. Thus, using the modulus of the volume average overestimates the quark number density. As soon as the expectation value of the Polyakov loop starts to rise, the two quantities $\langle |L| \rangle$ and $\langle L \rangle$ agree with each other. Further, in the regime of the heavy diquark gas (in our simulations the mass of the diquarks was fixed to $m_d = 20$ GeV) we saw that replacing $2m_q$ by m_d in the leading-order mean-field formula lead to a near-perfect, parameter free description of the density. Even though our diquarks are only loosely bound $2m_q - m_d = 2.8$ MeV this replacement made significant difference in the exponential

increase of the density. The fact that we are able to describe the density of the system over the whole range of chemical potentials and temperatures with the mean-field description of the Polyakov loop with only minor adjustments is rather surprising. The measured distributions of the local Polyakov loop are not sharply peaked around a mean value but are rather broad distributions, suggesting non-negligible fluctuations.
We were able to interpret the region between the kink in the logarithmic plot of the density and μ_{pc} as a thermal gas of heavy diquarks. We found no direct evidence for a Bose-Einstein condensation of those baryonic diquarks, probably because the temperatures in the range we investigated $T > 3.5$ MeV are higher than the binding energy of the diquarks. Our diquarks are effectively only held together by confinement, thus they are not deeply bound dimers in contrast to the usual scenario we find in BECs. Nevertheless, our extrapolation of the diquark onset to $T \to 0$ is in perfect agreement with $\mu_c = m_d/2$ as predicted by chiral perturbation theory. The extrapolation was done for several values of the lattice coupling β and proofed to be scale independent. Further, we were able to identify a region, where one might be able to find signs of a BEC in the future.
The phase diagram of cold, dense and heavy G_2-QCD also shows a sharp rise of the density and the Polyakov loop in the fundamental representations around $\mu \approx m_d/2$. For larger $\mu > m_d/2$ the density goes into saturation at $2 \cdot N_c = 14$. Again we are able to describe the density by a leading-order mean-field description. However here, we need a mean-field description for both fundamental Polyakov loops, in the seven and the fourteen dimensional representation $\langle\chi_7\rangle$ and $\langle\chi_{14}\rangle$. The expectation value of the Polyakov loops behave similar as in two-color QCD. At small μ the expectation values $\langle\chi_7\rangle$ and $\langle\chi_{14}\rangle$ stay constant at their $\mu = 0$ values until $\mu \approx m_d/2$ where they begin to rise. The Polyakov loop in the seven dimensional representation $\langle\chi_7\rangle$ rises earlier then the one in the fourteen dimensional representation $\langle\chi_{14}\rangle$. When we analyze the quark number density in a logarithmic scale, we can again distinguish different exponential regimes. Here we find three different exponential regimes corresponding to one-, two- and three-quark states. The three-quark state corresponds to a fermionic baryon as expected from the gauge invariant spectrum of G_2-QCD. By looking at the strong coupling limit of the leading-order partition function we would also expect to find expect to find exponential regimes corresponding to color singlet states made up of more than three quarks (up to seven quarks). Those exponentials are probably suppressed by the saturation of the lattice.
When we applied the effective theory outside the convergence region of the hopping expansion we found a small region in μ where we get artifacts in the density and the Polyakov loops caused by numerical instabilities when the chemical potential approaches the quark mass m_q. Outside this instability region we found the expected behavior. We were able to compare the results from the effective theory to data from full 4d G_2-QCD simulations for one parameter set, on the edge of the convergence region. The 4d data matches the results from the effective theory very well for chemical potentials up to the region where the numerical instabilities set in. Beyond the instability region and $\mu > m_d/2$, the data differ slightly until the saturation of the lattice. We are not too concerned about those deviations in the data as the region where the deviations

are visible the quark number density has already surpassed the half-filling point of the lattice, thus the density is dominated by lattice artifacts anyway. Unfortunately, we do not have many datapoints from the full theory to compare our data to, especially around $\mu \approx m_d/2$. This makes it e.g. impossible to compare, if the characteristic kinks in the logarithmic plots of the density from the effective theory are also present in the full theory and, should they appear, if they are at the same locations as in the effective theory. In the future, we need more data from full 4d G_2-QCD simulations, ideally in the hopping expansions region of convergence, to compare our data from the effective theory to and make robust quantitative comparisons. This lack of 4d data comes from the fact that simulating G_2-QCD is numerically very expensive, even in the case of fairly heavy quarks.

One way to work around the numerical costs to simulate G_2-QCD at finite baryon density might be simulations of dimensionally reduced G_2-QCD, in particular the Gießen group recently started simulations of G_2-QCD in 1+1 dimensions. Therefore, we have derived the effective theory for 1+1 dimensional G_2-QCD and taken the first steps to make the comparison to the full theory in the future. In the resulting 1d effective theory we noticed the absence of color singlet diquarks because the spin degrees of freedom are fundamentally different in 1+1 dimensions. In general, it will be interesting to see if a 1d effective theory can explain data of a higher dimensional underlying theory, in particular with regard to a possible first order liquid-gas phase transition.

In general we were able to show that effective Polyakov-loop theories for heavy quarks reflect important physical properties of the underlying QCD-like theories at finite baryon density and essential differences between the different theories we examined, e.g. the gauge invariant spectrum of the theory or the realization of the Silver Blaze property. We were able to generate lots of results from the effective theories, as numerical simulations with the effective actions are rather inexpensive. So far, however, there simply is not enough data from the full QCD-like theories to compare our results to. Still, we were able to make a qualitative check of the effective theories and some minor quantitative comparisons to the existing results from finite density, heavy G_2-QCD. These comparisons proved to be satisfying, yet a full-fledged quantitative analysis of the effective theory's validity was not possible with the few existing results from full QCD-like theories in the cold and dense regime. More extensive quantitative comparison to the results of full QCD-like theories and finding the range of validity for the effective theory will be interesting tasks for future work. This will be possible as soon as results for the full QCD-like theories with heavy quarks become available.

Even though the effective theory seems to realize the Silver Blaze property correctly we have to take our results with a grain of salt for we were not able to find evidence for any kind of phase transition connected to the onset of baryon density, even when we applied the theory at extremely low temperatures beyond the convergence of the hopping series. Maybe our quarks are simply to heavy for the theory to undergo any kind of phase transition. However, this question will hopefully be answered in the future when higher orders of the combined hopping and strong coupling expansion will be included to push the theory closer to the physical pion mass.

Another matter is, if the convergence properties of the combined strong coupling and

hopping expansion are such that we will be able to apply the effective theory to QCD with physical pion mass at finite baryon density. This is still under investigation and if it is possible, it will be a long and difficult way to identify and calculate all terms that have to be taken into account for reaching physical quark masses. Nevertheless, effective Polyakov-loop theories still provide valuable understanding about the features of QCD-like theories at finite baryon density on the lattice. This understanding is desirable, as the more we learn about the phase diagram of QCD-like theories at finite density it turns out to be challenging to disentangle lattice effects from continuum physics. Of course, this will eventually become important, if we will be able to solve the QCD sign problem in the future.

A

Basic Facts about Group Representations

In quantum mechanics a transformation is associated with a unitary operator acting on the Hilbert space.[11] Thus, a transformation group of the system is associated with a mapping of the group into a set of unitary operators

$$\rho \ : G \to U(H) \ . \tag{A.1}$$

This means, for every element g of the symmetry group G there is a $\rho(g)$ which is a unitary operator on the Hilbert space H. If the mapping preserves the algebraic structure, meaning

$$\rho(g \cdot h) = \rho(g) \cdot \rho(h) \qquad \forall g, h \in G \ , \tag{A.2}$$

we call the mapping ρ a representation of the group G. It will be convenient to think of representations both as linear operators and as matrices. The connection between them is easy. Take $|i\rangle$ to be an orthonormal basis of the Hilbert space. The matrix elements of the of the linear operator are

$$(\rho(g))_{ij} = \ \langle i|\rho(g)|j\rangle \ . \tag{A.3}$$

Since we are now able to think of representations as matrices we can make two more definitions. Two representations ρ and ρ' are equivalent if they are related by a similarity transformation

$$\rho'(g) = S\rho(g)S^{-1} \ , \tag{A.4}$$

for a fixed S and for all $g \in G$. If a representation can be brought into the form

$$\rho(g) = \begin{pmatrix} \rho_1(g) & X(g) \\ 0 & \rho_2(g) \end{pmatrix} \ , \tag{A.5}$$

[11] there is also the possibility of anti-unitary operators, but let us ignore them for now.

by a similarity tranformation for all $g \in G$ it is called *reducible*. A representation ρ is called *fully reducible* if it is equivalent to a block-diagonal representation ρ'

$$\rho'(g) = S\rho(g)S^{-1} = \begin{pmatrix} \rho'_1(g) & 0 \\ 0 & \rho'_2(g) \end{pmatrix} . \tag{A.6}$$

The Hilbert space H on which ρ acts then breaks down to two orthogonal invariant subspaces. The representation ρ' is said to be the direct sum of ρ'_1 and ρ'_2

$$\rho' = \rho'_1 \oplus \rho'_2 . \tag{A.7}$$

A representation is called *irreducible*, if it is not reducible. For the groups that we will study the irreducible representations are all unitary and finite dimensional. The groups we are studying are Lie groups. Therefore we will not give parameterizations of different representations but show the group's generators in the different representations. As a reminder, the connection between a given parametrization of a group element and the generators of the group is

$$U(\varphi_a) = \exp[i\varphi_a T_a] , \tag{A.8}$$

where $U(\varphi_a)$ is the group element, the φ_a are the variables parameterizing the group and the T_a are the generators of the group. The first example are the generators of the fundamental representation of SU(2), i.e. the smallest dimensional, non-trivial representation of SU(2): The well known Pauli matrices. The generators satisfy the following commutation relation

$$[T_a, T_b] = i f_{abc} T_c , \tag{A.9}$$

where in this case the structure constants f_{abc} are given by two times the totally antisymmetric tensor $f_{abc} = 2\epsilon_{abc}$. If the generators T_a of some representation ρ satisfy (A.9), the matrices $-T_a^*$ satisfy the same relation. Thus they also generate a representation of the group, since we have

$$\exp[-i\varphi_a T_a^*] = U^*(\varphi_a) . \tag{A.10}$$

We call this representation the complex conjugate representation of ρ and denote it by $\overline{\rho}$. The complex conjugate of the fundamental representation is also called the anti-fundamental representation.
The generators of a group also satisfy the Jacobi identity

$$[T_a, [T_b, T_c]] + \text{cyclic permutations} = 0 . \tag{A.11}$$

In terms of the structure constants the above equation becomes

$$f_{bcd} f_{ade} + f_{abd} f_{cde} + f_{cad} f_{bde} = 0 . \tag{A.12}$$

If we define a new set of matrices

$$\left(\tilde{T}_a\right)_{bc} = -i f_{abc} , \tag{A.13}$$

then (A.12) can be rewritten as

$$[\tilde{T}_a, \tilde{T}_b] = i f_{abc} \tilde{T}_c \ . \tag{A.14}$$

The representation generated by these matrices is called the adjoint representation. The dimension of a given representation is equal to the dimension of the Hilbert space it acts on. In case of the adjoint representation the dimension is equal to the number of generators. In the case of SU(2) the dimension of the adjoint representation is three.

A.1. Higher Dimensional Representations

We already saw that the direct sum of two representations ρ_1 and ρ_2 produces a reducible representation on the Hilbert space $H_1 \oplus H_2$. There is also the possibility to combine ρ_1 and ρ_2 via a tensor product

$$(\rho_1 \otimes \rho_2)(g) = \rho_1(g) \otimes \rho_2(g) \ . \tag{A.15}$$

This also gives a representation now acting on the Hilbert space $H_1 \otimes H_2$. The fundamental theorem on representations of unitary groups states that all irreducible representations of SU(N) can be generated by tensor products of the fundamental and anti-fundamental representations [105]. In principle one could build all irreducible representations of SU(N) by calculating tensor products. There is a clever way to work out all these tensor products in a graphical way. This technique to construct all irreducible unitary representations for SU(N) relies on so called Young tableaux (For a good overview about how to use Young tableaux, see e.g. [105] and [106]).

A.2. Characters Analysis

Similar to ordinary Fourier analysis, we can expand a function depending on group elements in terms of special functions of the group. Those functions are characteristic for different representations and are called group characters. The expansion of the gauge action in terms of group characters is one particular way to work out the strong coupling expansion of a gauge theory. Let us start with the definition of the group characters. The character χ_r of a representation $\rho_r(U)$ is given by

$$\chi_r(U) = \mathrm{tr}\, \rho_r(U) \ . \tag{A.16}$$

Its value at unity gives the dimension of the representation

$$\chi_r(1) = d_r \ . \tag{A.17}$$

It is a basic but important fact that the trace is independent of the choice of a basis of our Hilbert space

$$\chi_r(VUV^{-1}) = \chi_r(U) \ , \qquad U \ , V \ \in G \ . \tag{A.18}$$

We say that the character of a representation is a class function and only depends on the invariant angles of a representation. The characters of the irreducible, unitary representations of a group G are orthogonal

$$\int dU\ \overline{\chi}_r(U)\chi_s(U) = \delta_{rs}\ , \tag{A.19}$$

where $\overline{\chi}_r(U)$ is the character of the complex conjugate of the representation $\rho_r(U)$. For now, just assume we have a well defined way to integrate over the group manifold, in fact we will define the group integral with the so called Haar measure in the next section. Moreover, the theorem of Peter and Weyl states that the characters of the irreducible representations form an orthonormal basis of the Hilbert space of the square-integrable class functions [106]. That means that every square-integrable function on the group $f(U)$, obeying $f(U) = f(VUV^{-1})$ $U, V \in G$ can be expanded in terms of group characters

$$\begin{aligned} f(U) &= \sum_{r\in\hat{G}} = f_r\chi_r(U)\ , \\ f_r &= \int dU\ \overline{\chi}_r(U)f(U)\ . \end{aligned} \tag{A.20}$$

This is the harmonic analysis on group manifolds and for U(1) we have ordinary Fourier analysis. The completeness relation of characters is

$$\sum_{r\in\hat{G}} \chi_r(U)\overline{\chi}_r(V) = \delta(UV^{-1})\ , \tag{A.21}$$

where the delta function is defined as

$$\int dU\ f(U)\delta(UV^{-1}) = f(V)\ . \tag{A.22}$$

As an example let us take a look at the action of a single plaquette with Wilson's gauge action

$$\exp[-S_p(U_p)]\ . \tag{A.23}$$

We write its character expansion in the form

$$\exp[-S_p(U_p)] = \sum_{r\in\hat{G}} d_r c_r(\beta)\chi_r(U_p)\ , \tag{A.24}$$

where d_r is the dimension of the representation. The explicit coefficients $c_r(\beta)$ are

$$\begin{aligned} c_r &= I_r(\beta)e^{-\beta} && \text{for U(1)}, \\ c_r &= \frac{2}{\beta} I_{2r+1}(\beta)e^{-\beta} && \text{for SU(2)}. \end{aligned} \tag{A.25}$$

The I_r are modified Bessel functions of the first kind and we encountered these coefficients in the strong coupling expansion of the Yang-Mills action. For the gauge group SU(3) and other, more complicated gauge groups we are not able to write down the expansion coefficients in a closed form.

A.3. Invariant Integration on Groups

We will now take a close look at the integration over the group manifold that was already used in the last section. The first ingredient we need for a well defined integration procedure is an integration measure. It can be shown that there is a unique, normalized integration measure for every compact Lie-group, the *Haar measure*. It has the follwing properties

$$\begin{aligned} \int dg &= \int d(gh) = \int d(hg) = \int dg^{-1} \\ \int dg &= 1 \ , \end{aligned} \tag{A.26}$$

where g and h are elements of the group. From this we can read of that the integration measure is in fact invariant under gauge transformations. The Haar measure is completely defined by gauge invariance and normalization for every compact Lie group. For example one of the most important features of the Haar measure follows directly from gauge invariance:

$$\int dg \ f(g) = \int dg \ f(hg) \ . \tag{A.27}$$

Now we can imediately see that

$$\int dg \ g = 0 \ . \tag{A.28}$$

An explicit construction of the Haar measure can be obtained as an integral over the parameter space of the group and an according Jacobi determinant (metric tensor) [58]. However this construction can be quite tedious for larger groups. We will sketch a procedure where we do not need the explicit form of the Haar measure. In fact equations (A.26) and (A.28) completely determine all integrals over all possible functions of the group elements, since integrals over every product of group elements can be reduced to integrals over a single group element in some arbitrary representation by Clebsch-Gordan decomposition of the product. The general rule for group integration is

Every integral over an arbitrary function of the group elements is determined by the Clebsch-Gordan decomposition of the integrand. If the Clebsch-Gordon decomposition of the the integrand contains the trivial representation the integral will not vanish. The value of the integral is then given by the multiplicity of the trivial representation.

The general form of an integral emerging in strong coupling or hopping expansions is of the form

$$\int dg \ \chi_{r_1}(h_1 g) \cdot \cdots \cdot \chi_{r_i}(h_i g) \chi_{r_j}(h_j g^{-1}) \cdot \cdots \cdot \chi_{r_n}(h_n g^{-1}) \tag{A.29}$$

where χ_{r_l} is the character in the representation r_l. The general way to compute this integral is to calculate the Clebsch-Gordan decomposition of the product in the above equation. In particular, if the Clebsch-Gordan decomposition does not contain the trivial representation the integral vanishes, since:

$$\int dg \ \chi_r(g) = \delta_{r,0} \ . \tag{A.30}$$

Now we have to find the Clebsch-Gordon decomposition of (A.29). All of the decomposition except for terms proportional to the trivial character will vanish. So if the trivial representation is part of the Clebsch-Gordon decomposition then (A.29) will result in a some non-vanishing combination of the h_l, where the exact form of the combination is determined by the tensor structure of the trivial representation of the decomposition. The simplest example for the integration procedure is:

$$\int dg \chi_r(gh)\chi_{r'}(g^{-1}f) = \delta_{r,r'}\frac{1}{d_r}\chi_r(fh) \; . \tag{A.31}$$

So in general everything one has to do is work out the Clebsch-Gordon decomposition of (A.29) and determine the tensor structure of the trivial part of the decomposition. Even though this is straight forward and sounds quite simple it takes a lot of effort to do this correctly.

B

Character Expansion for G_2

We will now perform the character expansion of the G_2 plaquette action. Remember that according to eq. (A.24) and eq. (A.25) we can expand the action for a single plaqutte in the following form

$$\begin{aligned} \exp[-S_p(U)] &= \sum_{r\in\hat{G}} f_r \chi_r(U) \ , \\ f_r &= \int dU \bar{\chi}_r(U) \exp[-S_p(U)] \ , \end{aligned} \tag{B.1}$$

where $\bar{\chi}_r(U)$ is the character in the complex conjugate representation. for our purposes it will be sufficient to take only the first three representations namely the trivial (1) the fundamental (7) and the adjoint (14) representation into account. Since G_2 is real we find that also (7) and (14) are real representations. Therefore we have $\bar{\chi}_{(7)} = \chi_{(7)}$ and $\bar{\chi}_{(14)} = \chi_{(14)}$. For the trivial representation this is always the case. To carry out the integration we have to expand the exponential

$$\begin{aligned} f_r &= \int dU \chi_r(U) \sum_{n=0}^{\infty} \frac{1}{n!} \left[\frac{\beta}{2N_c} (\mathrm{tr}\, U + \mathrm{tr}\, U^\dagger) \right]^n \ , \\ &= \int dU \sum_{n=0}^{\infty} \frac{1}{n!} \left[\frac{\beta}{N_c} \right]^n \chi_r(U) \chi^n_{(1,0)}(U) \ , \end{aligned} \tag{B.2}$$

and find the Clebsch-Gordon decomposition of the character products. The first three expansion coefficients up to order β^5 read:

$$\begin{aligned} f_{(1)} &= 1 + \frac{\beta^2}{2!7^2} + \frac{\beta^3}{3!7^3} + 4\frac{\beta^4}{4!7^4} + 10\frac{\beta^5}{5!7^5} \,, \\ f_{(7)} &= \frac{\beta}{7} + \frac{\beta^2}{2!7^2} + 4\frac{\beta^3}{3!7^3} + 10\frac{\beta^4}{4!7^4} + 35\frac{\beta^5}{5!7^5} \,, \\ f_{(14)} &= \frac{\beta^2}{2!7^2} + 2\frac{\beta^3}{3!7^3} + 9\frac{\beta^4}{4!7^4} + 30\frac{\beta^5}{5!7^5} \,. \end{aligned} \tag{B.3}$$

The results were obtained with the aid of the computer algebra package LiE[12]. Now we compare the expansion coefficients from eq. (2.54) with the coefficients we just computed. They are related by

$$a_r = \frac{f_r}{f_{(1)} d_r} \,. \tag{B.4}$$

Therefore we find the expansion parameters

$$\begin{aligned} u = a_{(7)} &= \frac{x}{7} + \frac{x^2}{14} + \frac{x^3}{42} - \frac{x^5}{168} - \frac{x^6}{36} \,, \\ v = a_{(14)} &= \frac{x^2}{42} + \frac{x^3}{42} + \frac{5x^4}{336} + \frac{x^5}{504} - \frac{31x^6}{2016} \,. \end{aligned} \tag{B.5}$$

with $x = \frac{\beta}{7}$. We can immediately conclude that if x is such that u is a small parameter then v is suppressed by another factor of x.

[12] http://wwwmathlabo.univ-poitiers.fr/∼maavl/LiE/

C

Parametrization of G_2 Elements in Terms of Class-Angles

As G_2 is quite a 'large' group, numerical update algorithms for Monte-Carlo simulations of G_2 are very involved and therefore numerically expensive. Since all the terms in the effective actions in eqs. (2.141) and (2.155) only depend functions like the trace and the determinant of G_2 elements we can use a much simpler update algorithm. We already saw in section A.2 that the trace in the fundamental representation is a class function that is independent of the choice of a basis:

$$\mathrm{tr}\,(VUV^{-1}) = \mathrm{tr}\,U\ , \qquad U\ , V\ \in G\ . \tag{C.1}$$

This is of cause also true for the determinant:

$$\det(VUV^{-1}) = \det U\ , \qquad U\ , V\ \in G\ . \tag{C.2}$$

Since the effective action depends on the Polyakov loops only through class functions we can evaluate the effective action in an arbitrary basis, moreover we can choose to calculate every class function in the eigenbasis of its operand. Since all operands in the effective action (2.155) are of the form $(1 + hW)$ or $\frac{hW}{(1+hW)^n}$ the eigenbasis of the operands is the eigenbasis of W. The eigenvalues of W are functions of the class angles only. Hence, in a Monte-Carlo simulation we have to sample only over the class angles and not over the whole gauge group. For the case of G_2 this simplifies and speeds up our Metropolis algorithm drastically. The eigenvalues of a G_2 element in terms of the class angles can be found by diagonalizing the elements of the maximal torus T of G_2. Elements t of T can be parameterized as

$$t(x, y) = \exp[xC_5]\exp[\sqrt{3}yC_{11}]\ , \tag{C.3}$$

where C_5 and C_{11} are the fifth and eleventh Generator of G_2 according to [107]. This leads to the following diagonal form of t

$$t(x,y) = \begin{pmatrix} 1 & & & & & & & \\ & e^{-i(x-y)} & & & & & & \\ & & e^{i(x-y)} & & & & & \\ & & & e^{-2iy} & & & & \\ & & & & e^{2iy} & & & \\ & & & & & e^{-i(x+y)} & & \\ & & & & & & e^{i(x-y)} & \end{pmatrix}, \qquad x, y \in [0, \pi] \,. \tag{C.4}$$

When we integrate over class functions it is sufficient to integrate over the class angles only, this is done by using the *reduced Haar measure*. For G_2 the reduced Haar measure is given by [95]

$$\begin{aligned} d\mu_{\text{red}} =& (4\chi_{(7)}^3 - \chi_{(7)}^2 - 2\chi_{(7)} - 10\chi_{(7)}\chi_{(14)} + 7 - 10\chi_{(14)} - \chi_{(14)}^2) && \text{(C.5)} \\ & \cdot (7 - \chi_{(7)}^2 - 2\chi_{(7)} + 4\chi_{(14)}) d\phi_1 d\phi_2 && \text{(C.6)} \end{aligned}$$

Where $\chi_{(7)}$ and $\chi_{(14)}$ are the characters of the fundamental and the adjoint representation given by

$$\begin{aligned} \chi_{(7)} =& 1 + 2\cos\phi_1 + 2\cos\phi_2 + 2\cos(\phi_1 + \phi_2) \,, \\ \chi_{(14)} =& 2(1 + \cos\phi_1 + \cos(\phi_1 - \phi_2) + \cos\phi_2 + \cos(\phi_1 + \phi_2) \\ & + \cos(2\phi_1 + \phi_2) + \cos(\phi_1 + 2\phi_2)) \,. \end{aligned}$$

The angles x, y and ϕ_1, ϕ_2 are related by

$$x = \frac{\phi_1 - \phi_2}{2} \,, \qquad y = \frac{\phi_1 + \phi_2}{2} \,. \tag{C.7}$$

And thus the area of integration is $\phi_1, \phi_2 \in [0, 2\pi]$.

Bibliography

[1] P. Scior, D. Scheffler, D. Smith, and L. von Smekal, "Effective SU(2) Polyakov Loop Theories with Heavy Quarks on the Lattice," *PoS Lattice 2014* , arXiv:1412.7089.

[2] P. Scior and L. von Smekal, "Baryonic matter onset in two-color QCD with heavy quarks," *Phys. Rev. D* **92** (2015) 094504, arXiv:1508.00431.

[3] P. Scior and L. von Smekal, "Effective Polyakov loop models for QCD-like theories at finite chemical potential," *PoS Lattice 2015* , arXiv:1602.04614.

[4] T. Blum, A. Denig, I. Logashenko, E. de Rafael, B. L. Roberts, T. Teubner, and G. Venanzoni, "The Muon (g-2) Theory Value: Present and Future," arXiv:1311.2198.

[5] J. Olson and M. Kado, "ATLAS and CMS physics results from Run 2." https://indico.cern.ch/event/442432/.

[6] D. J. Gross and F. Wilczek, "Ultraviolet Behavior of Non-Abelian Gauge Theories," *Phys. Rev. Lett.* **30** (1973) 1343–1346.

[7] H. D. Politzer, "Reliable Perturbative Results for Strong Interactions?," *Phys. Rev. Lett.* **30** (1973) 1346–1349.

[8] B.-J. Schaefer and M. Wagner, "On the QCD phase structure from effective models," *Prog. Part. Nucl. Phys.* **62** (2009) 381–385, arXiv:0812.2855.

[9] J. Greensite, *An Introduction to the Confinement Problem*, vol. 821 of *Lecture Notes in Physics*. Springer, Berlin, Heidelberg, 2011.

[10] R. Devenish and A. Cooper-Sarkar, *Deep Inelastic Scattering*. Oxford University Press, Oxford, 2003.

[11] Z. Fodor and C. Hoelbling, "Light hadron masses from lattice QCD," *Rev. Mod. Phys.* **84** (2012) 449–495, arXiv:1203.4789.

[12] M. Constantinou, "Hadron Structure," *PoS Lattice 2014* , arXiv:1411.0078.

[13] A. Nicholson, E. Berkowitz, E. Rinaldi, P. Vranas, T. Kurth, B. Joo, M. Strother, and A. Walker-Loud, "Two-nucleon scattering in multiple partial waves," *PoS Lattice 2015* (2015) , arXiv:1511.02262.

[14] P. Braun-Munzinger and J. Stachel, "The quest for the quark-gluon plasma.," *Nature* **448** (2007) 302–9.

[15] P. Braun-Munzinger and J. Wambach, "The Phase Diagram of Strongly-Interacting Matter," *Rev. Mod. Phys.* **81** (2008) 20, arXiv:0801.4256.

[16] S. Borsányi, Z. Fodor, C. Hoelbling, S. D. Katz, S. Krieg, C. Ratti, and K. K. Szabó, "Is there still any T c mystery in lattice QCD? Results with physical masses in the continuum limit III," *J. High Energy Phys.* **2010** (2010) 73, arXiv:1005.3508.

[17] A. Bazavov, T. Bhattacharya, C. DeTar, H. T. Ding, S. Gottlieb, R. Gupta, P. Hegde, U. M. Heller, F. Karsch, E. Laermann, *et al.*, "The equation of state in (2+1)-flavor QCD," *Phys. Rev. D* **90** (2014) 094503, arXiv:1407.6387.

[18] C. Gattringer and K. Langfeld, "Approaches to the sign problem in lattice field theory," arXiv:1603.09517.

[19] B. Friman, C. Höhne, J. Knoll, S. Leupold, J. Randrup, R. Rapp, and P. Senger, eds., *The CBM Physics Book*, vol. 814 of *Lecture Notes in Physics*. Springer, Berlin, Heidelberg, 2011.

[20] L. McLerran and R. D. Pisarski, "Phases of Dense Quarks at Large N_c," *Nucl. Phys. A* **796** (2007) 83–100, arXiv:0706.2191.

[21] M. Buballa and S. Carignano, "Inhomogeneous chiral condensates," *Prog. Part. Nucl. Phys.* **81** (2015) 39–96, arXiv:1406.1367.

[22] M. G. Alford, A. Schmitt, K. Rajagopal, and T. Schäfer, "Color superconductivity in dense quark matter," *Rev. Mod. Phys.* **80** (2008) 1455–1515, arXiv:0709.4635.

[23] A. Collaboration, B. Alessandro, F. Antinori, J. A. Belikov, C. Blume, A. Dainese, P. Foka, P. Giubellino, B. Hippolyte, C. Kuhn, *et al.*, "ALICE: Physics Performance Report, Volume II," *J. Phys. G Nucl. Part. Phys.* **32** (2006) 1295–2040.

[24] L. Kumar, "STAR Results from the RHIC Beam Energy Scan-I," *Nucl. Phys. A* **904-905** (2013) 256c–263c, arXiv:1211.1350.

[25] A. W. Steiner, J. M. Lattimer, and E. F. Brown, "The Neutron Star Mass-Radius Relation and the Equation of State of Dense Matter," *Astrophys. J.* **765** (2012) L5, arXiv:1205.6871.

[26] B. J. Schaefer and J. Wambach, "Renormalization group approach towards the QCD phase diagram," *Phys. Part. Nucl.* **39** (2008) 1025–1032, arXiv:hep-ph/0611191.

[27] B.-J. Schaefer, J. M. Pawlowski, and J. Wambach, "Phase structure of the Polyakov-quark-meson model," *Phys. Rev. D* **76** (2007) 074023, arXiv:0704.3234.

[28] C. Jung, *Mesonic Spectral Functions of the Polyakov-Quark-Meson Model*. Master's thesis, TU Darmstadt, 2016.

[29] H. Hansen, W. M. Alberico, A. Beraudo, A. Molinari, M. Nardi, and C. Ratti, "Mesonic correlation functions at finite temperature and density in the Nambu–Jona-Lasinio model with a Polyakov loop," *Phys. Rev. D* **75** (2007) 065004.

[30] C. S. Fischer, J. Luecker, and C. A. Welzbacher, "Locating the critical end point of QCD," *Nucl. Phys. A* **931** (2014) 774–779, arXiv:1410.0124.

[31] G. Eichmann, C. S. Fischer, and C. A. Welzbacher, "Baryon effects on the location of QCD's critical end point," *Phys. Rev. D* **93** (2016) 034013, arXiv:1509.0208.

[32] P. de Forcrand and O. Philipsen, "QCD phase diagram for small densities from simulations at imaginary μ," *Nucl. Phys. B - Proc. Suppl.* **119** (2003) 535–537, arXiv:hep-ph/0301209.

[33] G. Endrődi, Z. Fodor, S. D. Katz, and K. K. Szabó, "The QCD phase diagram at nonzero quark density," *J. High Energy Phys.* **2011** (2011) 1, arXiv:1102.1356.

[34] O. Kaczmarek, F. Karsch, E. Laermann, C. Miao, S. Mukherjee, P. Petreczky, C. Schmidt, W. Soeldner, and W. Unger, "The phase boundary for the chiral transition in (2+1)-flavor QCD at small values of the chemical potential," *Phys. Rev. D* **83** (2010) 014504, arXiv:1011.3130.

[35] M. Cristoforetti, F. Di Renzo, G. Eruzzi, A. Mukherjee, C. Schmidt, L. Scorzato, and C. Torrero, "An efficient method to compute the residual phase on a Lefschetz thimble," *Phys. Rev. D* **89** (2014) 114505, arXiv:1403.5637.

[36] G. Aarts and I.-O. Stamatescu, "Stochastic quantization at finite chemical potential," *J. High Energy Phys.* **2008** (2008) 018–018, arXiv:0809.5227.

[37] D. Sexty, "Simulating full QCD at nonzero density using the complex Langevin equation," *Phys. Lett. B* **729** (2014) 108–111, arXiv:1307.7748.

[38] C. Gattringer, T. Kloiber, and V. Sazonov, "Dual representation for massless fermions with chemical potential and U(1) gauge fields," *Phys. Rev. D* **93** (2015) 034505, arXiv:1512.00995.

[39] P. de Forcrand, J. Langelage, O. Philipsen, and W. Unger, "Lattice QCD Phase Diagram In and Away from the Strong Coupling Limit," *Phys. Rev. Lett.* **113** (2014) 152002, arXiv:1406.4397 [hep-lat].

[40] M. Fromm, J. Langelage, S. Lottini, M. Neuman, and O. Philipsen, "Onset Transition to Cold Nuclear Matter from Lattice QCD with Heavy Quarks," *Phys. Rev. Lett.* **110** (2013) 122001, arXiv:1207.3005.

[41] M. Fromm, J. Langelage, S. Lottini, and O. Philipsen, "The QCD deconfinement transition for heavy quarks and all baryon chemical potentials," *J. High Energy Phys.* **2012** (2012) 24, arXiv:1111.4953.

[42] J. Langelage, S. Lottini, and O. Philipsen, "Centre symmetric 3d effective actions for thermal SU(N) Yang-Mills from strong coupling series," *J. High Energy Phys.* **2011** (2011) 57, arXiv:1010.0951.

[43] C. Wozar, T. Kaestner, A. Wipf, and T. Heinzl, "Inverse Monte Carlo determination of effective lattice models for SU(3) Yang-Mills theory at finite temperature," *Phys. Rev. D* **76** (2007) 085004, arXiv:0704.2570.

[44] J. Greensite and K. Langfeld, "Effective Polyakov line action from strong lattice couplings to the deconfinement transition," *Phys. Rev. D* **88** (2013) 074503, arXiv:1305.0048.

[45] J. Engels, J. Fingberg, and M. Weber, "Finite size scaling analysis of SU(2) lattice gauge theory in (3 + 1) dimensions," *Nucl. Phys. B* **332** (1990) 737–759.

[46] S. Hands, J. B. Kogut, M.-P. Lombardo, and S. E. Morrison, "Symmetries and spectrum of SU(2) lattice gauge theory at finite chemical potential," *Nucl. Phys. B* **558** (1999) 327–346, arXiv:hep-lat/9902034.

[47] S. Hands, S. Kim, and J.-I. Skullerud, "Deconfinement in dense two-color QCD," *Eur. Phys. J. C* **48** (2006) 193–206, arXiv:hep-lat/0604004.

[48] S. Cotter, P. Giudice, S. Hands, and J.-I. Skullerud, "Towards the phase diagram of dense two-color matter," *Phys. Rev. D* **87** (2013) 034507, arXiv:1210.4496.

[49] T. Boz, S. Cotter, L. Fister, D. Mehta, and J.-I. Skullerud, "Phase transitions and gluodynamics in 2-colour matter at high density," *Eur. Phys. J. A* **49** (2013) 11, arXiv:1303.3223.

[50] M. Pepe and U. J. Wiese, "Exceptional Deconfinement in G(2) Gauge Theory," *Nucl. Phys. B* **768** (2006) 20, arXiv:hep-lat/0610076.

[51] B. H. Wellegehausen, A. Maas, A. Wipf, and L. von Smekal, "Hadron masses and baryonic scales in G2-QCD at finite density," *Phys. Rev. D* **89** (2014) 056007, arXiv:1312.5579.

[52] F. Karsch and M. Lütgemeier, "Deconfinement and chiral symmetry restoration in an SU(3) gauge theory with adjoint fermions," *Nucl. Phys. B* **550** (1999) 449–464, arXiv:hep-lat/9812023.

[53] N. Strodthoff, B.-J. Schaefer, and L. von Smekal, "Quark-meson-diquark model for two-color QCD," *Phys. Rev. D* **85** (2012) 074007, arXiv:1112.5401.

[54] N. Strodthoff and L. von Smekal, "Polyakov-quark–meson–diquark model for two-color QCD," *Phys. Lett. B* **731** (2014) 350–357, arXiv:1306.2897.

[55] N. Nakanishi and I. Ojima, *Covariant operator formalism of gauge theories and quantum gravity*. World Scientific, Singapore, 1990.

[56] R.-A. Tripolt, L. von Smekal, and J. Wambach, "Flow equations for spectral functions at finite external momenta," *Phys. Rev. D* **90** (2014) 074031, arXiv:arXiv:1408.3512v2.

[57] M. Asakawa, T. Hatsuda, and Y. Nakahara, "Maximum Entropy Analysis of the Spectral Functions in Lattice QCD," *Prog. Part. Nucl. Phys.* **46** (2000) 459–508, arXiv:hep-lat/0011040.

[58] C. Gattringer and C. B. Lang, *Quantum Chromodynamics on the Lattice*, vol. 788 of *Lecture Notes in Physics*. Springer, Berlin, Heidelberg, 2010.

[59] H. Nielsen and M. Ninomiya, "A no-go theorem for regularizing chiral fermions," *Phys. Lett. B* **105** (1981) 219–223.

[60] L. H. Ryder, *Quantum Field Theory*. Cambridge University Press, Cambridge, UK, 1985.

[61] I. Montvay and G. Münster, *Quantum Fields on a Lattice*. Cambridge University Press, Cambridge, UK, 1994.

[62] H.-P. Schadler and C. Gattringer, "Quark number susceptibilities at finite chemical potential from fugacity expansion," *PoS Lattice 2014* , arXiv:1409.4672.

[63] A. Nakamura, S. Oka, and Y. Taniguchi, "QCD phase transition at real chemical potential with canonical approach," *J. High Energy Phys.* **2016** (2016) 54, arXiv:1504.04471.

[64] K. Langfeld and J. M. Pawlowski, "Two-color QCD with heavy quarks at finite densities," *Phys. Rev. D* **88** (2013) 071502, arXiv:1307.0455.

[65] D. Scheffler, *Two-Color Lattice QCD with Staggered Quarks*. PhD thesis, Technische Universität Darmstadt, 2015.

[66] J. B. Kogut, M. Stone, H. Wyld, S. Shenker, J. Shigemitsu, and D. Sinclair, "Studies of chiral symmetry breaking in SU(2) lattice gauge theory," *Nucl. Phys. B* **225** (1983) 326–370.

[67] J. B. Kogut, M. A. Stephanov, D. Toublan, J. J. M. Verbaarschot, and A. Zhitnitsky, "QCD-like theories at finite baryon density," *Nucl. Phys. B* **582** (2000) 477–513.

[68] F. J. Dyson, "The Threefold Way. Algebraic Structure of Symmetry Groups and Ensembles in Quantum Mechanics," *J. Math. Phys.* **3** (1962) 1199.

[69] S. L. Adler, "Axial-Vector Vertex in Spinor Electrodynamics," *Phys. Rev.* **177** (1969) 2426–2438.

[70] J. S. Bell and R. Jackiw, "A PCAC puzzle: $\pi 0 \to \gamma\gamma$ in the σ-model," *Nuovo Cim. A* **60** (1969) 47–61.

[71] J. Wirstam, "Chiral symmetry in two-color QCD at finite temperature," *Phys. Rev. D* **62** (2000) 045012, arXiv:hep-ph/9912446.

[72] A. J. Macfarlane, "Lie algebra and invariant tensor technology for g2," *Int. J. Mod. Phys. A* **16** (2001) 29, arXiv:math-ph/0103021.

[73] K. Holland, P. Minkowski, M. Pepe, and U. J. Wiese, "Exceptional confinement in G(2) gauge theory," *Nucl. Phys. B* **668** (2003) 207–236, arXiv:hep-lat/0302023.

[74] B. Svetitsky and L. G. Yaffe, "Critical behavior at finite-temperature confinement transitions," *Nucl. Phys. B* **210** (1982) 423–447.

[75] A. Velytsky, "Finite temperature SU(2) gauge theory: critical coupling and universality class," *Int. J. Mod. Phys. C* **19** (2007) 17, arXiv:0711.0748.

[76] N. Strodthoff, S. R. Edwards, and L. von Smekal, "SU(3) Deconfinement in (2+1)d from Twisted Boundary Conditions and Self-Duality," *PoS Lattice 2010* , arXiv:1012.0723.

[77] R. Pisarski, "Quark-gluon plasma as a condensate of Z(3) Wilson lines," *Phys. Rev. D* **62** (2000) 111501, arXiv:hep-ph/0006205.

[78] R. D. Pisarski, "Effective theory of Wilson lines and deconfinement," *Phys. Rev. D* **74** (2006) , arXiv:hep-ph/0608242.

[79] A. Vuorinen, "Z(3)-symmetric effective theory for pure gauge QCD at high temperature," *Nucl. Phys. A* **785** (2007) 190–193, arXiv:hep-ph/0608162.

[80] B. Svetitsky, "Symmetry aspects of finite-temperature confinement transitions," *Phys. Rep.* **132** (1986) 1–53.

[81] T. Heinzl, T. Kaestner, and A. Wipf, "Effective actions for the SU(2) confinement-deconfinement phase transition," *Phys. Rev. D* **72** (2005) 065005, arXiv:hep-lat/0502013.

[82] J. Greensite, "Potential of the effective Polyakov line action from the underlying lattice gauge theory," *Phys. Rev. D* **86** (2012) 114507, arXiv:1209.5697.

[83] J. Greensite and K. Langfeld, "Effective Polyakov line action from the relative weights method," *Phys. Rev. D* **87** (2013) 094501, arXiv:1301.4977.

[84] J. Langelage, M. Neuman, and O. Philipsen, "Heavy dense QCD and nuclear matter from an effective lattice theory," *J. High Energy Phys.* **2014** (2014) 131, arXiv:1403.4162.

[85] G. Münster, "High-temperature expansions for the free energy of vortices and the string tension in lattice gauge theories," *Nucl. Phys. B* **180** (1981) 23–60.

[86] J. Langelage, *private communication.*

[87] M. Creutz, "On invariant integration over SU(N)," *J. Math. Phys.* **19** (1978) 2043.

[88] J. Langelage and O. Philipsen, "The pressure of strong coupling lattice QCD with heavy quarks, the hadron resonance gas and the large N limit," *J. High Energy Phys.* **2010** (2010) 55, arXiv:1002.1507.

[89] N. Kawamoto, "Towards the phase structure of euclidean lattice gauge theories with fermions," *Nucl. Phys. B* **190** (1981) 617–669.

[90] M. Creutz, "Monte Carlo study of quantized SU(2) gauge theory," *Phys. Rev. D* **21** (1980) 2308–2315.

[91] P. de Forcrand and L. von Smekal, "'t Hooft Loops, Electric Flux Sectors and Confinement in SU(2) Yang-Mills Theory," *Phys. Rev. D* **66** (2001) 011504, arXiv:hep-lat/0107018.

[92] D. Smith, A. Dumitru, R. D. Pisarski, and L. von Smekal, "Effective potential for SU(2) Polyakov loops and Wilson loop eigenvalues," *Phys. Rev. D* **88** (2013) 054020, arXiv:1307.6339.

[93] I. Bogolubsky, V. Mitrjushkin, M. Müller-Preussker, A. Sergeev, and H. Stüben, "Polyakov loops and Binder cumulants in SU(2) theory on large lattices," *Nucl. Phys. B - Proc. Suppl.* **129-130** (2004) 611–613.

[94] G. Endrődi, C. Gattringer, and H.-P. Schadler, "Fractality and other properties of center domains at finite temperature Part 1: SU(3) lattice gauge theory," *Phys. Rev. D* **89** (2014) 054509, arXiv:1401.7228.

[95] B. H. Wellegehausen, A. Wipf, and C. Wozar, "Effective Polyakov loop dynamics for finite temperature G 2 gluodynamics," *Phys. Rev. D* **80** (2009) 065028, arXiv:0907.1450.

[96] B. H. Wellegehausen, *Effektive Polyakov-Loop-Modelle für SU(N)- und G2-Eichtheorien.* Diploma thesis, 2008.

[97] G. Cossu, M. D'Elia, A. Di Giacomo, B. Lucini, and C. Pica, "G_2 gauge theory at finite temperature," *J. High Energy Phys.* **2007** (2007) 100–100, arXiv:0709.0669.

[98] A. Maas, L. von Smekal, B. H. Wellegehausen, and A. Wipf, "Phase diagram of a gauge theory with fermionic baryons," *Phys. Rev. D* **86** (2012) 111901, arXiv:1203.5653v2.

[99] B. H. Wellegehausen, *private communication.*

[100] T. D. Cohen, "Functional integrals for QCD at nonzero chemical potential and zero density," *Phys. Rev. Lett.* **91** (2003) 222001, arXiv:hep-ph/0307089.

[101] B. H. Wellegehausen and L. von Smekal, "Lattice simulations of G_2-QCD at finite density," *PoS Lattice 2014* , arXiv:1501.06706.

[102] J. A. Cuesta and A. Sanchez, "General non-existence theorem for phase transitions in one-dimensional systems with short range interactions, and physical examples of such transitions," *J. Stat. Phys.* **115** (2003) 869–893, arXiv:cond-mat/0306354.

[103] C. Herzog, M. Olshanii, and Y. Castin, "A liquid-gas transition for bosons with attractive interaction in one dimension," *Comptes Rendus Phys.* **15** (2013) 285–296, arXiv:1311.3857.

[104] N. D. Mermin and H. Wagner, "Absence of ferromagnetism or antiferromagnetism in one- or two-dimensional isotropic Heisenberg models," *Phys. Rev. Lett.* **17** (1966) 1133–1136.

[105] C. Itzykson and M. Nauenberg, "Unitary Groups: Representations and Decompositions," *Rev. Mod. Phys.* **38** (1966) 95–120.

[106] S. Sternberg, *Group theory and physics.* Cambridge University Press, Cambridge, UK, 1994.

[107] S. L. Cacciatori, B. L. Cerchiai, A. Della Vedova, G. Ortenzi, and A. Scotti, "Euler angles for G2," *J. Math. Phys.* **46** (2005) 083512, arXiv:hep-th/0503106.

Acknowledgment

First of all I would like to thank Prof. Lorenz von Smekal for giving me the opportunity to do my PhD in his group. In my years as his Master's and PhD student we had many interesting and enlightening discussions, not only about physics. I would like to thank him for supporting me and especially for not forgetting me and visiting Darmstadt once per week while the rest of the group moved to Gießen.
I am also grateful to Prof. Jochen Wambach for his support in the last years and enriching discussion during the PhD committees.
Next up, I enjoyed working together with my collaborators Sam Edwards, Dominik Smith, David Scheffler, Lukas Holicki and Björn Wellegehausen - Thank you.
I also want to thank all my colleagues from the upper floor as we always had a nice atmosphere and good times unrelated to work. In particular, I would like to mention Chris Jung, Sven Möller, Anton Cyrol for discussion about 'the day, for which we are envied by the world', Stefano Carignano for his hatred of the world and people in general, the 'small' and the 'tall' Daniel, Pascal Büscher for supplying me with funny stuff from the Internet and introducing me to the Japanese cuisine outside of Sushi, Markus Q. Huber (and also his wife) for organizing countless game sessions at his place, and Marco Schramm for sharing my interest in Scottish Whisky, cooking meat and Eintracht Frankfurt.
Thank you also to Johannes Weyrich and his girlfriend Linda for numerous sessions on the 'Lungerbalken' and keeping me in touch with the world outside of physics.
My final thanks go to my girlfriend Michaela and my family for their ongoing support. Without you, I would have never made it this far.

Lebenslauf

Name	Philipp Friedrich Scior
Geburtstag	9. September 1985
Geburtsort	Groß-Umstadt
Staatsangehörigkiet	deutsch
Familienstand	ledig

2013 - 2016	Promotionsstudium im Fachbereich Physik
	an der Technischen Universität Darmstadt
2009 - 2012	Masterstudium Physik
	an der Technischen Universität Darmstadt
2009 - 2010	Auslandsstudium an der University of Saskatchewan, Saskatoon, Kanada
2006 - 2009	Bachelorstudium Physics
	an der Technischen Universität Darmstadt
2005 - 2006	Freiwilliges Soziales Jahr statt Zivildienst
	beim Rettungsdienst des DRK-KV Odenwaldkreis e. V.
2002 - 2005	Schulbesuch am Gymnasium Michelstadt
	Abschluss: allgmeine Hochschulreife (Abitur)

Erklärung zur Dissertation

Hiermit versichere ich, die vorliegende Dissertation ohne Hilfe Dritter, nur mit den angegebenen Quellen und Hilfsmitteln angefertigt zu haben. Diese Arbeit hat in gleicher oder ähnlicher Form noch keiner Prüfungsbehörde vorgelegen, weiter habe ich noch keinen Promotionsversuch unternommen.

Darmstadt, den 14.06.2016

_____

Philipp Scior